Università degli Studi di Catania

Facoltà di Scienze Matematiche, Fisiche e Naturali

Dipartimento di Matematica e Informatica

Dottorato di Ricerca in Matematica e Informatica

XXXII Ciclo

ITN ModCompShock

All-Mach Number Solvers for the Euler Equations and the Saint-Venant-Exner Model

Stavros Avgerinos

Supervisor
Prof. Giovanni Russo

November 2019

Στην αγαπημένη μου Δήμητρα

Abstract

We propose a simple second order semi-implicit scheme for the numerical solution of Euler equation of gas dynamics and the Exner model. The proposed scheme overpass the classical acoustic CFL restriction on the timestep. The core idea is that explicit differential operators in space relative to convective or material speeds are discretized by local Lax-Friedrics fluxes and the linear implicit operators, pertaining to acoustic waves or surface waves for the Exner model, are discretized by central differences. We run a series of tests in one and two dimension and we compare our results with classical configurations. New original tests are introduced in order to highlight all the aspects of the proposed scheme.

Acknowledgements

First of all, I would like to express my gratitude to my supervisor Giovanni Russo for the useful comments, remarks and engagement through the learning process of this PhD thesis. In these three years he taught me a lot, always communicating me his passion for research, making me grow scientifically but also as a person. Working with him has been a very rewarding experience on several levels. I would like to thank also my co-supervisor Manuel J. Castro, with whom I have discussed several times about my work, receiving great advises.

Most importantly, I would like to thank my parents, Ntina and Giorgos, and my brother Ioannis who guided me in their own way throughout these past few years. They were always encouraging me to continue and finish up what I had started. I thank them for their love and constant support.

I'd like to thank my colleagues in Catania and Malaga. Especially my friend Giovanni Nastazi who was helping me constantly and making my life easier in Italy. Also my friends from Malaga who made my time in Spain a great experience.

And then, I would like to thank Dimitra, who is by my side when we are close and when we are apart, always sharing every moment of our lives. Thanks for the for always pushing me in believing in myself and for putting up with me in my worst days. Thank for her patience and her unconditional love. Thanks for walking with me up here and for continuing on this road together.

Contents

List of Figures

List of Tables

For/Dedicated to/To my...

Chapter 1

Introduction

Numerical methods for the solution of hyperbolic systems of conservation laws has been a very active field of research in the last decades. Several very effective schemes are nowadays treated in textbooks which became a classic on the topic [78, 114, 48]. Because of the hyperbolic nature, all such systems develop waves that propagate at finite speeds. If one wants to accurately compute all the waves in a hyperbolic system, then one has to resolve all the space and time scales that characterize it. Most schemes devoted to the numerical solution of such systems are obtained by explicit time discretisation, and the time step has to satisfy a stability condition, known as CFL condition, which states that the time step should be limited by the space step divided by the fastest wave speed (times a constant of order 1). Usually such a restriction is not a problem: because of the hyperbolic nature of the system, if the order of accuracy is the same in space and time, accuracy restriction and stability restrictions are almost the same, and the system is not stiff. There are, however, cases in which some of the waves are not particularly relevant and one is not interested in resolving them. Let us consider as a prototype model the classical Euler equations of compressible gas dynamics. In the low Mach number regimes, it may happen that the acoustic waves carry a negligible amount of energy, and one is mainly interested in accurately capturing the motion of the fluid. In such a case the system becomes stiff: classical CFL condition on the time step is determined by the acoustic waves which have a negligible influence on the solution, but which deeply affect the efficiency of the method itself.

Another difficulty arising with standard Godunov-type schemes for low-Mach flows is that the amount of numerical viscosity on the slow waves introduced by upwind-type discretisation of the system would heavily degrade the accuracy. An account of the latter effect is analyzed in [41], where the relevance of centering pressure gradients in the limit of small Mach number is emphasized.

In order to overcome the drawback of the stiffness, one has to resort to implicit strategies for time discretisation, which avoid the acoustic CFL restriction and allow the use of a much large time step. Naive implementation of implicit schemes for the solution of the Euler equations presents however two kinds of problems. First, classical upwind discretisation (say Godunov methods based on exact or approximate Riemann solvers) are highly nonlinear and very difficult to solve implicitly. Second, the implicit version of classical schemes may introduce an excessive numerical dissipation on the slow wave, resulting in loss of accuracy. Investigation of the effect on fully implicit schemes (and preconditioning techniques adopted to cure the large numerical diffusion) are discussed for example in [117] and in [85], both inspired by an early work of Turkel [115]. In both cases, a modification to the absolute value of the Roe matrix is proposed by a suitable preconditioner that avoids excessive numerical diffusion of upwind-type discretisation at very low Mach.

Several techniques have been devised to treat problems in the low Mach number regimes, that alleviate both drawbacks. Paper [22] is certainly one of the first work in where staggered semi-implicit schemes have been adopted to solve transient compressible gas flows (although the equations were not written in conservative form, hence unable to deal with shock waves). Another example of an early paper that makes use of semi-implicit scheme for low Mach problem is is given by [71].

However, some of such techniques have been explicitly designed to treat low Mach number regimes, and are based on low Mach number asymptotics ([70], [69]). There are cases in which the Mach number can change by several orders of magnitude. The biggest challenges come from gas dynamic problems in astrophysics, where the range of scales of virtually all parameters vary over many orders of magnitude. An adaptive low Mach number scheme, based on a non conservative formulation, has been developed with the purpose of tackling complex gas dynamics problems in astrophysics (see [90] and references therein). When Mach number is very low the flow does not develop shock discontinuities, and the conservation form of the schemes is not mandatory. When Mach number is not small, then shock discontinuities may form. In such a cases it is necessary to resort to conservative schemes (see for example [85] for other astrophysical applications).

Some hyperbolic systems other than gas dynamics may be affected by the stiffness due to a large range of wave speed. In magneto-hydrodynamics, for example, fast magneto acoustic waves may be much faster than Alfvén waves, and in case they carry very little energy, they do not need to be resolved. A pioneering paper in this direction was written by Harned and Kerner [55], who proposed a semi-implicit method for compressible MHD,

which was able to filter out fast magneto-acoustic waves, so that the restriction on the time step was due to the much slower Alfvén waves.

Other physical systems, still in the context of gas dynamics, are affected by drastic changes of the sound speed. Such large variations may be due to geometrical effects, as for example in the case of the nozzle flow or to heterogeneity of the media. Air-water systems, for example, are characterized by density ratio of three orders of magnitude, while the ratio of sound speed is about five. Waves in heterogeneous solid materials may travel at very different speeds, depending on the local stiffness of the medium. The motivation for the construction of effective all Mach number solver is twofold: on one hand it is relevant to accurately simulate waves in heterogeneous materials without small time step restriction suffered by explicit schemes, on the other hand such simulations can be adopted as a tool to validate homogenized models, which at a more macroscopic scale can be described as a homogeneous medium with different mechanical properties. For example, in air-water flows, for a range of values of the void fraction, the measured sound speed is lower than both water and air sound speed [34].

Motivated by the above arguments, several researchers have devoted a lot of effort in the development of *all Mach number* solvers for gas dynamics. An early all Mach number scheme has been described in [59]. The method is based on a MAC-type staggered discretisation in space. A conservative scheme is stabilized by a pressure-correction technique. The method is applied to several one and two dimensional problems, although no numerical convergence studies are reported.

Another attempt in this direction is presented in [73], where the authors adopt a pressure stabilization technique to be able to go beyond the classical CFL restriction. The technique works well for moderate Mach number, but is not specifically designed to deal with very small Mach numbers.

A different stabilization technique has been proposed by Kadioglu and collaborators [66]. Here the authors present a stabilization method based on an implicit step (on the primitive variables) which is performed after a second order explicit prediction. The technique is successfully applied to single fluid as well as multi-fluid test cases. Related methods by the same author have been developed in [65], where an IMEX strategy has been adopted to solve hydrodynamical problems with non linear heat conduction, and in [67], where the implicit-explicit schemes in time have been used in the context of radiation hydrodynamics.

Paper [74] deals with a pressure implicit scheme, which allows the use of larger CFL numbers than classical explicit schemes. Here the authors adopt a pressure stabilization technique to be able to go beyond the classical CFL

restriction. The technique works well for moderate Mach number, but is not specifically designed to deal with very small Mach numbers.

In an impressive sequence of papers and conference proceedings, [31, 28, 30, 29, 27], F. Coquel and collaborators proposed a semi-implicit strategy, coupled with a multi resolution approach, for the numerical solution of hyperbolic systems of conservation laws with very well separated wave propagation speeds. In particular, they considered application to fluid mixtures, in which the propagation speed of acoustic waves, often carrying a negligible amount of energy, is much larger than the speed of the material wave traveling at the fluid velocity. The basic framework is set in [31]. The method is first explained in the context of linear hyperbolic systems. The eigenvalues are sorted and it is assumed that there is a clear separation between slow and fast waves. The Jacobian matrix is split into a slow and fast component, using the characteristic decomposition. The flux at cell boundaries is consequently split into a slow and fast term. The fast term is treated implicitly, while the slow one is treated explicitly. The approach is then generalized to the quasilinear case, making use of Roe-type approximation of flux difference. This allows to construct a simple semi-implicit formulation by leaving the Roe matrix of the fast waves at the previous time step, while only the field is computed at the new time step, leading to a linearly implicit scheme. The effectiveness of the approach is further improved by adopting spatial multi resolution: given a multi scale expansion of the numerical solution, the finest scale is maintained locally only where needed, while coarser scales are adaptively adopted in smoother regions, with a great savings in computational time. Different schemes, still adopting implicit-explicit time differentiation to filter out fast waves, are considered in [28], where a sort of arbitrary Lagrangian-Eulerian scheme is constructed: a fractional time step strategy is composed by an implicit Lagrangian step, which filters out acoustic waves, and an explicit Eulerian step, which takes into account the contribution of slow waves. The main application is still on a model for the evolution of gas-oil mixture. In order to simplify the treatment of a general equation of state, a relaxation method is adopted (which of course satisfies the Chen-Levermore-Liu sub-characteristic condition [23]). The problem of developing an adaptive (local) time step strategy is considered in the proceedings [30], and fully exploited in [29]. In [27], the authors further refine the technique, thus producing a positivity preserving, entropic semi-implicit scheme for Euler-like equations. The approach developed by Coquel and collaborators is certainly valuable, although it may be quite involved to be efficiently implemented for more complex, multidimensional situations.

A different approach has been adopted by Munz and collaborators, starting from the low Mach number asymptotic of Kleinerman and Majda. In

[87], the authors develop a very effective semi-implicit method which can be viewed as a generalization of a compressible solver to weakly compressible flows. The method is based on the asymptotic behavior of the Euler equation for low Mach number. Two pressures are defined, a thermodynamic one, which is essentially constant in space, and a dynamic one, which accounts for fluid motion. The method is based on a discretization of the system written in primitive variables. The approach, designed for low Mach flow, cannot be directly used when compressive effects are more pronounced. In a subsequent paper [94], Park and Munz extend the method, still using the pressure as basic unknown in place of the energy, but now they adopt a conservative formulation, thus being able to capture shocks when the Mach number is not so small. Several space discretizations as well as time discretization strategies are discussed, which allow to obtain second order accuracy in space and time. In addition, the paper contains a nice overview of other works on low Mach number flow.

More recently, the approach of Park and Munz has been extended to general equations of state [43], rewriting the method of Casulli and Greenspan of [22] in fully conservative form.

In [51] and in [40] the authors explore the construction of an all Mach-number finite volume scheme for the isentropic Euler and Navier-Stokes equations. In both cases, the approach consists in a sort of hyperbolic splitting, obtained by adding and subtracting a gradient-type term to the momentum equation. Such a term is an approximation of the pressure gradient, and is treated implicitly, while the (relatively small) difference with the physical pressure gradient is treated explicitly. The authors show the asymptotic preserving (AP) property of the schemes: when the Mach number approaches zero the schemes become a consistent and stable discretization of the incompressible Euler and Navier-Stokes equations. In a more recent paper, Cordier et al.[32] extend the technique to the full Euler and Navier-Stokes equations. In paper [38] a different approach has been adopted for the construction of asymptotic preserving schemes for the gas dynamics. The authors perform a *gauge* decomposition of the momentum density into a solenoidal and irrotational field. They show that this corresponds to a sort of micro-macro decomposition, in which the macroscopic variable describe the slow material wave, while the fast variable accounts for the fast acoustic waves. They apply their technique to isentropic and full Euler and Navier-Stokes, as well as to the isentropic Navier-Stokes-Poisson system.

A systematic description of the flux vector splitting approach is also described in [113]: the flux is split in two terms, one of which is treated explicitly and the other implicitly. Several splittings are considered and compared. A slightly different technique, still based on flux splitting, is adopted in [89].

Semi-implicit schemes have been proposed and adopted for a wide range of problems, and obtained by different techniques. In a quite remarkable recent paper by Dumbser et al [42] the authors develop a pressure-based semi-implicit finite volume solver for the equations of compressible ideal, viscous, and resistive magnetohydrodynamics. In addition to be conservative for mass, momentum and total energy, the scheme preserves the divergence-free property of the magnetic field at a discrete level. Following the approach proposed by Casulli, the implicit part is pressure-based, therefore the nonlinearity of the implicit step appears only on the diagonal. The method appears particularly suited for low Mach-number problems. Several additional references to other semi-implicit schemes available in the literature can be found in the references.

All Mach number solvers are particularly useful in the context of multifluid flow, where the sound speed may change by orders of magnitude. Here we mention the paper by Fusnet and Popinet [46], which deals with the simulation of bubble dynamics, or the paper by Jemison et al [62], which presents a semi-implicit scheme exactly preserving mass, momentum, and energy in a multifluid context. A very robust method for multiphase flow has been presented in [1], where a relaxation scheme has been used to be able to treat very general equations of state, which are able to models at the same time solids and fluids. The generality of the technique, however, comes at the cost of doubling the number of equations, therefore increasing the computational cost in some cases.

In the first part of this thesis we built a semi-implicit scheme for the Euler equation in gas dynamics which is linearly implicit in the acoustic waves, eliminating the acoustic CFL restriction, and does not introduce excessive numerical dissipation at low Mach number, thus providing accurate solution in such regimes. The timestep is determined from the material waves. We show with a series of tests, in one and two dimensions, that the scheme can capture efficiently even material and acoustic waves when the acoustic CFL condition is obeyed. The computational time is dramatically decreased and thus the numerical dissipation is much more less, compared with the explicit schemes. One and two dimensional schemes are presented accompanied by several numerical tests.

On the second part of the thesis, motivated from the nature of the Exner model and the analogy with the isentropic Euler equations, we built a semi-implicit scheme for the Exner model which deals with the sedimentation. In such cases when one is interested only for the evolution of the sediment for long runtimes, our scheme provides an extremely accurate dissipation-free solution. The computational time in incomparable with the runtime of the explicit schemes. Still, if one is interested for the surface water waves,

with the classical CFL condition the scheme is able to capture accurately also this kind of waves. Schemes for one and two dimensions are presented accompanied by the corresponding numerical tests.

Chapter 2

Euler Equations

In this chapter we want to end up to the Euler equations by using the simplest assumptions. Our goal is to derive the Euler equations in the conservation form by using the conservation laws of mass, momentum and energy. These equations are used to describe the fluids motion such as gases or liquids.

In order to describe the derivation of the equations, let us consider a region $D \subseteq \mathbb{R}^d$ filled with a fluid. Let $\mathbf{x} \in D$ be a point in the region D and consider a particle of fluid at the position $\mathbf{x}$ at time t.

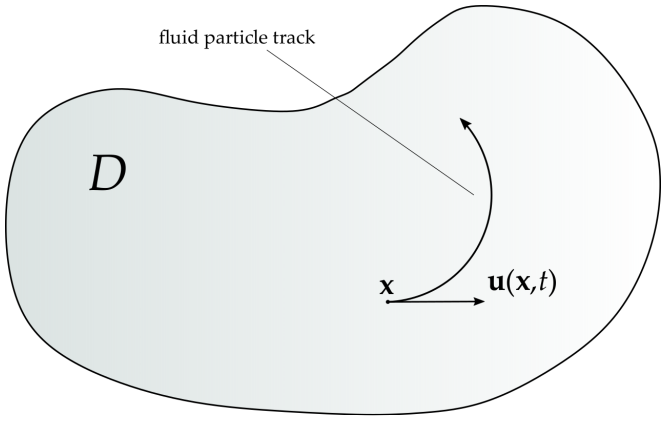

FIGURE 2.1: Motion of a fluid particle in the domain D.

2.1 Conservation of Mass

The first quantity we would like to introduce is the density $\rho(\mathbf{x}, t)$ which is defined as the mass per unit volume and it can be written as:

$$\rho(\mathbf{x}, t) = \lim_{\Delta V \to 0} \frac{\Delta m}{\Delta V}. \tag{2.1}$$

Now, for each time t we assume that the fluid has a well defined mass density $\rho(\mathbf{x}, t)$ such as, if W is an arbitrary subregion of D the mass of fluid in the subregion W is given by:

$$m(W, t) = \int_W \rho(\mathbf{x}, t) dV, \tag{2.2}$$

where dV is the volume element of W.

By assuming that the subregion W is fixed and does not change with time, we calculate the derivative with respect to time of Equation (2.2) and we obtain:

$$\frac{\partial}{\partial t} m(W, t) = \frac{\partial}{\partial t} \int_W \rho(\mathbf{x}, t) dV. \tag{2.3}$$

We denote the boundary of the fixed volume W by ∂W and we assume that is smooth. Moreover, we denote by $\mathbf{n} = n_x\mathbf{i} + n_y\mathbf{j} + n_z\mathbf{k}$ the outward unit normal vector defined at each point of ∂W, $\mathbf{i}, \mathbf{j}, \mathbf{k}$ the unit basis vectors and respectively n_x, n_y, n_z the components of the vector at the x, y and z direction. The volume flow rate across the surface ∂W for each unit area is $\mathbf{u} \cdot \mathbf{n}$ and respectively the mass flow is $\rho\mathbf{u} \cdot \mathbf{n}$.

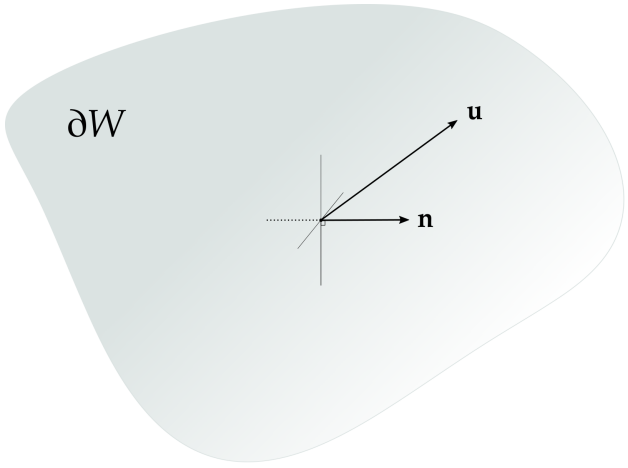

FIGURE 2.2: Mass flow through the boundary ∂W and the unit normal vector $\mathbf{n}$.

According to the principle of conservation of mass: the rate of increase of mass in the volume W is equal with the rate that mass crosses the boundary ∂W at the opposite direction of the outward normal vector, thus:

$$\frac{\partial}{\partial t}\int_W \rho(\mathbf{x},t)dV = -\int_{\partial W} \rho\mathbf{u}\cdot\mathbf{n}dA, \tag{2.4}$$

where dA is the surface element of ∂W.

By using the assumption that the subregion W is fixed and does not change with time, Equation (2.4) becomes:

$$\int_W \frac{\partial\rho}{\partial t}(\mathbf{x},t)dV = -\int_{\partial W} \rho\mathbf{u}\cdot\mathbf{n}dA, \tag{2.5}$$

which is the integral form of the law of conservation of mass.

By using the Divergence theorem to the right hand side of the (2.5), we obtain:

$$\int_W \left(\frac{\partial\rho}{\partial t} + \nabla\cdot(\rho\mathbf{u})\right) dV = 0. \tag{2.6}$$

Because the control volume W was arbitrary the integral vanishes and we obtain:

$$\frac{\partial\rho}{\partial t} + \nabla\cdot(\mathbf{m}) = 0, \tag{2.7}$$

where $\mathbf{m} = \rho\mathbf{u}$ stands for the momentum. Equation (2.7) is the differential form of the conservation of mass written in conservative form.

2.2 Momentum Equation

Let us consider again an arbitrary volume W of the region D. The forces acting on the fluid are separated to external volume forces per unit volume and the surface forces:

$$F = \int_W \mathbf{f}dV + \int_{\partial W} \sigma\mathbf{n}dA \tag{2.8}$$

Under the assumption that $f = 0$ and that the fluid is inviscid, i.e. $\sigma = -p\mathbf{I}$ where p stands for the pressure, we get:

$$F = -\int_{\partial W} p\mathbf{n}dA. \tag{2.9}$$

By using the Divergence theorem we obtain:

$$\begin{aligned} F &= -\int_{\partial W} p\mathbf{n}dA \\ &= -\int_{\partial W} p(n_x\mathbf{i} + n_y\mathbf{j} + n_z\mathbf{k})dA \\ &= -\left(\int_{\partial W} pn_x dA\right)\mathbf{i} - \left(\int_{\partial W} pn_y dA\right)\mathbf{j} - \left(\int_{\partial W} pn_z dA\right)\mathbf{k} \\ &= -\left(\int_W \frac{\partial p}{\partial x}dV\right)\mathbf{i} - \left(\int_W \frac{\partial p}{\partial y}dV\right)\mathbf{j} - \left(\int_W \frac{\partial p}{\partial z}dV\right)\mathbf{k} \\ &= -\int_W \left(\frac{\partial p}{\partial x}\mathbf{i} + \frac{\partial p}{\partial y}\mathbf{j} + \frac{\partial p}{\partial z}\mathbf{k}\right)dV = -\int_W \nabla p dV \end{aligned} \tag{2.10}$$

Thus, the force per unit volume is $-\nabla p$ on any particle of the fluid material. In order to use the Newton's second law, we must first define the acceleration of a moving fluid particle. This is done with the so-called material derivative, where the rate of the velocity of a given fluid particle which moves in the total fluid is:

$$\frac{D\mathbf{u}}{Dt} = \frac{\partial \mathbf{u}}{\partial t} + \mathbf{u}\cdot\nabla\mathbf{u}. \tag{2.11}$$

By using Newton's second law we obtain the differential form of the momentum equation:

$$\rho\frac{\partial \mathbf{u}}{\partial t} + \rho\mathbf{u}\cdot\nabla\mathbf{u} = -\nabla p. \tag{2.12}$$

In order to write the momentum equation in the conservation form we have to compute the derivative:

$$\frac{\partial(\rho\mathbf{u})}{\partial t} = \rho\frac{\partial \mathbf{u}}{\partial t} + u\frac{\partial \rho}{\partial t}. \tag{2.13}$$

Substituting the term $\rho(\partial\mathbf{u}/\partial t)$ on the Equation (2.12) by making use the Equation (2.13) we obtain:

$$\frac{\partial(\rho\mathbf{u})}{\partial t} - u\frac{\partial\rho}{\partial t} + \rho\mathbf{u}\cdot\nabla\mathbf{u} = -\nabla p. \tag{2.14}$$

Recalling the Equation (2.7) we substitute the term $\partial\rho/\partial t$ in Equation (2.14) and we obtain:

$$\begin{gathered}\frac{\partial(\rho\mathbf{u})}{\partial t} + u\nabla\cdot(\rho\mathbf{u}) + \rho\mathbf{u}\cdot\nabla\mathbf{u} = -\nabla p \Leftrightarrow \\ \frac{\partial\mathbf{m}}{\partial t} + \nabla\cdot\left(\frac{\mathbf{m}\otimes\mathbf{m}}{\rho} + p\mathbf{I}\right) = 0,\end{gathered} \tag{2.15}$$

which is the momentum equation written in the conservation form.

2.3 Energy Equation

Again we consider a control volume W of the domain D. We want to compute the total energy in this volume. By applying the first thermodynamics principle one gets:

$$\Delta E_{TOT} = \delta Q + \delta L. \tag{2.16}$$

We denote:

$$\delta Q = \left(-\int_{\partial W} q\cdot\mathbf{n}dA\right)dt, \tag{2.17}$$

where $q\cdot\mathbf{n}dA$ is the heat that flows inside to the control volume W per unit mass by crossing the surface of the volume.

The second term in Equation (2.17) is defined:

$$\delta L = \left(\int_W \rho\mathbf{f}\cdot\mathbf{u}dV + \int_{\partial W}\sigma\mathbf{u}\cdot\mathbf{n}dA\right)dt \tag{2.18}$$

where the first term is the work of surface forces and the second term is the work of body forces.

Using the the same assumption as before, that the the external forces are equal to zero and taking into account that for Euler equations the heat conduction is zero we obtain the total energy per unit volume:

$$\int_W E dV = \int_{\partial W} \sigma \mathbf{u} \cdot \mathbf{n} dA. \tag{2.19}$$

Using the assumption that the fluid is inviscid the stress tensor is equals: $\sigma = -p\mathbf{I}$. Thus the Equation (2.19) becomes:

$$\int_W E dV = -\int_{\partial W} p\mathbf{u} \cdot \mathbf{n} dA. \tag{2.20}$$

We compute the derivative with respect to time of the total Energy and we obtain:

$$\frac{d}{dt}\int_W E dV = \int_W \frac{\partial E}{\partial t} dV + \int_{\partial W} E\mathbf{u} \cdot \mathbf{n} dA. \tag{2.21}$$

Combining Equations (2.20) and (2.21) and by using the divergence theorem we obtain:

$$\int_W \frac{\partial E}{\partial t} dV + \int_W \nabla \cdot (E\mathbf{u}) dV = \int_W \nabla \cdot (p\mathbf{u}) dV. \tag{2.22}$$

The choice of the volume W was arbitrary, so the equation (2.22) is valid for each control volume W. Thus we obtain the Energy equation written in the conservative form:

$$\frac{\partial E}{\partial t} + \nabla \cdot ((E + p)\mathbf{u}) = 0. \tag{2.23}$$

Now, we introduce the total enthalpy $h = (E + p)/\rho$. Plugging the expression for the enthalpy in the Equation (2.23) we obtain the equation written in terms of enthalpy:

$$\frac{\partial E}{\partial t} + \nabla \cdot (h\mathbf{m}) = 0. \tag{2.24}$$

2.4 Equation of State

Let us now compute the total energy of a compressible fluid:

$$E = E_{KIN} + E_{INT}, \tag{2.25}$$

where E_{KIN} is the kinetic energy density correlated with the control volume which equals:

$$E_{KIN} = \frac{1}{2}\rho \mathbf{u}^2. \tag{2.26}$$

Moreover, E_{INT} is the internal energy per unit volume of the fluid which stands for:

$$E_{INT} = \rho e \tag{2.27}$$

where e is the internal energy per unit mass. For an ideal gas the specific internal energy is a function of temperature. Thus, the internal energy equals:

$$e = C_V T \tag{2.28}$$

where C_V the specific heat at constant volume. The specific heat constants for constant pressure and constant volume processes for an ideal gas are correlated to the gas constant R for a given gas such as:

$$C_P = C_V + R. \tag{2.29}$$

Thus, combining the Equations (2.26), (2.27) and (2.28) we obtain an expression for the the internal energy of the gas where:

$$E_{INT} = \rho C_V T = \rho \frac{C_V}{C_p - C_V} RT = \rho \frac{1}{1-\gamma} \frac{p}{\rho} = \frac{p}{\gamma - 1}, \tag{2.30}$$

where $\gamma = \frac{C_p}{C_V}$ is the polytropic gas constant. Finally, in order to compute the total energy we have to sum the kinetic energy and the internal energy. By substituting the kinetic and the internal energy terms in the Equation (2.25) by the terms from the Equations (2.26) and (2.30) we obtain the equation of state (EOS) for a perfect gas:

$$E = \frac{1}{2}\rho \mathbf{u}^2 + \frac{p}{\gamma - 1}. \tag{2.31}$$

With this equation introduced the system of differential equations now is closed by adding this liner correlation between the pressure and the energy variables. For a detailed derivation of the Euler equations see [25].

2.5 Hyperbolicity

The Euler equations in one dimension can be written in the following form:

$$\begin{cases} \dfrac{\partial \rho}{\partial t} + \dfrac{\partial m}{\partial x} = 0, \\ \dfrac{\partial m}{\partial t} + \dfrac{\partial}{\partial x}(mu + p) = 0, \\ \dfrac{\partial E}{\partial t} + \dfrac{\partial}{\partial x}(hm) = 0. \end{cases} \tag{2.32}$$

The system is closed with the equation of state for a perfect gas, where:

$$E = \frac{1}{2}\rho u^2 + \frac{p}{\gamma - 1}. \tag{2.33}$$

For the sake of simplicity we are going to build the scheme using just this equation of state, but it is straightforward that any equation of state can be used specifically for the explicit schemes.

Let us now write the System (2.32), using the primitive variables, in the following form:

$$W_t + A(W)W_x = 0, \tag{2.34}$$

where:

$$W = \begin{pmatrix} \rho \\ u \\ p \end{pmatrix}, \qquad A(W) = \begin{pmatrix} u & \rho & 0 \\ 0 & u & 1/\rho \\ 0 & \rho a^2 & u \end{pmatrix}$$

where $a = \sqrt{\frac{\gamma p}{\rho}}$ is the sound speed.

The eigenvalues of the matrix A can be computed easily and one gets three distinct eigenvalues λ_k:

$$\lambda_1 = u - a, \qquad \lambda_2 = u, \qquad \lambda_3 = u + a \tag{2.35}$$

These eigenvalues are real, thus the System (2.32) is hyperbolic. Moreover, these eigenvalues are the speeds at which information propagates for the fluid equations. Since $A = A(W)$ the System (2.32) is called quasi-linear.

2.6 Incompressible Euler Equations

Let us now present the rescaled (non-dimensionalised) compressible Euler equations:

$$\begin{cases} \dfrac{\partial \rho}{\partial t} + \nabla \cdot (\mathbf{m}) = 0, \\ \dfrac{\partial \mathbf{m}}{\partial t} + \nabla \cdot \left(\dfrac{\mathbf{m} \otimes \mathbf{m}}{\rho} \right) + \dfrac{1}{\epsilon^2} \nabla p = 0, \\ \dfrac{\partial E}{\partial t} + \nabla \cdot (h\mathbf{m}) = 0, \end{cases} \tag{2.36}$$

where ϵ stands for the dimensionless reference Mach number. The system is closed with the suitable scaled equation of state, where:

$$p = (\gamma - 1) \left(E - \frac{\epsilon^2}{2} \rho u^2 \right). \tag{2.37}$$

Let us now consider an asymptotic expansion ansatz for the following variables:

$$\begin{aligned} p(x,t) &= p_0(x,t) + \epsilon p_1(x,t) + \epsilon^2 p_2(x,t) + \cdots \\ \mathbf{u}(x,t) &= \mathbf{u_0}(x,t) + \epsilon \mathbf{u_1}(x,t) + \cdots \\ E(x,t) &= E_0(x,t) + \epsilon E_1(x,t) + \cdots \end{aligned} \tag{2.38}$$

Plugging this expansion in the momentum equation of (2.36) and considering terms $\mathcal{O}(1/\epsilon)$ and $\mathcal{O}(1/\epsilon^2)$, we obtain that:

$$\nabla p_0 = \nabla p_1 = 0. \tag{2.39}$$

This leads to the conjecture that pressure must be constant in space up to order ϵ. Thus from (2.38) we obtain:

$$p(x,t) = p_0(t) + \epsilon^2 p_2(x,t) + \cdots \tag{2.40}$$

that allows only temporal variations.

The expansion in Mach number is also applied to the equation of state, where:

$$p_0 = (\gamma - 1) E_0 \tag{2.41}$$

Plugging the relation (2.39) and (2.41) into the equation for the energy from (2.36), by taking the $\mathcal{O}(1)$ terms, one writes:

$$\begin{cases} \rho_t + \nabla \cdot (\rho \mathbf{u_0}) = 0, \\ (\rho \mathbf{u_0})_t + \nabla \cdot (\rho \mathbf{u_0} \otimes \mathbf{u_0}) + \nabla p_2 = 0, \\ \nabla \cdot \mathbf{u_0} = -\dfrac{1}{\gamma p_0(t)} \dfrac{dp_0}{dt}. \end{cases} \tag{2.42}$$

Under the assumption that we use periodic boundary conditions, i.e.:

$$\int_\Omega \nabla \cdot \mathbf{u_0} dx = 0,$$

we integrate the last equation of (2.42) and we obtain $dp_0/dt = 0$. This leads to the deduction that the pressure $p_0 = p^*$ is constant and thus we get that $\nabla \cdot \mathbf{u_0} = 0$.

Using these relations, the density equation becomes:

$$\rho_t + \mathbf{u_0} \cdot \nabla \rho = 0. \tag{2.43}$$

This means that in the limit case where $\epsilon = 0$ the density will be advected along the particle paths and if it's constant at the initial time, it should remain constant at any time.

We impose that $\rho(x, 0) = \rho^*(x)$, where ρ^* is a strictly positive function such that $\rho^* = \mathcal{O}(1)$. Using well-prepared initial conditions where:

$$\begin{cases} \rho(x,0) = \rho^*(x) + \epsilon^2 \rho_2(x), \\ p(x,0) = p^* + \varepsilon^2 p_2(x), \\ \nabla \cdot \mathbf{u}(x,0) = \mathbf{u_0}(x) + \mathcal{O}(\epsilon). \end{cases} \tag{2.44}$$

we obtain, at low Mach number ($\epsilon \to 0$), with $\nabla \cdot \mathbf{u_0} = 0$, the solution $(\rho, \mathbf{u}, p)$ of the compressible Euler system (2.36) converges to the solution of the incompressible Euler system:

$$\begin{cases} \rho_t + \mathbf{u} \cdot \nabla \rho = 0, \\ \rho \left(\mathbf{u}_t + (\mathbf{u} \cdot \nabla \mathbf{u}) \right) + \nabla p_2 = 0, \\ \nabla \cdot \mathbf{u} = 0, \\ p = (\gamma - 1) E = p^*. \end{cases} \tag{2.45}$$

where

$$p_2 = \lim_{\epsilon \to 0} \frac{1}{\epsilon^2}(p - p^*)$$

This is implicitly defined by the constraint $\nabla \cdot \mathbf{u} = 0$ and explicitly given by the equation:

$$-\Delta p_2 = \rho_0 \nabla^2 (\mathbf{u} \otimes \mathbf{u}). \tag{2.46}$$

Compressible Euler equations converge to incompressible equations when the Mach number becomes small. This was the motivation for building an all Mach number semi-implicit scheme. When the Mach number is of order one, modern shock capturing methods are able to capture shocks and other complex structures with high numerical resolutions. A difficulty in the construction such schemes consists in the different nature of the equations and then in different numerical techniques traditionally used for solving them: methods for compressible Euler is usually based on a conservative form, explicit schemes in time and non-linear reconstruction, while the methods for Euler incompressible are usually based on a non-conservative formulation, on the implicit treatment of the pressure and on reconstructions which are often linear. In Chapter 4 we present a semi-implicit all Mach number scheme but first we have to present some well known techniques from the literature.

Chapter 3

Explicit Scheme for 1D Euler Equations

In this chapter we present an explicit numerical method in order to build the required background for the derivation of the semi-implicit scheme. We present a first order finite volume scheme in space and time. The purpose of this chapter is to present some well known techniques we used for the development of our scheme. More details concerning finite volume scheme can be found at the following classical books [111, 112, 6, 78, 79, 101].

We adopt a collocated grid for the spatial discretization which is more common in finite volumes for compressible flows. The choice of this grid also reduces the implementation complexity, specifically in modern distributed memory machine architectures.

3.1 Upwind Scheme

Standard centered difference in space and forward Euler in time gives a numerical scheme that converges only under the restriction $\Delta t = O(\Delta x^2)$, which is not natural for hyperbolic problems. One can show that using three level Runge-Kutta time discretization coupled with centered difference leads to a scheme which is stable for $c\Delta t < K\Delta x$, where K is a constant that depends on the scheme. On the other hand, it is possible to combine space and time discretization, and obtain one level scheme (in time) which are stable. The upwind scheme uses a first order approximation of the space derivative.

For the scalar conservation law:

$$u_t + c\, u_x = 0,$$

upwinding time discretization is obtained by discretizing the space derivatives as follows:

$$\left.\frac{\partial u}{\partial x}\right|_{x_i} \approx \begin{cases} \dfrac{u_i - u_{i-1}}{\Delta x} & \text{if } c \geq 0 \\ \dfrac{u_{i+1} - u_i}{\Delta x} & \text{if } c < 0 \end{cases}$$

First order upwinding is obtained by explicit Euler and first order upwind space discretization[1] :

$$\frac{u_i^{n+1} - u_i^n}{\Delta t} + c\frac{u_i^n - u_{i-1}^n}{\Delta x} = 0 \quad \text{if } c \geq 0,$$

$$\frac{u_i^{n+1} - u_i^n}{\Delta t} + c\frac{u_{i+1}^n - u_i^n}{\Delta x} = 0 \quad \text{if } c < 0.$$

The scheme can be written in a compact form as:

$$u_i^{n+1} = u_i^n - c_+\frac{\Delta t}{\Delta x}(u_i^n - u_{i-1}^n) - c_-\frac{\Delta t}{\Delta x}(u_{i+1}^n - u_i^n)$$

where

$$c_+ = \max(c, 0) \qquad c_- = \min(c, 0)$$

For a linear system one has:

$$\frac{\partial u}{\partial t} + A\frac{\partial u}{\partial x} = 0, \quad A \in \mathbb{R}^{m\times m}, u \in \mathbb{R}^m \tag{3.1}$$

where $u(x,t) \in \mathbb{R}^m$ is the unknown vector field and it is not clear where to apply right or left difference.

Upwind schemes for a linear system can be constructed by diagonalizing the system. Let Q be the matrix formed by the m independent right eigenvectors of A and Λ the diagonal matrix containing the corresponding eigenvalues. Then one has

$$A\,Q = Q\,\Lambda \tag{3.2}$$

The diagonalization is always possible if we assume that the system is hyperbolic. Let us express the vector field u as a linear combination of eigenvectors of A:

$$u = Qv \quad v \in \mathbb{R}^m \tag{3.3}$$

[1]For the moment we do not specify the range of the cell index i, which depends also on the boundary conditions and on the order of accuracy of the method

Then, substituting into (3.1) one has

$$\frac{\partial v}{\partial t} + \Lambda \frac{\partial v}{\partial x} = 0. \tag{3.4}$$

This means that the equations decouple, and one can apply the upwind scheme to each scalar equation of system (3.4),

$$v_i^{n+1} = v_i^n - \frac{\Delta t}{\Delta x}\left[\Lambda_+(v_i^n - v_{i-1}^n) + \Lambda_-(v_{i+1}^n - v_i^n)\right] \tag{3.5}$$

where

$$\Lambda_+ = \text{diag}\left((\lambda_1)_+, \ldots, (\lambda_m)_+\right)$$
$$\Lambda_- = \text{diag}\left((\lambda_1)_-, \ldots, (\lambda_m)_-\right)$$

and λ_k, $k = 1, \ldots, m$ denotes the eigenvalues of A.
Using transformation (3.3) to go back to the original variable u one has the upwind scheme for u in the form

$$u_i^{n+1} = u_i^n - \frac{\Delta t}{\Delta x}\left(A_+(u_i^n - u_{i-1}^n) + A_-(u_{i+1}^n - u_i^n)\right)$$

with

$$A_+ = Q\Lambda_+Q^{-1} \qquad A_- = Q\Lambda_-Q^{-1}$$

What is the restriction on the time step? The restriction is that for all eigenvalues λ_k, condition

$$|\lambda_k|\frac{\Delta t}{\Delta x} \leq 1 \quad k = 1, \ldots, m$$

has to be satisfied. This condition can be written in the form

$$\rho(A)\frac{\Delta t}{\Delta x} \leq 1$$

where

$$\rho(A) \equiv \max_{1 \leq k \leq m} |\lambda_k(A)|$$

denotes the spectral radius of matrix A, i.e. the maximum eigenvalue of the matrix (in absolute value).

The geometric interpretation of the stability condition is the following. For each eigenvalue λ_k one uses left or right difference on the characteristic variable according to whether $\lambda_k > 0$ or $\lambda_k < 0$. The characteristic emanating back from point (x_i, t_{n+1}) will intercept the line $t = t_n$ at a point which lies between x_{i-1} and x_i (if $\lambda_k > 0$) or between x_i and x_{i+1} if (if $\lambda_k < 0$).

This condition is a particular case of a more general stability condition for systems, known as CFL condition, which states that a necessary condition for stability is that the analytical domain of dependence of a given grid point has to be contained by the numerical domain of dependence. Using the same argument of the diagonalization, one can show that stability condition for Lax-Friedrichs and Lax-Wendroff scheme is also:

$$\rho(A)\frac{\Delta t}{\Delta x} \leq 1$$

3.2 The Riemann problem

How can one generalize upwind schemes to nonlinear conservation laws? A popular method, that can be considered the ancestor of many modern schemes for the numerical approximation of conservative laws, is the Godunov method. This method is based on the solution of the Riemann problem.

A Riemann problem is an initial value problem for which the initial data is piecewise constant:

$$\begin{aligned} &\frac{\partial u}{\partial t} + \frac{\partial f}{\partial x} = 0, \\ &u(x,0) = \begin{cases} u_l, & x < 0, \\ u_r, & x > 0 \end{cases} \end{aligned}$$

The solution of the Riemann problem is known for several hyperbolic systems of conservation laws with great relevance in the applications, as is the case of gas dynamics (see, for example, [78]). The solution to the Riemann problem centered at the origin is a similarity solution that depends on x/t , $u = u(x/t; u_l, u_r)$. In many cases, however, its solution is not available analytically, or it is quite expensive to compute. In such cases one uses either approximate Riemann solvers, or schemes that do not require the solution to the Riemann problem. For the moment we shall assume that we know the solution of the Riemann problem.

3.3 Godunov Scheme

Let us assume that at time t_n we know an approximation of the cell average, $\{\bar{u}_i^n\}$, and that the solution is a piecewise constant function:

$$u(x, t_n) \simeq \sum_i \bar{u}_i^n \chi_i(x) \tag{3.6}$$

where

$$\chi_i(x) = \begin{cases} 1 & x \in [x_{i-1/2}, x_{i+1/2}] \\ 0 & \text{otherwise} \end{cases}$$

For short later times the field vector $u(x,t)$ will be the solution of several Riemann problems, centered in $x_{i+1/2}$.

Let us integrate the conservation law in the cell $I_i \times [t_n, t_{n+1}]$. Then one has:

$$\bar{u}_i^{n+1} = \bar{u}_i^n - \frac{1}{\Delta x} \int_{t_n}^{t_{n+1}} [f(u(x_{i+1/2}, t)) - f(u(x_{i-1/2}, t))]\, dt \tag{3.7}$$

Now if the Riemann fan do not interact (which is obtained if the time step Δt satisfies a suitable CFL condition) then the function $u(x_{i+1/2}, t)$ can be obtained from the solution of the Riemann problem with states u_i and u_{i+1} across the interface:

$$u(x_{i+1/2}, t) = u^*(0; \bar{u}_i, \bar{u}_{i+1}) =: u^*(\bar{u}_i, \bar{u}_{i+1})$$

This quantity does not depend on time, and therefore Eq.(3.7) becomes

$$\bar{u}_i^{n+1} = \bar{u}_i^n - \frac{\Delta t}{\Delta x} [f(u^*(\bar{u}_i, \bar{u}_{i+1})) - f(u^*(\bar{u}_{i-1}, \bar{u}_i))] \tag{3.8}$$

If the function $u(x, t_n)$ is really a piecewise constant function, then Equation (3.8) gives the correct average of the solution at time t_{n+1}. In order to proceed from time t_{n+1} to time t_{n+2} applying the same technique, one has to approximate the solution at time t_{n+1} as a piecewise constant function. It is essentially this projection that introduces the approximation.

When applied to a linear system, Godunov scheme reduces to first order upwind. To see this, let us consider an interface, let us say at $x_{i+1/2}$, and let us write

$$\bar{u}_{i+1/2} = \bar{u}_{i+1} - \bar{u}_i = \sum_k \alpha_k^{(i+1/2)} r_k$$

where r_k are the right eigenvectors of matrix A that defines the linear flux:

$$f(u) = A\, u$$

Then the solution of the Riemann problem can be written as

$$\begin{aligned} u^*(\bar{u}_i, \bar{u}_{i+1}) &= \bar{u}_i + \sum_{\lambda_k < 0} \alpha_k^{(i+1/2)} r_k \\ &= \bar{u}_{i+1} - \sum_{\lambda_k > 0} \alpha_k^{(i+1/2)} r_k \end{aligned}$$

since the contribution to the jump with $\lambda_k < 0$ will propagate to the left, and the contribution with $\lambda_k > 0$ will propagate to the right.
Substituting this expression into (3.8) one has

$$\begin{aligned}\bar{u}_i^{n+1} &= \bar{u}_i^n - \frac{\Delta t}{\Delta x}\left[A\left(\bar{u}_i + \sum_{\lambda_k<0}\alpha_k^{(i+1/2)} r_k\right) - A\left(\bar{u}_i + \sum_{\lambda_k>0}\alpha_k^{(i-1/2)} r_k\right)\right] \\ &= \bar{u}_i^n - \frac{\Delta t}{\Delta x}\left[\sum_{\lambda_k<0}\alpha_k^{(i+1/2)}\lambda_k r_k + \sum_{\lambda_k>0}\alpha_k^{(i-1/2)}\lambda_k r_k\right]\end{aligned}$$

Multiplying by Q^{-1}, and considering that $Q^{-1}r_k = e_k$, one has

$$v_i^{n+1} = v_i^n - \frac{\Delta t}{\Delta x}\left[\sum_{\lambda_k<0}\lambda_k(v_{i+1}^{(k)} - v_i^{(k)})e_k + \sum_{\lambda_k>0}\lambda_k(v_i^{(k)} - v_{i-1}^{(k)})e_k\right]$$

where $\bar{u}_i^n = Q\, v_i^n$, v_i being characteristic variables, $\alpha_k^{(i+1/2)} = v_{i+1}^{(k)} - v_i^{(k)}$, and e_k is the k-th column of the $m \times m$ identity matrix. This relation can be written as

$$v_i^{n+1} = v_i^n - \frac{\Delta t}{\Delta x}\left(\Lambda_-(v_{i+1} - v_i) + \Lambda_+(v_i - v_{i-1})\right),$$

which is the same as Eq.(3.5).

Godunov scheme is therefore first order accurate in space and time. The Godunov method is based on the solution of the Riemann problem, which makes it expensive to use in many circumstances. Several approximate Riemann solvers have been developed, that make Godunov methods more efficient. The most popular is the one derived by Phil Roe [99]. Another approximate Riemann solver has been proposed by Harten, Lax and Van Leer [57]. For more details concerning the Riemann solvers we refer the reader to the books by LeVeque [78, 79].

3.4 Finite Volume Scheme

Higher order extension of the Godunov method can be obtained by several techniques. One is to use a more accurate reconstruction of the function from cell averages, such as, for example, a piecewise linear function, and then solve the generalized Riemann problem.

A second alternative is to use a semidiscrete scheme of the following form. In a finite volume scheme, the basic unknown is the cell average $\bar{u}_j$. We have

seen that the solution $u(x,t)$ satisfies the equation:

$$\frac{d < u >_i}{dt} + \frac{f(u(x_{i+1/2},t)) - f(u(x_{i-1/2},t))}{h} = 0$$

where:

$$< u >_i \equiv \frac{1}{h}\int_{I_i} u(x,t)\,dt$$

.

First order (in space) semidiscrete schemes can be obtained using $F_{i+1/2} = F(\bar{u}_i, \bar{u}_{i+1})$ in place of $f(u(x_{i+1/2},t))$:

$$\frac{d\bar{u}_i}{dt} = -\frac{F(\bar{u}_i, \bar{u}_{i+1}) - F(\bar{u}_{i-1}, \bar{u}_i)}{h}.$$

A scheme based on this formula, however, is restricted to first order accuracy.

3.4.1 High Order Finite Volume Discretization

Higher order schemes are obtained by using a piecewise polynomial reconstruction in each cell, and evaluating the numerical flux on the two sides of the interface.

$$\frac{d\bar{u}_i}{dt} = -\frac{F(u^-_{i+1/2}, u^+_{i+1/2}) - F(u^-_{i-1/2}, u^+_{i-1/2})}{h}, \tag{3.9}$$

where $F(u^-, u^+)$ can be, for example, the flux function defining a Godunov scheme $F(u^-, u^+) = f(u^*(u^-, u^+))$, or some other numerical flux function, and the values $u^+_{i+1/2}$, $u^-_{i+1/2}$ are obtained by a suitable reconstruction from cell averages.

A second order scheme constructed by using a piecewise linear reconstruction is obtained as follows. Given $\{u^n_i\}$, compute a piecewise linear reconstruction

$$L(x) = \sum_i L_i(x)\chi_i(x)$$

with $L_i = \bar{u}_i + u'_i(x - x_i)$.

The quantity u'_i is a suitable (first order) approximation of the space derivative of the profile $u(x)$ at x_i.

The numerical approximation of the first derivative is a very important point, since the accuracy and TVD properties of the scheme depend on it. If, for

example, one uses standard central difference, then the reconstructed piecewise linear function will have spurious extrema, and its total variation will be larger that the total variation of the discrete data.

In order to prevent the formation of spurious extrema, the derivative has to be reconstructed by a suitable limiter.

Minmod Flux Limiter

The simplest one is the so called minmod limiter [98], defined as:

$$\text{minmod}\,(a_1, a_2, a_3) = \begin{cases} \text{sgn}(a_1)\min\limits_{i=1}^{3} |a_i|, & \text{if all } a_i \text{ have the same sign,} \\ 0, & \text{otherwise.} \end{cases}$$

For the computation of the reconstruction of the derivative, using the minmod limiter, one writes:

$$u_i' = \text{minmod}\left(\theta\frac{u_{i+1}-u_i}{\Delta x}, \frac{u_{i+1}-u_{i-1}}{2\Delta x}, \theta\frac{u_i-u_{i-1}}{\Delta x}\right), \tag{3.10}$$

where the parameter $\theta \in [1, 2]$ is a smoothness indicator.

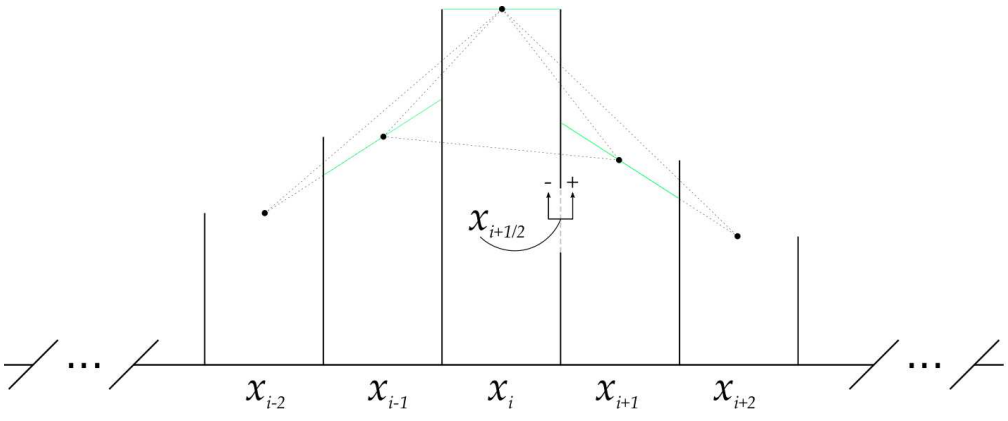

FIGURE 3.1: Reconstruction using the minmod flux limiter with $\theta = 1$ on each cell interface.

3.4.2 Numerical Flux Function

There are many options that one can use for the definition of the numerical flux function. One of the original ideas, concerning the finite volumes schemes, was built from Godunov when he proposed an ingenious way to compute the numerical flux. Godunov defined a Riemann problem at each cell interface $x_{i+1/2}$ and thus the flux function (for scalar cases) is defined as follows:

$$F_{i+1/2} = \begin{cases} \min\limits_{u_i \le w \le u_{i+1}} f(w), & \text{if } u_i^n \le u_{i+1}^n \\ \max\limits_{u_{i+1} \le w \le u_i} f(w), & \text{if } u_i^n > u_{i+1}^n. \end{cases} \tag{3.11}$$

Another option for the numerical flux is the Lax-Friedrichs numerical flux function where:

$$F_{i+1/2} = \frac{1}{2}\left[f\left(u_i^n\right) + f\left(u_{i+1}^n\right)\right] - \frac{\Delta t}{2\Delta x}\left[u_{i+1}^n - u_i^n\right]. \tag{3.12}$$

However the parameter $\frac{\Delta x}{2\Delta t}$ may introduce a large amount of numerical diffusion. For this reason a most sophisticated version of the Lax-Friedrichs flux function is introduced, the so-called local Lax-Friedrichs flux function (also called Rusanov flux), where:

$$F_{i+1/2} = \frac{1}{2}\left[f\left(u_i^n\right) + f\left(u_{i+1}^n\right)\right] - \frac{\alpha_{i+1/2}}{2}\left[u_{i+1}^n - u_i^n\right] \tag{3.13}$$

The choice of the parameter α is crucial for the stability of the scheme and the efficiency. In the classical explicit schemes the parameter is computed as the locally determined maximum value between the cells i and $i+1$ of the wave speeds and is given by:

$$\alpha_{i+1/2} = \max\left(|u_i| + a_i, |u_{i+1}| + a_{i+1}\right), \tag{3.14}$$

where $a = \sqrt{\frac{\gamma p}{\rho}}$ is the sound speed.

Several other numerical flux functions can be obtained by approximate Riemann solvers, such as the Roe solver [98] of the HLL solver [57]. For an account of several approximate solvers and numerical flux functions see, for example, the book by LeVeque [78].

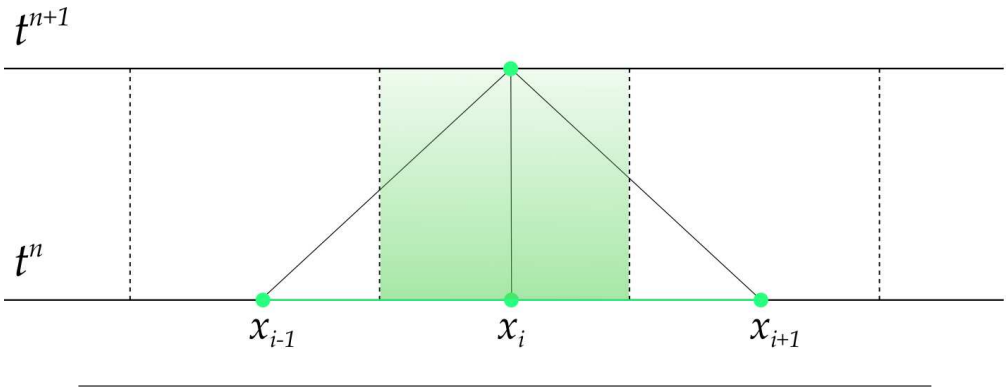

FIGURE 3.2: Integration over a finite volume on a collocated grid.

3.5 Discretization in Time

Here we would like to introduce some well known time discretization techniques.

Now, we want to introduce another family of time integration numerical techniques that we need for the development of the semi-implicit scheme.

For a scalar conservation law:

$$u_t + u_x = 0,$$

we introduce a compact form by assuming a suitable spatial discretization for the derivatives in space:

$$\begin{cases} \dfrac{dU}{dt}(t) = \mathcal{H}\left(U(t)\right), \quad \forall t \geq t_0 \\ U\left(t_0\right) = U_0. \end{cases} \tag{3.15}$$

Here U stands for the discrete approximation of u and $\mathcal{H}$ for the approximation of $-\partial f(u)/\partial x$ achieved by a suitable spatial discretization.

3.5.1 Runge-Kutta Schemes

Once the system of PDE's has been reduced to a system of ODE's, it may be solved numerically by some standard ODE solver, for example, Runge-Kutta.

Apply to the initial value problem (3.15) an explicit Runge-Kutta scheme with s stages:

$$U^{n+1} = U^n + \Delta t \sum_{i=1}^{s} b_i K^{(i)}. \tag{3.16}$$

The $K^{(i)}$ are called Runge-Kutta fluxes and are defined by:

$$K^{(i)} = \mathcal{H}(U^{(i)}) \quad \text{with} \quad U^{(1)} = U^n, \quad i = 1, \cdots, s, \tag{3.17}$$

where the $U^{(i)}$ will be called intermediate values, and, for an explicit scheme, are given by:

$$U^{(i)} = U^n + \Delta t \sum_{j=1}^{i-1} a_{ij} K^{(j)}, \quad i = 1, \cdots, s-1. \tag{3.18}$$

The matrix $A = \left(a_{i,j}\right)$, and the vector b define uniquely the RK scheme. With the present notation, A is a $s \times s$ lower triangular matrix, with zero elements on the diagonal.

SSP Schemes

When constructing numerical schemes for conservation laws, one has to take a great care in order to avoid spurious numerical oscillations arising near discontinuities of the solution. This is avoided by a suitable choice of space discretization and time discretization. Solution of scalar conservation equations, and equations with a dissipative source have some norm that decreases in time. It would be desirable that such property is maintained at a discrete level by the numerical method.

Definition: A sequence $\{U^n\}$ is said to be strongly stable in a given norm $\|\cdot\|$ provided that $\left\|U^{n+1}\right\| \leq \|U^n\|$ for all $n \geq 0$. The most commonly used norms are the TV-norm and the infinity norm. A numerical scheme that maintains strong stability at discrete level is called Strong Stability Preserving (SSP).

Here we review some basic facts about RK-SSP schemes. First, it has been shown [50] under fairly general conditions that high order SSP schemes are necessarily explicit. Second, observe that a generic explicit RK scheme can be written as:

$$
\begin{aligned}
U^{(0)} &= U^n, \\
U^{(i)} &= \sum_{j=0}^{i-1} \left(\alpha_{ij} U^{(j)} + \Delta t \beta_{ij} L(U^{(j)}) \right), \quad i = 1, \ldots, s, \\
U^{n+1} &= U^{(s)},
\end{aligned}
\tag{3.19}
$$

where $\alpha_{ij} \geq 0$ and $\alpha_{ij} = 0$ only if $\beta_{ij} = 0$. This representation of RK schemes (which is not unique) can be converted to a standard Butcher form in a straightforward manner. Observe that for consistency, one has $\sum_{j=0}^{i-1} \alpha_{ij} = 1$. It follows that if the scheme can be written in the form (3.19) with non-negative coefficients $\beta_{i,j}$ then it is a convex combination of Forward Euler steps, with step sizes $\beta_{ij}/\alpha_{ij}\Delta t$. A consequence of this is that if Forward Euler is SSP for $\Delta t \leq \Delta t^*$, then the RK scheme is also SSP for $\Delta t \leq c\Delta t^*$, with $c = \min_{ij} \left(\alpha_{ij}/\beta_{ij} \right)$ [107].

The constant c is a measure of the efficiency of the SSP-RK scheme, therefore for the applications it is important to have c as large as possible. For a detailed description of optimal SSP schemes and their properties see [104].

TVD Runge-Kutta

To achieve higher order accuracy in the discretization in time, one can use Total Variation Diminishing (TVD) Runge-Kutta (RK) methods [108, 107, 78]. These methods guarantee that the total variation of the solution does not increase, i.e. no new extrema are generated. Below we consider 1st order and 2nd order TVD RK.

• 1st order,

The 1st order TVD RK is identical to forward Euler and 1st order RK. It is given by:

$$
\frac{U^{n+1} - U^n}{\Delta t} = \mathcal{H}(U^n) \tag{3.20}
$$

• 2nd order,

The 2nd order TVD RK method is also known as 2nd order RK and Heun's predictor-corrector method.

First, an Euler step is taken to advance the solution to time $t^n + \Delta t$:

$$\frac{U^{(1)} - U^n}{\Delta t} = \mathcal{H}(U^n), \tag{3.21}$$

followed by a second Euler step:

$$\frac{U^{(2)} - U^n}{\Delta t} = \mathcal{H}(U^{(1)}), \tag{3.22}$$

followed by an averaging step:

$$U^{n+1} = \frac{U^{(1)} + U^{(2)}}{2}. \tag{3.23}$$

that takes a convex combination of the initial data and the result of two Euler steps. The final averaging step produces the second order accurate TVD approximation to U at time $t^n + \Delta t$.

Higher order TVD RK schemes there exist but there are beyond the scope of this thesis. For a detailed description we refer the reader to [108, 107, 49]

Projection method

Let us now recall the incompressible Euler equations from Chapter 2. Assuming, without loss of generality, that the density is constant and equal to one, one writes:

$$\begin{aligned} &\mathbf{u}_t + \mathbf{u} \cdot \nabla \mathbf{u} + \nabla p = 0 \\ &\nabla \cdot \mathbf{u} = 0. \end{aligned} \tag{3.24}$$

This system models the flow of an inviscid, incompressible fluid with constant density. The vector-valued function $\mathbf{u}(\mathbf{x}, t)$ is the velocity of the fluid and the scalar-valued function $p(\mathbf{x}, t)$ is the pressure.

Using the standard techniques for the numerical solution of differential equations, one would probably think of (3.24) as some kind of heat equation and try the simplest possible scheme in time, namely an explicit forward step:

$$\frac{\mathbf{u}^{n+1} - \mathbf{u}^n}{\Delta t} = -\mathbf{u}^n \cdot \nabla \mathbf{u}^n - \nabla p^n \tag{3.25}$$

where Δt is the timestep and n denotes the time level. The equation can be trivially solved for u^{n+1}, after having introduced, e.g., finite elements,

finite differences, finite volumes, or spectral methods to discretize the spatial operators.

However, the fundamental problem with this approach is that the new velocity $\mathbf{u}^{n+1}$ does not, in general, satisfy the equation $\nabla \cdot \mathbf{u}^{n+1} \neq 0$. Moreover, there is no natural computation of p^{n+1}.

A possible remedy is to introduce a pressure at p^{n+1}, which leaves two unknowns, $\mathbf{u}^{n+1}$ and p^{n+1}, and hence requires a simultaneous solution of both the incompressible Euler equations:

$$\begin{cases} \dfrac{\mathbf{u}^{n+1} - \mathbf{u}^n}{\Delta t} = -\mathbf{u}^n \cdot \nabla \mathbf{u}^n - \nabla p^{n+1} \\ \nabla \cdot \mathbf{u}^{n+1} = 0. \end{cases} \tag{3.26}$$

More implicitness of the velocity terms can easily be introduced. One can, for example, try a semi-implicit approach, based on a Backward Euler scheme, using an old velocity (as a linearization technique) in the convective term $\mathbf{u} \cdot \nabla \mathbf{u}$.

However, this scheme are highly inefficient since it requires, at each time step, the solution of (3.26) which is coupled system for $\mathbf{u}^{n+1}, p^{n+1}$. This is precisely the reason for proposing the projection method, as a numerical device to decouple the computation of $\mathbf{u}^{n+1}$and p^{n+1} [24].

Instead of simultaneously satisfying the momentum equation and the incompressibility constraint, projection method proceeds by first ignoring the incompressibility constraint, compute an intermediate velocity field $\mathbf{u}^*$ using the momentum equation and then project $\mathbf{u}^*$ back to the space of incompressible vector fields to obtain $\mathbf{u}^{n+1}$and p^{n+1}. The actual realization of this procedure for the first order scheme can be summarized as :

- First we compute an intermediate velocity, $\mathbf{u}^*$, explicitly using the momentum equation by ignoring the pressure gradient term:

$$\frac{\mathbf{u}^* - \mathbf{u}^n}{\Delta t} = -\mathbf{u}^n \cdot \nabla \mathbf{u}^n. \tag{3.27}$$

- In the second half of the algorithm, the projection step, we correct the intermediate velocity to obtain the final solution of the time step $\mathbf{u}^{n+1}$:

$$\begin{cases} \dfrac{\mathbf{u}^{n+1} - \mathbf{u}^*}{\Delta t} = -\mathbf{u}^n \cdot \nabla \mathbf{u}^n - \nabla p^{n+1} \\ \nabla \cdot \mathbf{u}^{n+1} = 0. \end{cases} \tag{3.28}$$

Alternatively a fully implicit approach can be obtained using a backward Euler scheme for (3.24) where the convective term $\mathbf{u} \cdot \nabla \mathbf{u}$ is evaluated as $\mathbf{u}^{n+1} \cdot \nabla \mathbf{u}^{n+1}$, leads to a nonlinear equation in $\mathbf{u}^{n+1}$.

For the moment it is sufficient to describe the aforementioned techniques for treating implicity the stiff terms of the incompressible Euler equations. This technique it is crucial for the derivation of the semi-implicit scheme that we will describe later in Chapter 4.

3.6 Boundary Conditions

Now we introduce the different kind of boundary conditions that we use in order to perform the numerical tests. The method that we are using is the ghost cell method. First we present the transmissive boundary conditions. Such conditions are used in some tests when we have pulses and we want to monitor the acoustic wave and the material wave separately without interaction for a short time. On the other hand, reflective boundary conditions are used when we want to preserve all the quantities since nothing exits the computational domain. In the case of reflective boundary conditions large runtimes can be used and check the results after many interactions between the two types of waves. The same property also exists in the final set of boundary conditions the so-called periodic. These artificial conditions are used only for computational purpose. In these case, whatever exits from the one side of the computational domain enters from the other side and thus all the quantities are preserved. Usually these boundary conditions are used for very long runtimes tests.

Let us now describe the technical details about how to implement such boundary conditions. Assume that the discretization consists by N uniform cells. Because of the use of the collocated grid the values of the solutions are obtained at the cell centers i.e., the numerical solution U_i^n is computed at the center of the cell i which in 1D has coordinates x_i. In order to introduce the boundary conditions at the edges of the grid, we extend the grid from N cells to $N+2$ cells by adding on cell at each edge. These extra cells are called ghost cells and their presence is indispensable for the implementation of the boundary conditions. Defining the values U_1 and U_{N+2} at the ghost cells, we can choose what type of boundary conditions we want to use.

3.6.1 Transmissive Boundary Conditions

Assume that U is the vector of the numerical solution of the Euler equations in 1D, where $U = (\rho, m, E)^T$. In the case of transmissive boundary conditions the values at the ghost cells are the following:

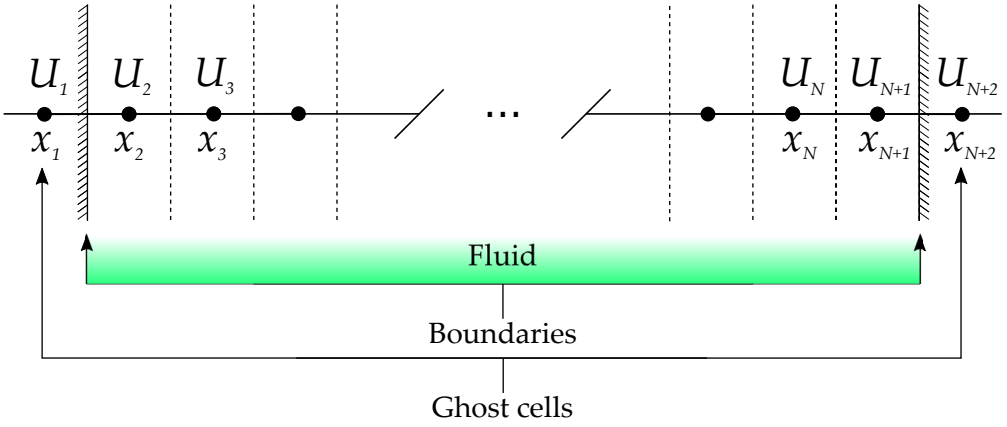

FIGURE 3.3: Grid setup.

$$U_1 = U_2 \Leftrightarrow \begin{pmatrix} \rho_1 \\ m_1 \\ E_1 \end{pmatrix} = \begin{pmatrix} \rho_2 \\ m_2 \\ E_2 \end{pmatrix}, \tag{3.29}$$

$$U_{N+2} = U_{N+1} \Leftrightarrow \begin{pmatrix} \rho_{N+2} \\ m_{N+2} \\ E_{N+2} \end{pmatrix} = \begin{pmatrix} \rho_{N+1} \\ m_{N+1} \\ E_{N+1} \end{pmatrix}. \tag{3.30}$$

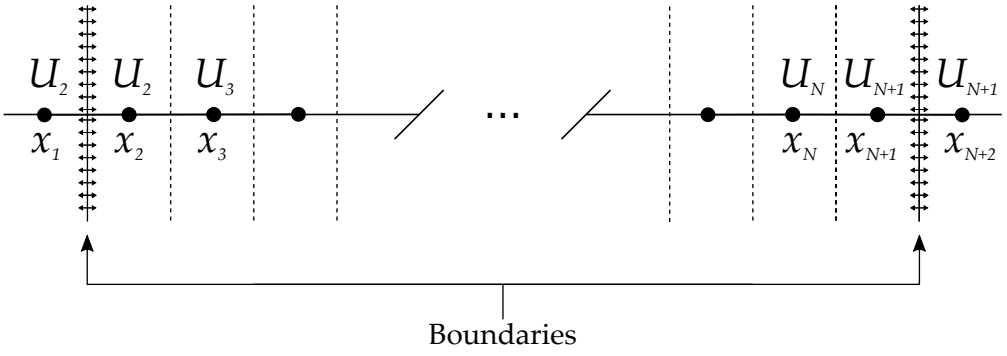

FIGURE 3.4: Transmissive boundary conditions.

3.6.2 Reflective Boundary Conditions

Using the same notation as before, we introduce the reflective boundary conditions or wall boundary conditions. In this case the ghost cell values are computed as the transmissive boundary conditions case with the exception

of the momentum quantity which receives the neighbor value but with minus sing, i.e.:

$$\begin{pmatrix} \rho_1 \\ m_1 \\ E_1 \end{pmatrix} = \begin{pmatrix} \rho_2 \\ -m_2 \\ E_2 \end{pmatrix}, \quad \begin{pmatrix} \rho_{N+2} \\ m_{N+2} \\ E_{N+2} \end{pmatrix} = \begin{pmatrix} \rho_{N+1} \\ -m_{N+1} \\ E_{N+1} \end{pmatrix}. \tag{3.31}$$

3.6.3 Periodic Boundary Conditions

Finally we may use periodic boundary conditions for sake of simplicity in some tests. In some cases when we want to check the stability of the scheme by using stationary solutions we use periodic boundary conditions. The implementation is straightforward where by using the same notation one writes:

$$U_1 = U_{N+1} \Leftrightarrow \begin{pmatrix} \rho_1 \\ m_1 \\ E_1 \end{pmatrix} = \begin{pmatrix} \rho_{N+1} \\ m_{N+1} \\ E_{N+1} \end{pmatrix}, \tag{3.32}$$

$$U_{N+2} = U_2 \Leftrightarrow \begin{pmatrix} \rho_{N+2} \\ m_{N+2} \\ E_{N+2} \end{pmatrix} = \begin{pmatrix} \rho_2 \\ m_2 \\ E_2 \end{pmatrix}. \tag{3.33}$$

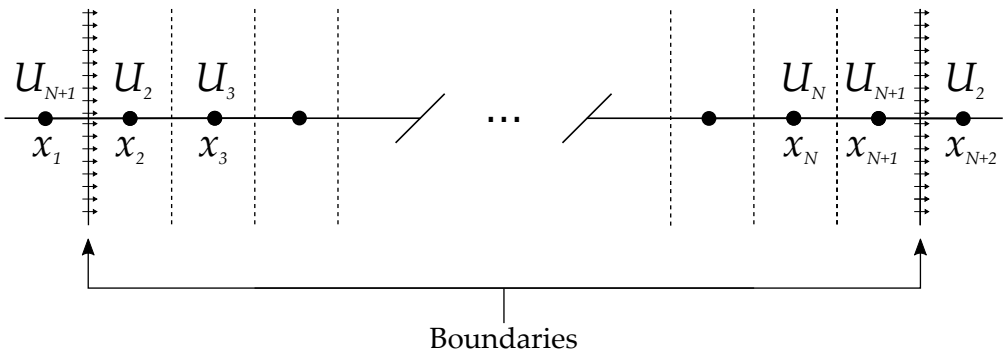

FIGURE 3.5: Periodic boundary conditions.

Chapter 4

Semi-Implicit Scheme for 1D Euler Equations

Numerical methods for the solution of hyperbolic systems of conservation laws has been a very active field of research in the last decades. Several very effective schemes are nowadays treated in textbooks which became a classic on the topic [78, 114, 48]. Because of the hyperbolic nature, all such systems develop waves that propagate at finite speeds. If one wants to accurately compute all the waves in a hyperbolic system, then one has to resolve all the space and time scales of the system. Most schemes devoted to the numerical solution of such systems are obtained by explicit time discretization, and the time step has to satisfy a stability condition, known as CFL condition. Usually such a restriction is not a problem: because of the hyperbolic nature of the system, if the order of accuracy is the same in space and time, accuracy restriction and stability restrictions are almost the same, and the system is not stiff. There are, however, cases in which some of the waves are not particularly relevant and one is not interested in resolving them. Let us consider as a prototype model the classical Euler equations of compressible gas dynamics. In the low Mach number regimes, it may happen that the acoustic waves carry a negligible amount of energy, and one is mainly interested in accurately capturing the motion of the fluid. In this chapter we propose propose a simple second order accurate scheme for the numerical solution of Euler equation of gas dynamics that are (linearly) implicit in the acoustic waves, eliminating the acoustic CFL restriction on the time step. The general idea is that explicit differential operators in space relative to convective or material speeds are discretized by local Lax-Friedrics fluxes and the linear implicit operators, pertaining to acoustic waves, are discretized by central differences. First we present the first order scheme in space and time. We adopt a collocated grid for the spatial discretization which is more common in finite volumes for compressible flows. The choice of this grid also reduces the implementation complexity, specifically in modern distributed memory

machine architectures.

Let us now introduce the Euler equations in one dimension which come from the equations derived in Chapter 2:

$$\begin{cases} \dfrac{\partial \rho}{\partial t} + \dfrac{\partial m}{\partial x} = 0, \\ \dfrac{\partial m}{\partial t} + \dfrac{\partial}{\partial x}(mu + p) = 0, \\ \dfrac{\partial E}{\partial t} + \dfrac{\partial}{\partial x}(hm) = 0. \end{cases} \tag{4.1}$$

The equation of state for a perfect gas stands for:

$$E = \frac{1}{2}\rho \mathbf{u}^2 + \frac{p}{\gamma - 1}. \tag{4.2}$$

Here, we use this equation of state in order to derive our scheme, but the scheme can be easily adapted to a more general equation of state. It's straightforward that we can use, with minor changes, any equation of state where the energy and the pressure terms are linearly correlated but also more general equations of state.

The idea of the proposed scheme is to treat with two different ways the waves of the system. More specifically, we choose to treat the acoustic waves implicitly, while the material waves explicitly. The terms that describe material waves will be with some sort of an upwind discretization in space while the terms which are responsible for the acoustic waves will be discretized in space with central difference.

The System of equations (4.1) has the structure of a quasi linear hyperbolic system of conservation laws and it can be written in the following form:

$$\frac{\partial W}{\partial t} = -\frac{\partial \mathcal{F}(W)}{\partial x}, \tag{4.3}$$

where $W = (\rho, m, E)^T$ and $\mathcal{F} = (m, mu + p, hm)$.

Now we can rewrite the system in a compact form, assuming that we approximate the spatial derivatives that appear in the system by suitable discrete operators, as follows:

$$\begin{cases} \dfrac{dU}{dt}(t) = \mathcal{H}\left(U_E(t), U_I(t)\right), \quad \forall t \geq t_0 \\ U\left(t_0\right) = U_0. \end{cases} \tag{4.4}$$

We denote by U the discrete approximation of W which can be splitted into two parts. The first part is the non-stiff part which is correlated with the material waves and thus we treat it with an explicit way, so-called U_E. The second part is the stiff one corresponding with the acoustic waves, so we choose to treat these terms implicitly and we name them U_I. Finally, $\mathcal{H}$ denotes the the approximation of the right hand side of Equation (4.3) which is going to be described in detail later.

4.1 1st Order Discretization in Time

In order to obtain a first order scheme, first we have to discretize the governing equations in time. To achieve this we discretize the time derivative of (4.4) using backward differences over a time step Δt, thus the first-order accurate temporal discretization is given by:

$$\frac{U^{n+1} - U^n}{\Delta t} = \mathcal{H}\left(U^n, U^{n+1}\right), \tag{4.5}$$

where $n+1$ denotes the value at the next time step $t + \Delta t$. Now we have to describe the spatial discretization of the term $\mathcal{H}\left(U^n, U^{n+1}\right)$.

4.2 1st Order Discretization in Space

Let us now present the semi-implicit scheme derived from the implicit treatment of the pressure term in the momentum equation. Combining the semi-discrete form of Equation (4.5) and the System of equations (4.1) we have the fully discrete form of the numerical scheme.

We discretize the System (4.1) at a time interval $[t_n, t_{n+1}]$:

$$\begin{cases} \rho^{n+1} = \rho^n - \Delta t \hat{D}_x\left(m^n\right), & \text{(4.6a)} \\ m^{n+1} = m^n - \Delta t \hat{D}_x\left(m^n u^n\right) - \Delta t D_x(p^{n+1}), & \text{(4.6b)} \\ E^{n+1} = E^n - \Delta t D_x(h^n m^{n+1}), & \text{(4.6c)} \end{cases}$$

where with $\hat{D}_x$ we denote the upwind discrete derivative given by

$$\hat{D}_x(F_i) = \frac{F_{i+1/2} - F_{i-1/2}}{\Delta x}. \tag{4.7}$$

Here we choose to use the local Lax-Friedrichs flux function (for more details see Section 3.4) for the finite volume derivatives, where:

$$F_{i+1/2} = \frac{1}{2}\left[\mathcal{F}\left(U_i^n\right) + \mathcal{F}\left(U_{i+1}^n\right)\right] - \frac{\alpha_{i+1/2}}{2}\left[U_{i+1}^n - U_i^n\right] \tag{4.8}$$

In classical explicit schemes it is a bound on the maximum wave speeds, and is given by

$$\alpha_{j+1/2} = \max(|u_j| + a_j, |u_{j+1}| + a_{j+1}),$$

where $a^2 = \gamma p/\rho$ denotes the square of the sound speed. In our case, since the acoustic waves are treated implicitly, we use α proportional to the material speed. We expect that for very low Mach number, $\alpha \approx |u|$ should be sufficient, while for Mach number larger than one, the speed of sound is bounded by the fluid speed. For this reason, we choose

$$\alpha_{j+1/2} = \max(|u_j|, |u_{j+1}|), \tag{4.9}$$

On the other hand, D_x will be computed with a centred scheme:

$$D_x(F_i) = \frac{\mathcal{F}(U_{i+1/2}) - \mathcal{F}(U_{i-1/2})}{\Delta x}. \tag{4.10}$$

In practice, $\mathcal{F}^j(U_{i-1/2})$ will be approximated by $(\mathcal{F}^j(U_{i-1}) + \mathcal{F}^j(U_i))/2$, therefore Equation (4.10) becomes the classical centred approximation of the first derivative.

4.3 Pressure Splitting

Let us now recall the discretization of the Euler equations, i.e. System (4.6). This technique was originally proposed in our recent published paper [5]. In order to substitute the pressure term p^{n+1} in Equation (4.6b), we recall the Equation of state for a perfect gas in one dimension:

$$p^{n+1} = (\gamma - 1)\left(E^{n+1} - \frac{m^n u^n}{2}\right). \tag{4.11}$$

We choose to treat implicitly the Energy term while the kinetic energy part of the equation of state is computed explicitly.

Plugging Equation (4.11) into Equation (4.6b) we obtain:

$$m^{n+1} = \underbrace{m^n - \left(\frac{3-\gamma}{2}\right)\Delta t \hat{D}_x\left(m^n u^n\right)}_{m^*} - (\gamma-1)\Delta t D_x(E^{n+1}), \tag{4.12}$$

where we denote with m^* the terms that are treated explicitly.

Substituting the term m^{n+1} by using the Equation (4.12) on the Equation (4.6c) one gets:

$$E^{n+1} = \underbrace{E^n - \Delta t \hat{D}_x\left(h^n m^*\right)}_{E^*} + (\gamma-1)\Delta t^2 D_x\left(h^n D_x\left(E^{n+1}\right)\right), \tag{4.13}$$

where with E^* we denote the explicit part which is also the right hand side of the linear system whose the solution gives the energy at the new time $n+1$.

On a cell i of a collocated grid, one can write the fully discrete expression which occurs from the Equation (4.13) as follows:

$$E_i^{n+1} = E_i^* + (\gamma-1)\frac{\Delta t^2}{\Delta x^2}\left(h_{i+1/2}^n\left(E_{i+1}^{n+1} - E_i^{n+1}\right) - h_{i-1/2}^n\left(E_i^{n+1} - E_{i-1}^{n+1}\right)\right) \tag{4.14}$$

Writing the Equation (4.14) in the form of a linear system of equations one gets:

$$E_{i-1}^{n+1}(-ch_{i-1/2}) + E_i^{n+1}(1 + c(h_{i-1/2} + h_{i+1/2})) + E_{i+1}^{n+1}(-ch_{i+1/2}) = E_i^*, \tag{4.15}$$

where the parameter $c = (\gamma-1)\Delta t^2/\Delta x^2$, under the assumption that the grid is uniform. This is a tridiagonal sparse linear system of equations (see Figure 4.1) that can be solved in order to obtain the solution. The literature concerning the solution of such systems is very rich and one can find plethora of methods (iterative methods, direct solvers etc.).

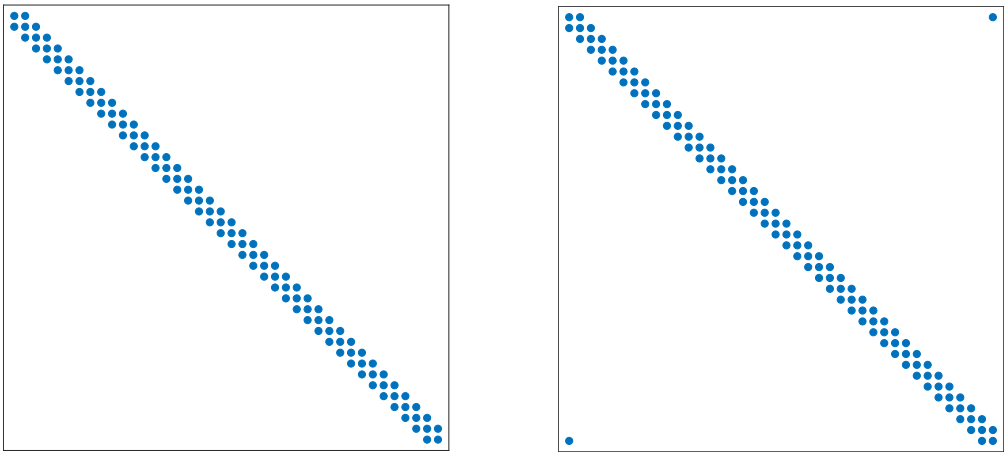

(a) Reflective BC. (b) Periodic BC.

FIGURE 4.1: Sparsity pattern of the matrix that occurs from the implicit terms at the energy equation.

4.4 Extension to Second Order

In order to derive second order accurate scheme we use for the finite volume approximations, namely $\hat{D}_x$, the MUSCL scheme equipped with the θ-minmod limiter which are described in detain in Section 3.4. For the centred derivatives, in order to obtain a second order accurate in space derivative, we use the following approximation:

$$D_x\left(D_x(\mathcal{F}(U_i))\right) = \frac{\mathcal{F}\left(U_{i+1}\right) - 2\mathcal{F}\left(U_i\right) + \mathcal{F}\left(U_{i-1}\right)}{\Delta x^2}. \tag{4.16}$$

Finally for the time derivatives we use the implicit-explicit Runge-Kutta method which is described below in Subsection 4.4.1.

This combination of the conservative linear reconstruction technique and the implicit-explicit Runge-Kutta scheme is expandable to higher order (for the case of Euler equations of isentropic gas dynamics see [19]). By using a higher order non-oscillatory reconstruction for the finite volume derivatives and higher order central space discretization for the stiff terms combined with an appropriate Runge-Kutta scheme one can achieve higher order semi-implicit schemes.

4.4.1 2nd Order Discretization in Time

Until now the proposed schemes are second order accurate in space but still first order accurate in time. In order to achieve second order of accuracy also

in the time domain, we use an implicit-explicit Runge-Kutta method which was originally proposed in [11].

After the system is discretized in space with the aforementioned technique, we can write it as a set of ordinary differential equations for a vector $U(t) \in \mathbb{R}^{Nm}$, where N is the number of cells for the space discretization and m the numbers of equations. With the objective to solve this system of ODE's we use an implicit-explicit Runge-Kutta scheme. An s-stage implicit-explicit Runge-Kutta method can be represented, by adopting the usual notation, with the following double Butcher tableaux:

$$\begin{array}{c|c} \hat{c} & \hat{A} \\ \hline & \hat{b}^\top \end{array} \qquad \begin{array}{c|c} c & A \\ \hline & b^\top \end{array}, \tag{4.17}$$

where $\hat{A}$, $A \in \mathcal{M}_{s,s}(\mathbb{R})$ and the coefficients $\hat{c}$, c, $\hat{b}$, $b \in \mathbb{R}^s$. In the case of non-autonomous systems the coefficients $\hat{c}$ and c are related with the matrices $\hat{A}$ and A as follows:

$$\hat{c}_i = \sum_j \hat{a}_{ij}, \quad c_i = \sum_j a_{ij} \tag{4.18}$$

where i and j are the row and the column indices respectively.

Let us now describe in detail the Butcher tableaux we are using in order to obtain second order accuracy in time. The matrices $\hat{A}$ and A are lower triangular and specifically the matrix $\hat{A}$ has all the diagonal elements equal to zero. Moreover, in this particular IMEX-RK scheme we have $\hat{b} = b$. Thus, the detailed form of the tableaux is:

$$\begin{array}{c|cc} 0 & 0 & 0 \\ \hat{c} & \hat{c} & 0 \\ \hline & 1-\beta & \beta \end{array} \qquad \begin{array}{c|cc} \beta & \beta & 0 \\ 1 & 1-\beta & \beta \\ \hline & 1-\beta & \beta \end{array}, \tag{4.19}$$

where we choose $\beta = 1 - 1/\sqrt{2}$ which is value is the root of the polynomial $\beta^2 - 2\beta + 1/2 = 0$ and $\hat{c} = 1/(2\beta)$. This IMEX-RK method is a combination of a second order Runge-Kutta method, for the explicit part, and an L-stable second order singly diagonal stiffly accurate Runge-Kutta method (SDIRK) for the implicit part, and the combination is called LSDIRK2.

Let us now describe the algorithm that is the outcome of the proposed Runge-Kutta method. Assume that the numerical solution U^n is known at the

timestep n and we want to compute the numerical solution U^{n+1} at the timestep $n+1$. First we have to compute the stage values:

$$U_E^{(i)} = U^n + \Delta t \sum_{j=1}^{i-1} \hat{a}_{ij} \mathcal{H}\left(U_E^{(j)}, U_I^{(j)}\right), \tag{4.20}$$

$$U_I^{(i)} = U_*^{(i)} + (\Delta t) a_{ii} \mathcal{H}\left(U_E^{(i)}, U_I^{(i)}\right), \tag{4.21}$$

where $i = 1 \ldots s$. We denote by $U_*^{(i)}$, at each stage i, the following:

$$U_*^{(i)} = U^n + \Delta t \sum_{j=1}^{i-1} a_{ij} \mathcal{H}\left(U_E^{(j)}, U_I^{(j)}\right). \tag{4.22}$$

There is a major advantage concerning the proposed scheme. The only step that requires implicit calculation is at the Equation (4.21) in order to compute the value of $U_I^{(i)}$. After the aforementioned evaluations the solution at the new timestep $n+1$ is computed as follows:

$$U^{n+1} = U^n + \Delta t \sum_{j=1}^{s} b_i \mathcal{H}\left(U_E^{(i)}, U_I^{(i)}\right). \tag{4.23}$$

In order to simplify the implementation procedure we can rewrite the calculations needed at the Runge-Kutta method steps as follows. We define:

$$U_I = \mathcal{S}\left(U_*, U_E, \Delta t\right), \tag{4.24}$$

where S is the function (solver) which returns the first order in time solution of the following problem:

$$U_I = U_* + \Delta t \mathcal{H}\left(U_E, U_I\right). \tag{4.25}$$

Using this notation the two-step ($s = 2$) method can be summarized in the following equations:

$$U_I^{(1)} = \mathcal{S}(U^n, U^n, \beta\Delta t), \tag{4.26}$$

$$U_E^{(2)} = \left(1 - \frac{\hat{c}}{\beta}\right) U^n + \frac{\hat{c}}{\beta} U_I^{(1)}, \tag{4.27}$$

$$U_*^{(2)} = \frac{2\beta - 1}{\beta} U^n + \frac{1 - \beta}{\beta} U_I^{(1)}, \tag{4.28}$$

$$U_I^{(2)} = \mathcal{S}(U_*^{(2)}, U_E^{(2)}, \beta\Delta t). \tag{4.29}$$

Finally we obtain the second order in time and space solution at the new timestep $n+1$ where $U^{n+1} = U_I^{(2)}$.

Chapter 5

Numerical Tests for 1D Euler Equations

In this chapter we perform multiple tests but first we have to introduce some useful numbers. The Mach number stands for $M = u_0/c_0$ where u_0 is the fluid typical velocity and a the typical speed of sound in the medium:

$$a = \sqrt{\frac{\gamma p}{\rho}}. \tag{5.1}$$

The typical CFL number or acoustic CFL number creates a condition which states that the time step should be limited by the space step divided by the fastest wave speed. Thus the timestep Δt is defined:

$$\Delta t = CFL \frac{\Delta x}{\max |u| + a} \tag{5.2}$$

For classical schemes the classical CFL restriction states that the CFL number is less than one. In the case of the semi-implicit scheme we can overpass this restriction. The only condition that we have to obey is that the material CFL number must be less than one. The timestep Δt by using the material CFL number is defined as follows:

$$\Delta t = \mathrm{CFL}_{\mathrm{IM}} \frac{\Delta x}{\max |u|} \tag{5.3}$$

First, we run the classical tests of Sod shock tube and Lax shock tube in order to verify the shock capturing ability of the proposed scheme for intermediate values of Mach numbers. The use of CFL numbers bigger than one for these test is forbidden and this is not the scope of these runs. The purpose of the

shock tests is to check our scheme in terms of robustness and stability in classical cases which are well known from the literature.

Afterwards, we present a test case with a stronger shock in order to check the robustness of the semi-implicit scheme. Again, the acoustic CFL condition is obeyed due to the fact of the presence of a shock.

Then we run a test with two colliding acoustic pulses in order to check the capability of the scheme to filtering out the acoustic waves. Bu using the classical definition of Courant number where CFL $= (\Delta t \max(|u| + a))/\Delta x$ we show that the proposed scheme for small CFL numbers captures the acoustic waves, while using greater than one CFL numbers it filters them out.

Another test with material and acoustic waves is presented. In this test we manipulate two waves, an acoustic pulse and a material wave, and we compare the results with variable CFL numbers in order to show how one can benefit form this scheme if is not interested in the acoustic waves.

5.1 Sod Shock Tube

This is a classical shock tube test where the domain is $[0, 1]$ and is discretized with 100 equal cells. The final time for this test is $T = 0.168$. Initially the discontinuity is placed at $x = 0.5$ with the initial conditions at the left and the right respectively:

$$\begin{pmatrix} \rho \\ u \\ p \end{pmatrix}_L = \begin{pmatrix} 1 \\ 0 \\ 1 \end{pmatrix}, \qquad \begin{pmatrix} \rho \\ u \\ p \end{pmatrix}_R = \begin{pmatrix} 0.125 \\ 0 \\ 0.1 \end{pmatrix}.$$

We compare our semi-implicit scheme with an explicit scheme equipped with local Lax-Friedrichs flux. The Mach number for this test is $M \simeq 1$. In Figure 5.1 we compare the density profiles for first and second order accurate schemes. We observe, as in velocity plot (see Figure 5.2) and pressure plot (see Figure 5.3), that the two solutions are almost indistinguishable.

In this test the results are obtained, in both cases (explicit and semi-implicit), with CFL $= 0.5$. We perform a series of classical tests in order to check the scheme for robustness even if we don't gain any performance improvement, in term of acceleration of the computations by using bigger CFL numbers.

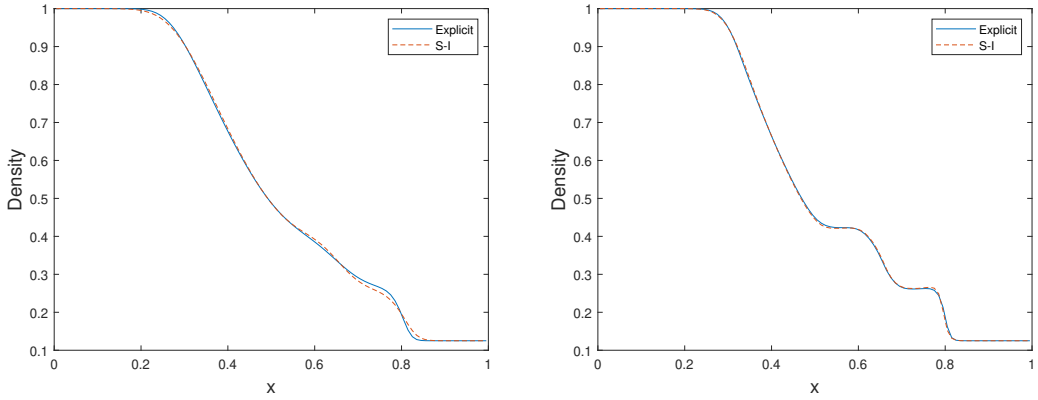

(a) First Order. (b) Second Order.

FIGURE 5.1: Density profiles for Sod shock tube test at the final time $t = 0.168$, with $N = 100$ and CFL $= 0.5$ for explicit and semi-implicit.

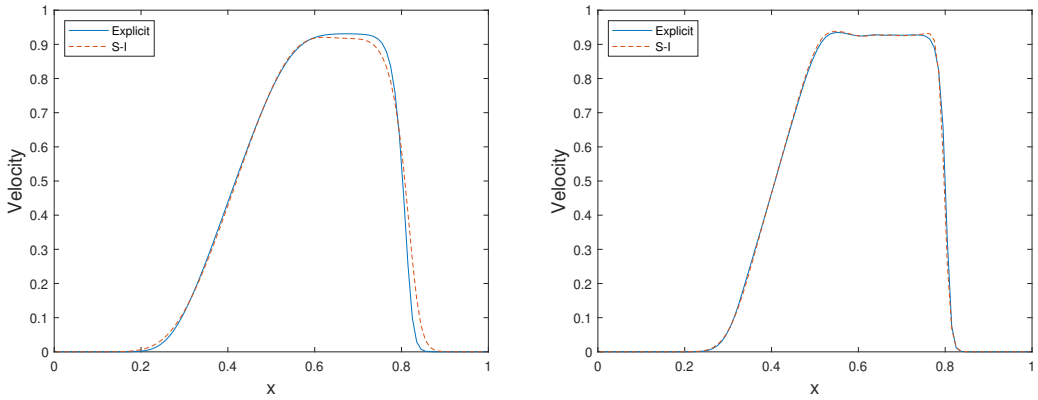

(a) First Order. (b) Second Order.

FIGURE 5.2: Velocity profiles for Sod shock tube test at the final time $t = 0.168$, with $N = 100$ and CFL $= 0.5$ for explicit and semi-implicit.

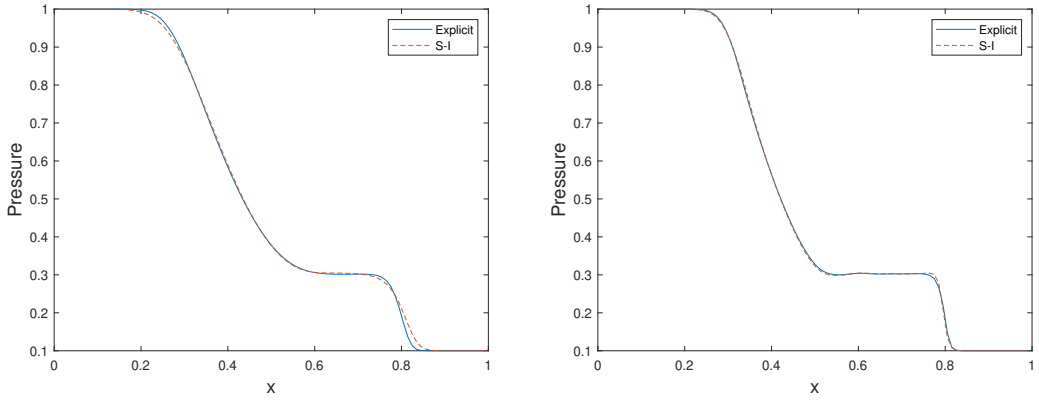

(a) First Order.

(b) Second Order.

FIGURE 5.3: Pressure profiles for Sod shock tube test at the final time $t = 0.168$, with $N = 100$ and CFL $= 0.5$ for explicit and semi-implicit.

5.2 Lax Shock Tube

Now we perform another classical well known numerical test. The initial conditions are defined by using the Sod shock tube notation where initially the discontinuity is place at $x = 0.5$ and the corresponding initials conditions to the left and the right are given:

$$\begin{pmatrix} \rho \\ u \\ p \end{pmatrix}_L = \begin{pmatrix} 0.445 \\ 0.6989 \\ 3.5277 \end{pmatrix}, \qquad \begin{pmatrix} \rho \\ u \\ p \end{pmatrix}_R = \begin{pmatrix} 0.5 \\ 0 \\ 0.5710 \end{pmatrix}.$$

The domain here is $[0, 1]$ and now we discretize with a uniform grid that consists of 200 cells. It's a test same as the Sod shock tube but with a stronger shock while the Mach numbers remain at same order $M \simeq 1$. Here we use CFL $= 0.5$ and again are not seeking for better performance by using greater than one CFL numbers, but we just want to compare our semi-implicit scheme results with well known from the literature examples.

The difference in the computation time between the two run tests (explicit and semi-implicit) is negligible due to the fact that the size of the system that the semi-implicit scheme requires to solve is very small. Thus, even with the same CFL numbers, if we are comparing the explicit with semi-implicit scheme using small discretizations, the computation time is roughly the same.

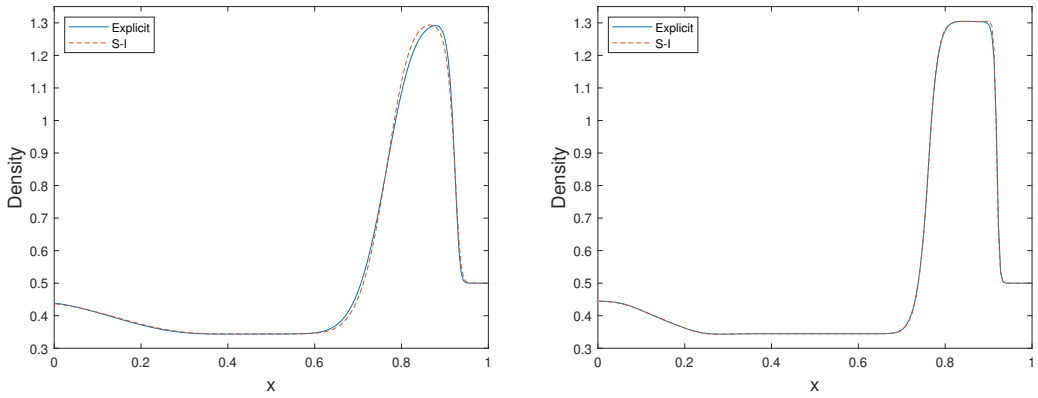

(a) First Order. (b) Second Order.

FIGURE 5.4: Density profiles for Lax shock tube test at the final time $t = 0.168$, with $N = 200$ and CFL $= 0.5$ for explicit and semi-implicit.

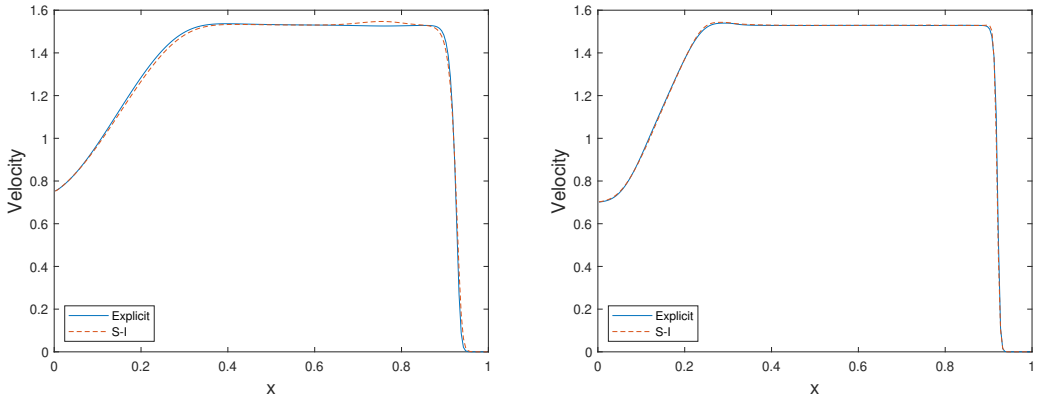

(a) First Order. (b) Second Order.

FIGURE 5.5: Velocity profiles for Lax shock tube test at the final time $t = 0.168$, with $N = 200$ and CFL $= 0.5$ for explicit and semi-implicit.

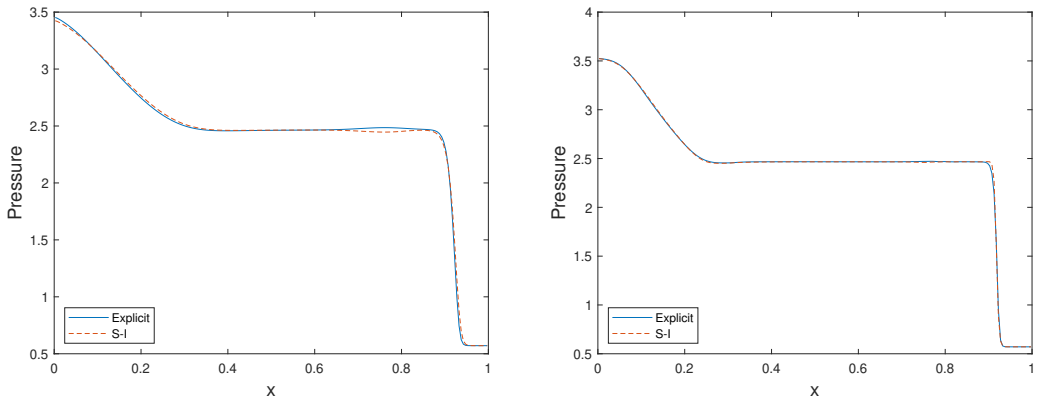

(a) First Order. (b) Second Order.

FIGURE 5.6: Pressure profiles for Lax shock tube test at the final time $t = 0.168$, with $N = 200$ and CFL $= 0.5$ for explicit and semi-implicit.

5.3 High Mach Tube

Let us now perform an extreme test in order to check the robustness of the scheme. In this case we initialize the tube with the discontinuity placed at $x = 0.5$ on the domain $[0, 1]$ and the following initial conditions to the left and the right respectively:

$$\begin{pmatrix} \rho \\ u \\ p \end{pmatrix}_L = \begin{pmatrix} 10 \\ 2000 \\ 500 \end{pmatrix}, \qquad \begin{pmatrix} \rho \\ u \\ p \end{pmatrix}_R = \begin{pmatrix} 20 \\ 0 \\ 500 \end{pmatrix}.$$

We run this test with $CFL = 0.5$ on a uniform grid with 200 cells, for both schemes , explicit and semi-implicit, and the final time is $T = 1.75\text{e-}4$.

We observe a good agreement between the explicit and semi-implicit solutions. A better resolution is obtained by the semi-implicit scheme specifically in the density profile (See Figure 5.7a).

5.4 Acoustic Pulses

This test case is adopted from [32]. With this test we want to check the ability of the proposed scheme, in low Mach regimes, to filter out the acoustic waves when a material CFL condition is adopted rather than an acoustic.

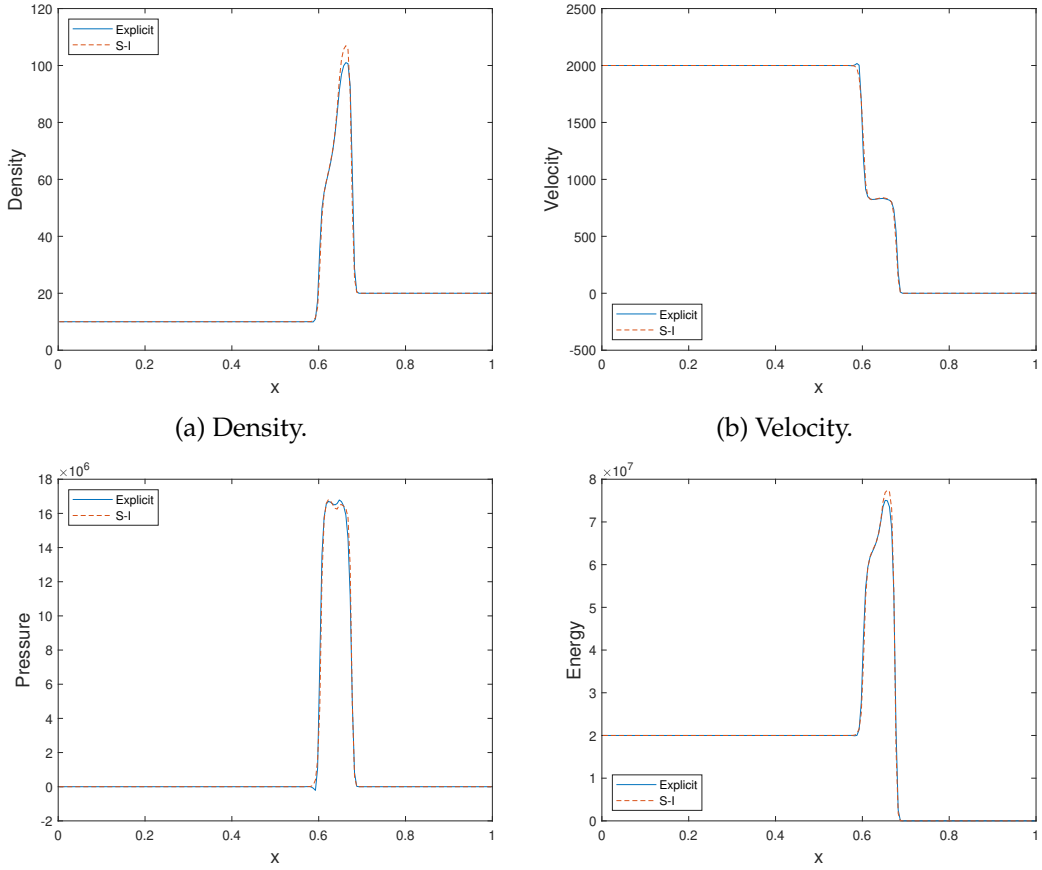

(a) Density.

(b) Velocity.

(c) Pressure.

(d) Energy.

FIGURE 5.7: Second order density and velocity profiles for High Mach tube test at $t = 1.75\text{e-}4$, with $N = 200$ and CFL $= 0.5$ for explicit and semi-implicit.

In order to initialize this test we have to use a rescaled version of the equations. To do that we introduce the parameter ϵ which stands for the ratio between the fluid velocity and the thermal speed:

$$\epsilon = \frac{u_0}{\sqrt{p_0/\rho_0}} = M\sqrt{\gamma} \tag{5.4}$$

We rewrite the System of equation (2.32) by using the rescaling parameter ϵ and we obtain:

$$\begin{cases} \dfrac{\partial \rho}{\partial t} + \dfrac{\partial m}{\partial x} = 0, \\ \dfrac{\partial m}{\partial t} + \dfrac{\partial}{\partial x}(mu) + \dfrac{1}{\epsilon^2}\dfrac{\partial p}{\partial x} = 0, \\ \dfrac{\partial E}{\partial t} + \dfrac{\partial}{\partial x}(hm) = 0. \end{cases} \tag{5.5}$$

The system is closed with the equation of state where also the rescaling parameter ϵ appears, where:

$$E = \frac{\epsilon^2}{2}\rho u^2 + \frac{p}{\gamma - 1}. \tag{5.6}$$

We choose to use the parameter ϵ instead of the Mach number in order to present the same numerical test with same notation as in the literature.

The length of the domain for this test is L. It depend on the parameter ϵ and it is symmetrically split $-L/2 = -1/\epsilon$ and $L/2 = 1/\epsilon$. Using the aforementioned notation, the initial conditions are:

$$\begin{aligned} &\rho_0 = 0.955, \qquad \rho_1 = 2, \qquad \rho = \rho_0 + 0.5\rho_1\epsilon\left(1 - \cos\frac{2\pi x}{L}\right), \\ &u_0 = 2\sqrt{\gamma}, \qquad\qquad\quad u = -0.5\,\mathrm{sgn}(x)u_0\left(1 - \cos\frac{2\pi x}{L}\right), \\ &p_0 = 1, \qquad\quad p_1 = 2 \qquad p = p_0 + 0.5p_1\epsilon\left(1 - \cos\frac{2\pi x}{L}\right). \end{aligned}$$

We run this test with second order accurate schemes, using two values of the parameter ϵ in order to present two regimes of Mach numbers and we adopt acoustic CFL numbers notation.

5.4.1 $\epsilon = 1/11$

Here we choose $\epsilon = 1/11$ and we plot the pressure profiles with two different CFL numbers. We compare an explicit solution, equipped with the Lax–Friedrichs flux, obtained with 1600 cells, with the semi-implicit scheme solution obtained with 400 cells.

We observe on Figure 5.8 that for CFL$=$ 0.5 the two solutions are indistinguishable for the intermediate and the final time of the test.

Similar result we obtain on Figure 5.9 where we adopt an acoustic CFL number equal to 4 for the semi-implicit scheme which corresponds to material CFL equal to 0.7 As expected, for intermediate values of Mach numbers the solution is well captured even if the classical acoustic CFL condition is overpassed.

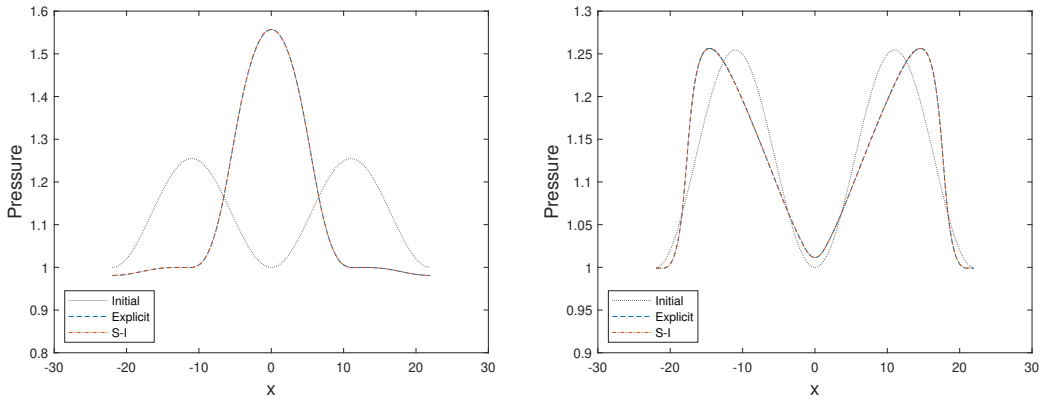

(a) Pressure at $t = 0.815$.

(b) Pressure at $t = 1.63$.

FIGURE 5.8: Pressure profiles with $\epsilon = 1/11$ and CFL$=$ 0.5 for both schemes, with $N = 400$ for the semi-implicit scheme and $N = 1600$ for the explicit scheme.

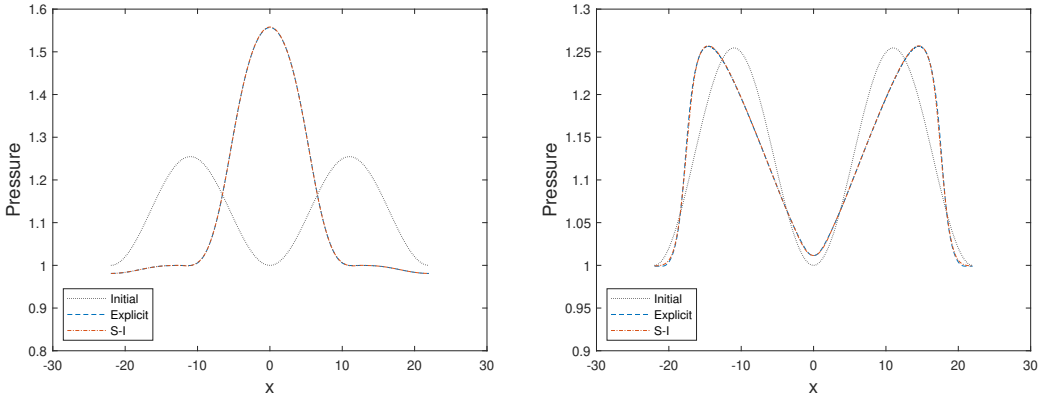

(a) Pressure at $t = 0.815$.

(b) Pressure at $t = 1.63$.

FIGURE 5.9: Pressure profiles with $\epsilon = 1/11$, CFL$= 0.5$ and $N = 1600$ for the explicit scheme and CFL$= 4$ for the semi-implicit scheme with $N = 400$.

5.4.2 $\epsilon = 1/1000$

Here, we run the same test but in the low-Mach regime. We compare the same solution as before and we observe that if we obey the acoustic CFL restriction for the semi-implicit scheme (CFL=0.5), the solution is well captured (see Figure 5.10).

On the other hand if we use an acoustic CFL number equal to 100 for the semi-implicit scheme, we expect that the acoustic waves will be filtered out which is the result that we obtain in Figure 5.11.

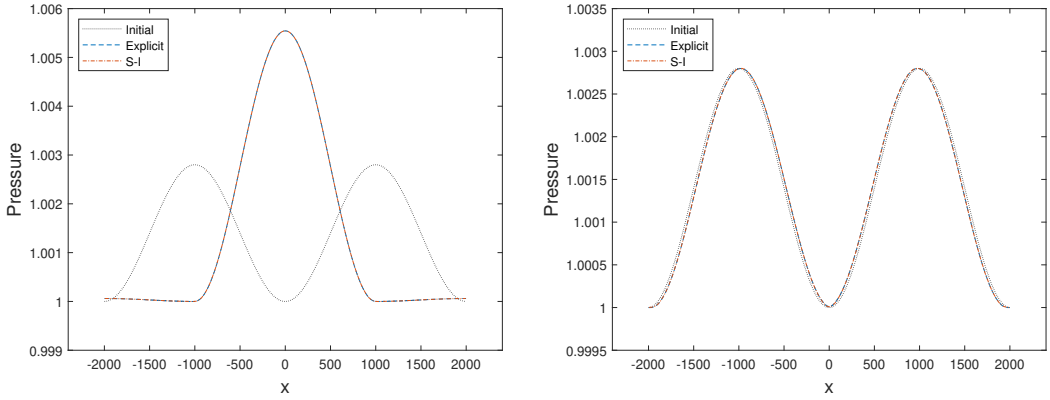

(a) Pressure at $t = 0.815$. (b) Pressure at $t = 1.63$.

FIGURE 5.10: Pressure profiles with $\epsilon = 1/1000$ and CFL= 0.5 for both schemes, with $N = 400$ for the semi-implicit scheme and $N = 1600$ for the explicit scheme.

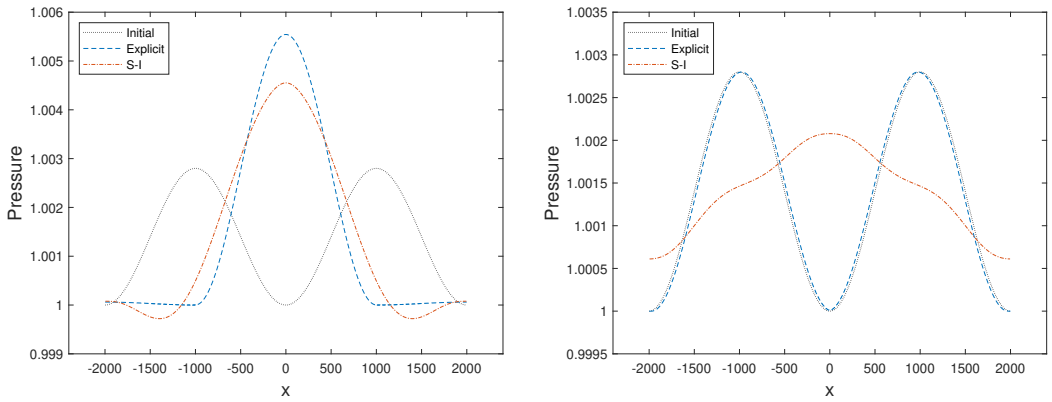

(a) Pressure at $t = 0.815$. (b) Pressure at $t = 1.63$.

FIGURE 5.11: Pressure profiles with $\epsilon = 1/1000$, CFL= 0.5 and $N = 1600$ for the explicit scheme and CFL= 100 for the semi-implicit scheme with $N = 400$.

5.5 Material and Acoustic Waves

This test is proposed in order to prove that the scheme captures the material waves very accurately even if we use large CFL numbers. If one is interested only in the material waves we observe that it is better to use a large CFL number and filter out the acoustic waves. When using smaller CFL numbers, numerical diffusion occurs which results to a less accurate solution.

The domain in this test is $[0, 4]$ and by choosing ρ_0, u_0 and p_0, we can compute the initial soundspeed $a_0 = \sqrt{\gamma \frac{p_0}{\rho_0}}$ and initialize the test case as follows:

$$
\begin{aligned}
a &= a_0 + \left(\frac{\gamma - 1}{2}\right) \beta_1 a_0 \exp\left(\frac{(x - 0.5)^2}{0.02}\right) \\
\rho &= \rho_0 \left(\frac{a}{a_0}\right)^{\frac{2}{\gamma - 1}} + \beta_2 \exp\left(\frac{(x - 1.5)^2}{0.02}\right) \\
u &= u_0 + \beta_1 a_0 \exp\left(\frac{(x - 0.5)^2}{0.02}\right) \\
p &= p_0 \left(\frac{a}{a_0}\right)^{\frac{2\gamma}{\gamma - 1}}
\end{aligned}
$$

where β_1 and β_2 are two parameters with which we manipulate the acoustic and the material waves. In the case where $\beta_1 = 0$ and $\beta_2 \neq 0$ we have a purely material wave and respectively when $\beta_1 \neq 0$ and $\beta_2 = 0$ we introduce a purely acoustic wave.

5.5.1 Convergence Test

In this test we run two different cases where first we introduce a purely acoustic wave and then a purely material wave in order to check the convergence of the proposed semi-implicit scheme.

For the acoustic pulse we initialize the test by setting $\rho_0 = 1$, $u_0 = 0.08$ and $p_0 = 1$ while the regulating parameters are $\beta_1 = 0.1$ and $\beta_2 = 0$. The final time is $T = 0.2$ in order to compute the order off accuracy before a shock forms. We plot in Figure 5.12a the CFL numbers we use (in a range that we obey the material CFL restriction) versus the logarithmic error. We observe that for very small CFL numbers the numerical diffusion increases the error. As expected for a purely acoustic wave, when we overpass the acoustic CFL restriction the error increases and the optimal CFL number for this case is close to one.

On the other hand for the purely material wave we set $\rho_0 = 1$, $u_0 = 0.5$ and $p_0 = 1$ while the regulating parameters are set to $\beta_1 = 0$ and $\beta_2 = 0.1$. The final time is $T = 1$ and we plot the same data (see Figure 5.12b) as the acoustic case. Note here that after the acoustic CFL condition is overpassed the error remains almost the same as long as we obey the material CFL condition.

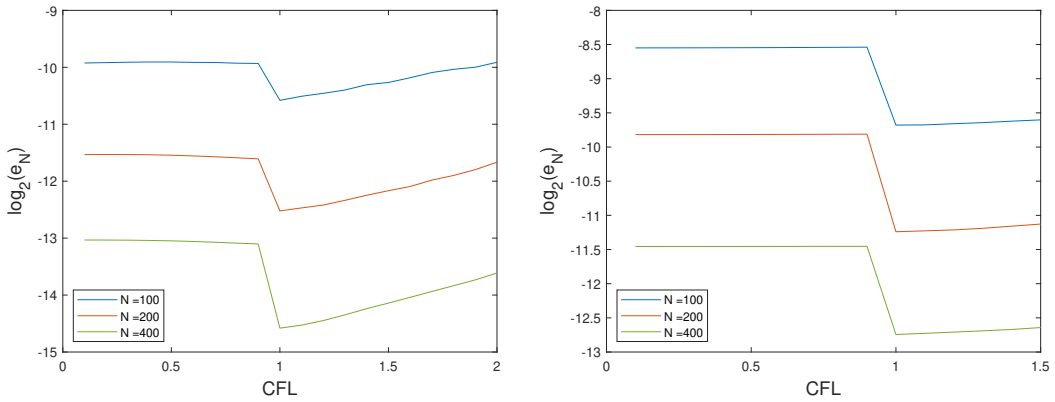

(a) Acoustic wave.

(b) Material wave.

FIGURE 5.12: CFL number versus the logarithmic error of the acoustic and material cases.

5.5.2 Material and Acoustic Waves

For this case we set $\rho_0 = 1, \quad u_0 = 0.08$ and $p_0 = 1$. We compute the initial soundspeed $a_0 = \sqrt{\gamma \frac{p_0}{\rho_0}}$ where $\gamma = 1.4$ and the test case in initialized as follows:

Here we initialize the test by setting $\rho_0 = 1$, $u_0 = 0.08$, $p_0 = 1$ and $\gamma = 1.4$. The parameters which manipulate the waves are regulated to $\beta_1 = 0.1$ and $\beta_2 = 1$ in order to introduce both types of waves in the same setup. We use periodic boundary condition and we set the final time $T = 13.25$ in order for the acoustic pulse to return to its initial position after approximately four full periods. In Figure 5.13 we plot the initial conditions and in Figure 5.14 we compare the solution obtained from the semi-implicit scheme with a solution obtained from an explicit F-V scheme in very fine mesh.

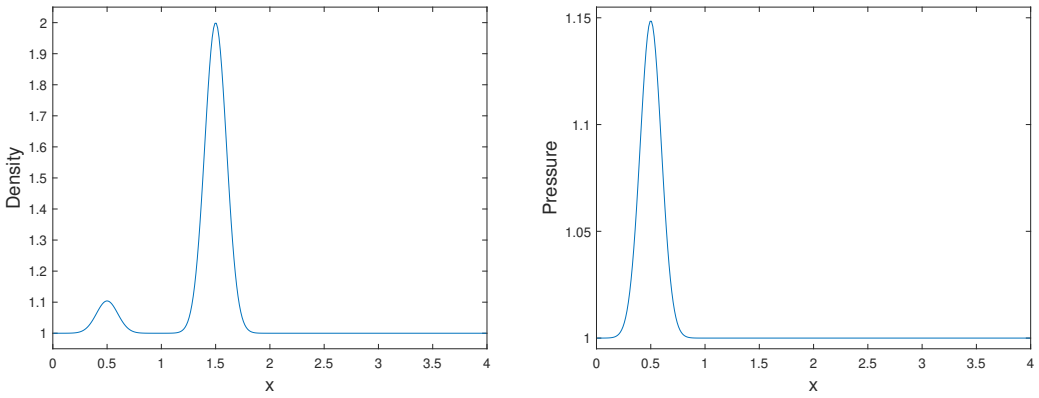

(a) Density. (b) Pressure.

FIGURE 5.13: Material and acoustic waves initial conditions.

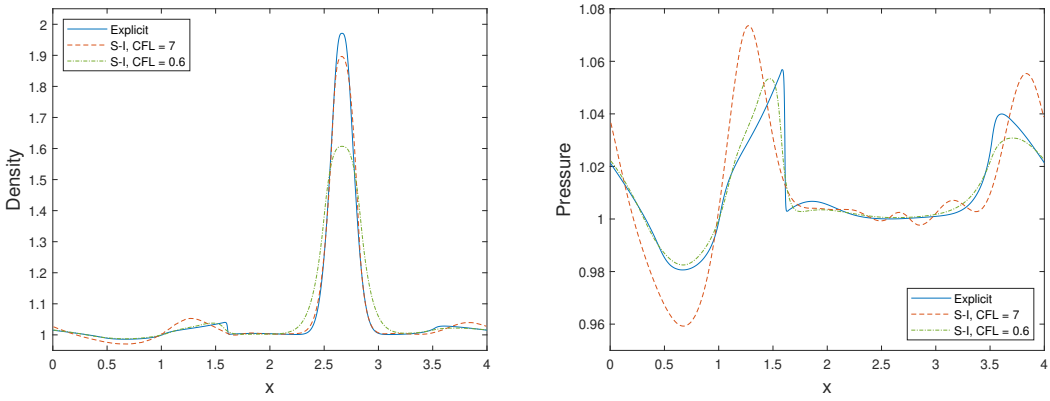

(a) Density. (b) Pressure.

FIGURE 5.14: Material and acoustic waves solution at t=13.25 with $N = 3200$ for the explicit scheme and $N = 320$ grid points for the solution obtained with the semi-implicit scheme.

5.5.3 Stiffened Gas

The same test is performed but here we use the Noble-Abel stiffened gas equation of state [76] in order to check the efficiency of the semi implicit scheme even in extreme cases with stiffened gas. Such equation of state is given by:

$$p = (\gamma - 1)(E - \frac{\rho u^2}{2}) - \gamma p_\infty. \tag{5.7}$$

where p_∞ is a stiffness parameter, and for $p_\infty = 0$ one recovers the ideal gas case.

Again, the domain for this test is $[0,4]$ and we set $\rho_0 = 1, \quad u_0 = 0.08$ and $p_0 = 1$. Here the initial sound speed is computed as follows:

$$a_0 = \sqrt{\gamma \frac{p_0 + p_\infty}{\rho_0}},$$

where $\gamma = 1.4$, $p_\infty = 10^3$ and the test is initialized as before (Subsection 5.5.2), except for the pressure that is written as:

$$p = (p_0 + p_\infty)\left(\frac{a}{a_0}\right)^{\frac{2\gamma}{\gamma-1}} - p_\infty.$$

We initialize the test by keeping the same values for $\beta_1 = 0.1 \quad$ and $\quad \beta_2 = 1$ in order to introduce both types of waves and we use periodic boundary condition. The final time here is $T = 0.42$ in the same philosophy as before i.e. the acoustic pulse to return to its initial position after four full periods. As before, we observe in Figure 5.16a that the scheme, when large CFL numbers are used, preserves the material waves but it doesn't captures accurately the acoustic waves. This can be seen in the pressure plot Figure 5.16b, that a small CFL number leads to a more accurate solution concerning the acoustic wave.

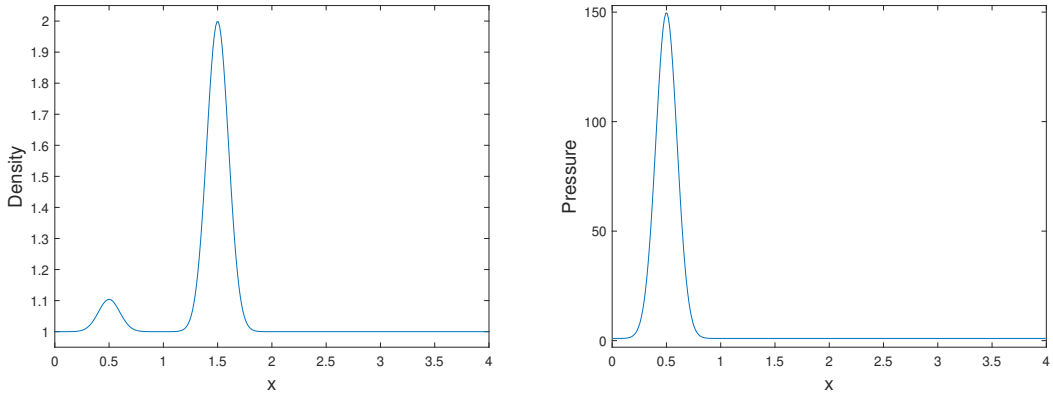

(a) Density. (b) Pressure.

FIGURE 5.15: Initial conditions of material and acoustic waves with p_∞ .

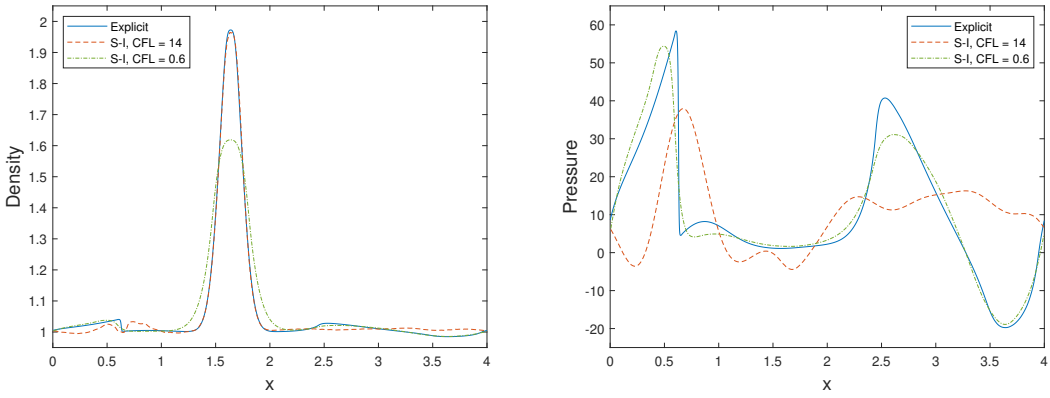

(a) Density. (b) Pressure.

FIGURE 5.16: Material and acoustic waves solution at t=0.42 with $N = 3200$ for the explicit scheme and $N = 320$ grid points for the solution obtained with the semi-implicit scheme.

Chapter 6

Explicit Scheme for 2D Euler Equations

In this chapter we present an explicit scheme for Euler equations in two dimensions. First, we present a first order accurate in space finite volume scheme.

Recalling the Euler equations in vector form in two dimensions from Chapter 2 we have:

$$\begin{cases} \dfrac{\partial \rho}{\partial t} + \nabla \cdot \mathbf{m} = 0, \\ \dfrac{\partial \mathbf{m}}{\partial t} + \nabla \cdot \left(\dfrac{\mathbf{m} \otimes \mathbf{m}}{\rho} \right) + \nabla p = 0, \\ \dfrac{\partial E}{\partial t} + \nabla \cdot (h\mathbf{m}) = 0, \end{cases} \tag{6.1}$$

where $\mathbf{m} = (\mathsf{m}, \mathsf{n})$ stands for the vector form of the momentum in the x and y direction receptively.

The system is closed with the Equation of state in two dimensions:

$$p = (\gamma - 1) \left(E - \frac{\rho}{2} \left(u^2 + v^2 \right) \right), \tag{6.2}$$

where $u = \mathsf{m}/\rho$ and $v = \mathsf{n}/\rho$ are the velocities in x and y direction.

In order to discretize the System (6.1), we have to write it in scalar form where:

$$\begin{cases} \dfrac{\partial \rho}{\partial t} + \dfrac{\partial \mathsf{m}}{\partial x} + \dfrac{\partial \mathsf{n}}{\partial y} = 0, \\ \dfrac{\partial \mathsf{m}}{\partial t} + \dfrac{\partial}{\partial x}(\mathsf{m}u) + \dfrac{\partial}{\partial y}(\mathsf{m}v) + \dfrac{\partial p}{\partial x} = 0, \\ \dfrac{\partial \mathsf{n}}{\partial t} + \dfrac{\partial}{\partial x}(\mathsf{n}u) + \dfrac{\partial}{\partial y}(\mathsf{n}v) + \dfrac{\partial p}{\partial y} = 0, \\ \dfrac{\partial E}{\partial t} + \dfrac{\partial}{\partial x}(h\mathsf{m}) + \dfrac{\partial}{\partial y}(h\mathsf{n}) = 0. \end{cases} \tag{6.3}$$

Using this notation we can define now the numerical discretization in space. The differences that occur from 1D are just in the fluxes.

6.1 1st Order Discretization in Time

Following the same procedure and notation as Section (3.5) we can write the semi discrete form of the System (6.3) as follows:

$$\frac{U^{n+1} - U^n}{\Delta t} = \mathcal{H}(U^n). \tag{6.4}$$

Now we obtained a first order accurate in time domain scheme. The next step is to describe the numerical discretization in space domain.

6.2 Finite Volume Scheme

Assume that the problem is defined in a square domain $[a, b] \times [a, b]$. Discretizing the System (6.3) at a time interval $[t_n, t_{n+1}]$ one gets:

$$\begin{cases} \rho^{n+1} = \rho^n - \Delta t \hat{D}_x(\mathsf{m}^n) - \Delta t \hat{D}_y(\mathsf{n}^n), & \text{(6.5a)} \\ \mathsf{m}^{n+1} = \mathsf{m}^n - \Delta t \hat{D}_x(\mathsf{m}^n u^n) - \Delta t \hat{D}_y(\mathsf{m}^n v^n) - \Delta t \hat{D}_x(p^n), & \text{(6.5b)} \\ \mathsf{n}^{n+1} = \mathsf{n}^n - \Delta t \hat{D}_x(\mathsf{n}^n u^n) - \Delta t \hat{D}_y(\mathsf{n}^n v^n) - \Delta t \hat{D}_y(p^n), & \text{(6.5c)} \\ E^{n+1} = E^n - \Delta t \hat{D}_x(h^n \mathsf{m}^n) - \Delta t \hat{D}_y(h^n \mathsf{n}^n). & \text{(6.5d)} \end{cases}$$

where $\hat{D}_x$ and $\hat{D}_y$ stand for the finite volume approximation of the spatial derivatives in x and y direction respectively. We shall now define the computation of such terms.

6.2.1 Definition of $\hat{D}$

On a collocated grid in 2D we use a pair of indices i, j, where we denote with i the index of the cells on the discretization on y and with j on x respectively.

We compute $\hat{D}_x$ as the flux derivative that is discretized as the difference of the numerical fluxes between two adjacent cells on the x direction, i.e. $i, j + 1/2$ and $i, j - 1/2$, as:

$$\hat{D}_x(F_{i,j}) = \frac{F_{i,j+1/2} - F_{i,j-1/2}}{\Delta x}, \tag{6.6}$$

where Δx is the discretization step corresponding to the x direction.

Respectively $\hat{D}_y$ stands for the finite volume flux derivative, which is computed now as the difference of the numerical fluxes between two adjacent cell at the y direction, meaning $i + 1/2, j$ and $i - 1/2, j$, where:

$$\hat{D}_y(F_{i,j}) = \frac{F_{i+1/2,j} - F_{i-1/2,j}}{\Delta y}, \tag{6.7}$$

where again Δy stands for the discretization step in y. In the case where the grid is uniform we have $\Delta x = \Delta y$.

6.3 Boundary Conditions

Let us now introduce how we implement the different types of boundary conditions in 2D. Assume that we use a $N \times N$ grid. We extend the grid in both directions, thus the dimension becomes $N + 2 \times N + 2$. Now we have in every side a column-row of ghost cells. This procedure is depicted in Figure 6.1.

After the ghost cells are introduced, we can initialize the test cases using a range of boundary conditions. As in 1D we have several types of boundary conditions. The reason we use different kinds of BC is explained in detail at Section 3.6.

6.3.1 Transmissive Boundary Conditions

First we present the transmissive case in two dimensions where then values at the ghost columns are:

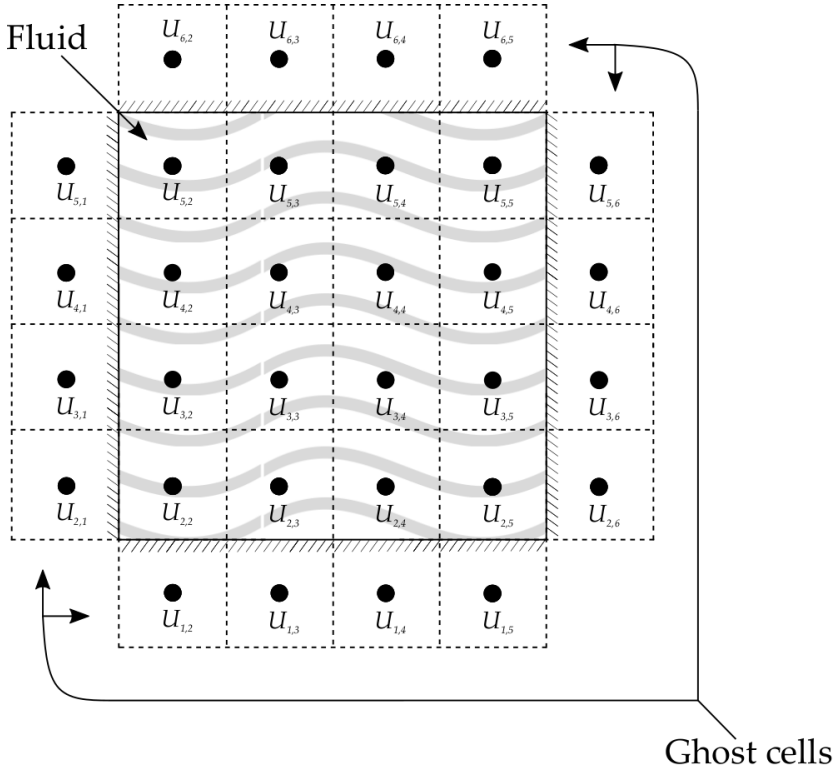

FIGURE 6.1: 2D grid setup with ghost cells ($N = 4$).

$$\begin{pmatrix} \rho_{i,1} \\ \mathsf{m}_{i,1} \\ \mathsf{n}_{i,1} \\ E_{i,1} \end{pmatrix} = \begin{pmatrix} \rho_{i,2} \\ \mathsf{m}_{i,2} \\ \mathsf{n}_{i,2} \\ E_{i,2} \end{pmatrix}, \quad \begin{pmatrix} \rho_{i,N+2} \\ \mathsf{m}_{i,N+2} \\ \mathsf{n}_{i,N+2} \\ E_{i,N+2} \end{pmatrix} = \begin{pmatrix} \rho_{i,N+1} \\ \mathsf{m}_{i,N+1} \\ \mathsf{n}_{i,N+1} \\ E_{i,N+1} \end{pmatrix}, \quad i = 2 \dots N+1, \tag{6.8}$$

while at the ghost rows:

$$\begin{pmatrix} \rho_{1,j} \\ \mathsf{m}_{1,j} \\ \mathsf{n}_{1,j} \\ E_{1,j} \end{pmatrix} = \begin{pmatrix} \rho_{2,j} \\ \mathsf{m}_{2,j} \\ \mathsf{n}_{2,j} \\ E_{2,j} \end{pmatrix}, \quad \begin{pmatrix} \rho_{N+2,j} \\ \mathsf{m}_{N+2,j} \\ \mathsf{n}_{N+2,j} \\ E_{N+2,j} \end{pmatrix} = \begin{pmatrix} \rho_{N+1,j} \\ \mathsf{m}_{N+1,j} \\ \mathsf{n}_{N+1,j} \\ E_{N+1,j} \end{pmatrix}, \quad j = 2 \dots N+1. \tag{6.9}$$

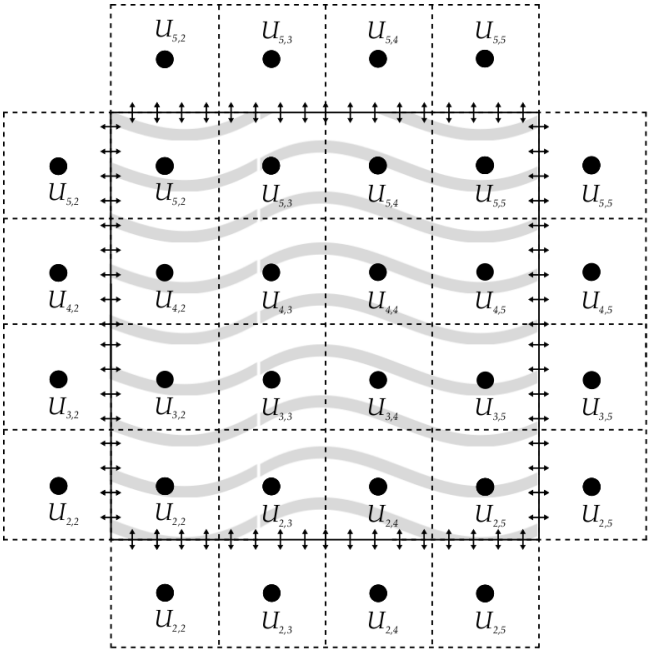

FIGURE 6.2: Transmissive boundary conditions in 2D where $N = 4$.

6.3.2 Reflective Boundary Conditions

Another possibility is to use reflective boundary conditions. In some cases a mixture of boundary conditions can be used and for this reason we present in detail all the kinds of boundary conditions. In the case of reflective boundary conditions all the values are still the same as the transmissive case except from the momentum which takes the opposite sign, i.e. the ghost columns are computed like:

$$\begin{pmatrix} \rho_{i,1} \\ \mathsf{m}_{i,1} \\ \mathsf{n}_{i,1} \\ E_{i,1} \end{pmatrix} = \begin{pmatrix} \rho_{i,2} \\ -\mathsf{m}_{i,2} \\ -\mathsf{n}_{i,2} \\ E_{i,2} \end{pmatrix}, \quad \begin{pmatrix} \rho_{i,N+2} \\ \mathsf{m}_{i,N+2} \\ \mathsf{n}_{i,N+2} \\ E_{i,N+2} \end{pmatrix} = \begin{pmatrix} \rho_{i,N+1} \\ -\mathsf{m}_{i,N+1} \\ -\mathsf{n}_{i,N+1} \\ E_{i,N+1} \end{pmatrix}, \quad i = 2 \dots N+1, \tag{6.10}$$

while the rows like:

$$\begin{pmatrix} \rho_{1,j} \\ \mathsf{m}_{1,j} \\ \mathsf{n}_{1,j} \\ E_{1,j} \end{pmatrix} = \begin{pmatrix} \rho_{2,j} \\ -\mathsf{m}_{2,j} \\ -\mathsf{n}_{2,j} \\ E_{2,j} \end{pmatrix}, \quad \begin{pmatrix} \rho_{N+2,j} \\ \mathsf{m}_{N+2,j} \\ \mathsf{n}_{N+2,j} \\ E_{N+2,j} \end{pmatrix} = \begin{pmatrix} \rho_{N+1,j} \\ -\mathsf{m}_{N+1,j} \\ -\mathsf{n}_{N+1,j} \\ E_{N+1,j} \end{pmatrix}, \quad j = 2 \dots N+1. \tag{6.11}$$

6.3.3 Periodic Boundary Conditions

Finally, in some test we use artificial periodic boundary conditions. In order to initialize the test we calculate the values at the ghost cells as follows. We assume periodic boundary conditions in both directions, thus concerning the x direction we set the ghost columns values as follows:

$$\begin{pmatrix} \rho_{i,1} \\ \mathsf{m}_{i,1} \\ \mathsf{n}_{i,1} \\ E_{i,1} \end{pmatrix} = \begin{pmatrix} \rho_{i,N+1} \\ \mathsf{m}_{i,N+1} \\ \mathsf{n}_{i,N+1} \\ E_{i,N+1} \end{pmatrix}, \quad \begin{pmatrix} \rho_{i,N+2} \\ \mathsf{m}_{i,N+2} \\ \mathsf{n}_{i,N+2} \\ E_{i,N+2} \end{pmatrix} = \begin{pmatrix} \rho_{i,2} \\ \mathsf{m}_{i,2} \\ \mathsf{n}_{i,2} \\ E_{i,2} \end{pmatrix}, \quad i = 2 \dots N+1, \tag{6.12}$$

where respectively for the y direction we set the ghost rows values as:

$$\begin{pmatrix} \rho_{1,j} \\ \mathsf{m}_{1,j} \\ \mathsf{n}_{1,j} \\ E_{1,j} \end{pmatrix} = \begin{pmatrix} \rho_{N+1,j} \\ \mathsf{m}_{N+1,j} \\ \mathsf{n}_{N+1,j} \\ E_{N+1,j} \end{pmatrix}, \quad \begin{pmatrix} \rho_{N+2,j} \\ \mathsf{m}_{N+2,j} \\ \mathsf{n}_{N+2,j} \\ E_{N+2,j} \end{pmatrix} = \begin{pmatrix} \rho_{2,j} \\ \mathsf{m}_{2,j} \\ \mathsf{n}_{2,j} \\ E_{2,j} \end{pmatrix}, \quad j = 2 \dots N+1. \tag{6.13}$$

Chapter 7

Semi-Implicit Scheme for 2D Euler Equations

In this chapter we present the semi-implicit scheme for the two dimensional Euler equations. After we presented all the needed tools for the derivation of this scheme we are going to explain in detail the semi-implicit technique. Let us now recall from Chapter 2 the Euler equations in two dimensions:

$$\begin{cases} \dfrac{\partial \rho}{\partial t} + \nabla \cdot \mathbf{m} = 0, \\ \dfrac{\partial \mathbf{m}}{\partial t} + \nabla \cdot \left(\dfrac{\mathbf{m} \otimes \mathbf{m}}{\rho} \right) + \nabla p = 0, \\ \dfrac{\partial E}{\partial t} + \nabla \cdot (h\mathbf{m}) = 0, \end{cases} \tag{7.1}$$

where $\mathbf{m} = (\mathsf{m}, \mathsf{n})$ stands for the vector form of the momentum in the x and y direction with $u = \mathsf{m}/\rho$ and $v = \mathsf{n}/\rho$ the corresponding velocities.

The system is closed with the Equation of state in two dimensions:

$$p = (\gamma - 1) \left(E - \frac{\rho}{2} \left(u^2 + v^2 \right) \right). \tag{7.2}$$

Again, we can use a wide range of equations of state where the pressure and the energy are linearly related. Moreover, we can extend the scheme for more general equations of state using the appropriate linearization techniques.

7.1 1st Order Discretization in Time

Let us now rewrite the System (7.1) in the following form:

$$\begin{cases} \dfrac{\partial \rho}{\partial t} + \dfrac{\partial \mathsf{m}}{\partial x} + \dfrac{\partial \mathsf{n}}{\partial y} = 0, \\ \dfrac{\partial \mathsf{m}}{\partial t} + \dfrac{\partial}{\partial x}(\mathsf{m}u + p) + \dfrac{\partial}{\partial y}(\mathsf{m}v) = 0, \\ \dfrac{\partial \mathsf{n}}{\partial t} + \dfrac{\partial}{\partial x}(\mathsf{n}u) + \dfrac{\partial}{\partial y}(\mathsf{n}v + p) = 0, \\ \dfrac{\partial E}{\partial t} + \dfrac{\partial}{\partial x}(h\mathsf{m}) + \dfrac{\partial}{\partial y}(h\mathsf{n}) = 0. \end{cases} \tag{7.3}$$

The System of equations (7.3) has the structure of a quasi linear hyperbolic system of conservation laws and it can be written in the following form:

$$\frac{\partial W}{\partial t} = -\frac{\partial \mathcal{F}(W)}{\partial x} - \frac{\partial \mathcal{G}(W)}{\partial y}, \tag{7.4}$$

where $W = (\rho, \mathsf{m}, \mathsf{n}, E)^T$, $\mathcal{F} = (\mathsf{m}, \mathsf{m}u + p, \mathsf{n}u, h\mathsf{m})$ and $\mathcal{G} = (\mathsf{n}, \mathsf{m}v, \mathsf{n}v + p, h\mathsf{n})$.

Using the same technique as 1D we can rewrite the System (7.3) in the following semi-discrete form:

$$\begin{cases} \dfrac{dU}{dt}(t) = \mathcal{H}\left(U_E(t), U_I(t)\right), \quad \forall t \geq t_0 \\ U\left(t_0\right) = U_0. \end{cases} \tag{7.5}$$

In the same philosophy as 1D, we denote by U the discrete approximation of W which can be splitted into two parts. The first part is the non-stiff part which is correlated with the material waves and thus we treat it with an explicit way, so-called U_E. The second part is the stiff one corresponding with the acoustic waves, so we choose to treat these terms implicitly and we name them U_I. Finally, $\mathcal{H}$ denotes the the approximation of the right hand side of Equation (7.4).

In order to achieve a first order in time scheme we discretize the time derivative of (7.5) using backward differences over a time step Δt, thus the first-order accurate temporal discretization is given by:

$$\frac{U^{n+1} - U^n}{\Delta t} = \mathcal{H}\left(U^n, U^{n+1}\right), \tag{7.6}$$

where $n+1$ denotes the value at the next time step $t + \Delta t$. Now we are going to describe the spatial discretization of the term $\mathcal{H}\left(U^n, U^{n+1}\right)$.

7.2 1st Order Discretization in Space

In the same philosophy as 1D we choose to treat implicitly the pressure terms at the momentum equations. Using the semi-discrete form of Equation (7.5) and the System (7.1) we discretize the system at a time interval $[t^n, t^{n+1}]$ and we obtain:

$$\begin{cases} \rho^{n+1} = \rho^n - \Delta t \hat{D}_x(\mathsf{m}^n) - \Delta t \hat{D}_y(\mathsf{n}^n), & \text{(7.7a)} \\ \mathsf{m}^{n+1} = \mathsf{m}^n - \Delta t \hat{D}_x(\mathsf{m}^n u^n) - \Delta t \hat{D}_y(\mathsf{m}^n v^n) - \Delta t D_x(p^{n+1}), & \text{(7.7b)} \\ \mathsf{n}^{n+1} = \mathsf{n}^n - \Delta t \hat{D}_x(\mathsf{n}^n u^n) - \Delta t \hat{D}_y(\mathsf{n}^n v^n) - \Delta t D_y(p^{n+1}), & \text{(7.7c)} \\ E^{n+1} = E^n - \Delta t D_x(h^n \mathsf{m}^{n+1}) - \Delta t D_y(h^n \mathsf{n}^{n+1}), & \text{(7.7d)} \end{cases}$$

where $\hat{D}$ stands for the finite volume computed derivatives and D for the centred.

Again we use for the finite volume derivatives the local Lax-Friedrichs flux function which for x direction stands for:

$$F_{i,j+1/2} = \frac{1}{2}\left[\mathcal{F}\left(U^n_{i,j}\right) + \mathcal{F}\left(U^n_{i,j+1}\right)\right] - \frac{\alpha_{i,j+1/2}}{2}\left[U^n_{i,j+1} - U^n_{i,j}\right], \tag{7.8}$$

while for y direction:

$$F_{i+1/2,j} = \frac{1}{2}\left[\mathcal{F}\left(U^n_{i,j}\right) + \mathcal{F}\left(U^n_{i+1,j}\right)\right] - \frac{\alpha_{i+1/2,j}}{2}\left[U^n_{i+1,j} - U^n_{i,j}\right]. \tag{7.9}$$

Now we have to define the local viscosity terms.

7.2.1 Definition of D

Let us now describe the computation of the terms that are treated with a centred approximation. Such terms are occur when we solve at the energy equation using the pressure splitting technique. The only term that we are interested to use this approximation is the second order derivative of the energy term. Thus, in the same philosophy as 1D one obtains:

$$D_x\left(D_x(\mathcal{F}(U_{i,j}))\right) = \frac{\mathcal{F}\left(U_{i,j+1}\right) - 2\mathcal{F}\left(U_{i,j}\right) + \mathcal{F}\left(U_{i,j-1}\right)}{\Delta x^2}, \tag{7.10}$$

which is the second order derivative on the x direction and second order accurate. Respectively for the y direction we get:

$$D_y\left(D_y(\mathcal{F}(U_{i,j}))\right) = \frac{\mathcal{F}\left(U_{i+1,j}\right) - 2\mathcal{F}\left(U_{i,j}\right) + \mathcal{F}\left(U_{i+1,j}\right)}{\Delta y^2}, \tag{7.11}$$

Because of the implicit treatment of the acoustic waves we can regulate the parameter α proportional to the material velocity in the low Mach number regime. Moreover for high Mach cases the, the soundspeed is bounded by the fluid velocity, thus is enough to choose the parameter for x and y direction respectively:

$$\begin{aligned} \alpha_{i,j+1/2} &= \max\left(\left|u_{i,j}\right|, \left|u_{i,j+1}\right|\right), \\ \alpha_{i+1/2,j} &= \max\left(\left|u_{i,j}\right|, \left|u_{i+1,j}\right|\right), \end{aligned} \tag{7.12}$$

7.3 Pressure Splitting

In the same philosophy as Section 4.3 we choose to treat with an implicit way the pressure terms. After we discretize the System (7.1) between a time t^n and a time t^{n+1} we make use of the equation of state (7.2), where

$$p^{n+1} = (\gamma - 1)\big(E^{n+1} - \frac{1}{2}((\mathsf{m}^n u^n + \mathsf{n}^n v^n)\big), \tag{7.13}$$

and we substitute this expression in Equations (7.7b) and (7.7c). We choose to treat implicitly the energy term and upwind the rest. Thus, we obtain:

$$\begin{aligned} \mathsf{m}^{n+1} = \mathsf{m}^n - \left(\frac{3-\gamma}{2}\right)\Delta t\hat{D}_x(\mathsf{m}^n u^n) - \left(\frac{1-\gamma}{2}\right)\Delta t\hat{D}_x(\mathsf{n}^n v^n) \\ -\Delta t\hat{D}_y(\mathsf{m}^n v^n) - (\gamma-1)\Delta t D_x(E^{n+1}), \end{aligned} \tag{7.14}$$

$$\begin{aligned} \mathsf{n}^{n+1} = \mathsf{n}^n - \left(\frac{3-\gamma}{2}\right)\Delta t\hat{D}_y(\mathsf{n}^n v^n) - \left(\frac{1-\gamma}{2}\right)\Delta t\hat{D}_y(\mathsf{m}^n u^n) \\ -\Delta t\hat{D}_x(\mathsf{n}^n u^n) - (\gamma-1)\Delta t D_y(E^{n+1}). \end{aligned} \tag{7.15}$$

For sake of simplicity, we denote:

$$\mathsf{m}^* = \mathsf{m}^n - \left(\frac{3-\gamma}{2}\right)\Delta t\hat{D}_x(\mathsf{m}^n u^n) - \left(\frac{1-\gamma}{2}\right)\Delta t\hat{D}_x(\mathsf{n}^n v^n) - \Delta t\hat{D}_y(\mathsf{m}^n v^n), \tag{7.16}$$

and respectively

$$\mathsf{n}^* = \mathsf{n}^n - \left(\frac{3-\gamma}{2}\right)\Delta t\hat{D}_y(\mathsf{n}^n v^n) - \left(\frac{1-\gamma}{2}\right)\Delta t\hat{D}_y(\mathsf{m}^n u^n) - \Delta t\hat{D}_x(\mathsf{n}^n u^n). \quad (7.17)$$

Using this notation the Equations (7.14) and (7.15) become:

$$\mathsf{m}^{n+1} = \mathsf{m}^* - (\gamma-1)\Delta t D_x(E^{n+1}), \quad (7.18)$$

$$\mathsf{n}^{n+1} = \mathsf{n}^* - (\gamma-1)\Delta t D_y(E^{n+1}). \quad (7.19)$$

Plugging these expressions in the Equation for the Energy (7.7d) one obtains:

$$\begin{aligned} E^{n+1} = E^n - \Delta t\hat{D}_x(h^n\mathsf{m}^*) + (\gamma-1)\Delta t^2 D_x(h^n D_x(E^{n+1})) \\ -\Delta t\hat{D}_y(h^n\mathsf{n}^*) + (\gamma-1)\Delta t^2 D_y(h^n D_y(E^{n+1})). \end{aligned} \quad (7.20)$$

Posing $E^* = E^n - \Delta t\hat{D}_x(h^n\mathsf{m}^*) - \Delta t\hat{D}_y(h^n\mathsf{n}^*)$ the Equation (7.20) becomes:

$$E^{n+1} = E^* + (\gamma-1)\Delta t^2 D_x(h^n D_x(E^{n+1})) + (\gamma-1)\Delta t^2 D_y(h^n D_y(E^{n+1})). \quad (7.21)$$

Now we can solve this system in order to compute E^{n+1} and then plug it in the momentum equations to compute m^{n+1} and n^{n+1}.

7.3.1 Extension to 2nd Order

Again we are using the same techniques described in Section 3.4.1. The only difference that occurs naturally is that the same procedure must be done for both dimensions in order to compute the reconstructed values for the fluxes. Apart from this detail, the rest procedure still the same as before.

In order to achieve second order accuracy in the time domain, we use the same technique as 1D described in 4.4.1. The implementation it's straightforward without any difference from 1D. We choose this approximation because it's efficient and easily implementable.

Chapter 8

Numerical Tests for 2D Euler Equations

In this chapter we perform multiple tests in order to check the robustness the accuracy and the convergence of the proposed 2D scheme. First we introduce some useful quantities. The timestep by using the so-called acoustic CFL number in two dimension is define as:

$$\Delta t = \mathrm{CFL}\frac{\Delta x}{\max(|u|+a) + \max(|v|+a)}, \tag{8.1}$$

where a stands for the soundspeed:

$$a = \sqrt{\frac{\gamma p}{\rho}}. \tag{8.2}$$

In some tests a modified version of the classical acoustic CFL number is needed, so we introduce a new quantity namely the material CFL number (notation $\mathrm{CFL}_{\mathrm{IM}}$) where the timestep is computed as:

$$\Delta t = \mathrm{CFL}_{\mathrm{IM}}\frac{\Delta x}{\max|u| + \max|v|} \tag{8.3}$$

At the beginning we run some classical Riemann problems. The scope of these tests is to reproduce some well-known results from the literature, when we obey the classical acoustic CFL condition. Moreover we run an original test where we compare the 2D scheme with the 1D by initializing a classical Sod shock tube in two dimensions on the counter diagonal of the domain.

8.1 Sod Shock Tube

This test shows that the scheme is able to work on a wide range of Mach numbers. We compare the 2D scheme with the 1D scheme by doing the following. We choose a square domain $\Omega = [0, \sqrt{0.5}] \times [0, \sqrt{0.5}]$. In order to initialize the test, we place the discontinuity along the main diagonal, thus the domain is divided into the upper and lower part and the initial conditions (with index U and L respectively, Figure 8.1) are:

$$\begin{pmatrix} \rho \\ u \\ v \\ p \end{pmatrix}_U = \begin{pmatrix} 1 \\ 0 \\ 0 \\ 1 \end{pmatrix}, \qquad \begin{pmatrix} \rho \\ u \\ v \\ p \end{pmatrix}_L = \begin{pmatrix} 0.125 \\ 0 \\ 0 \\ 0.1 \end{pmatrix}.$$

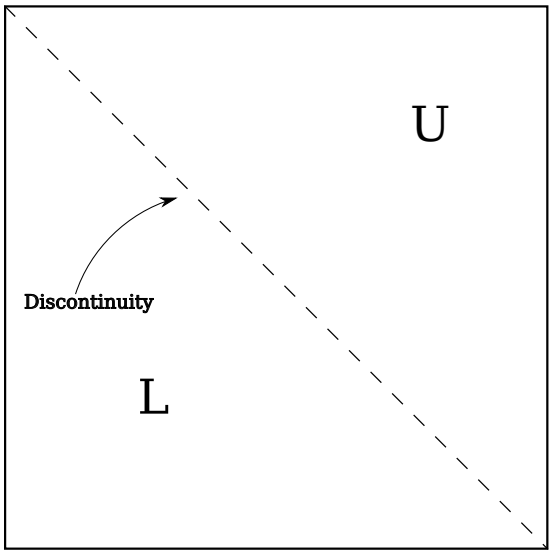

FIGURE 8.1: Initial conditions of Sod shock tube in 2D.

Then we keep as solution the vector that contains the N elements of the counter diagonal of the $N \times N$ solution matrix obtained by the 2D method (Figure 8.2). This test is performed in order to compare in a quantitatively way the solutions obtained with the 1D and 2D code. We adjust the CFL number in such a way that the timestep in both cases is the same (0.7 for the 2D scheme). We observe that the 2D code is much more accurate even if we use half of the points per direction we are using in the 1D computation. In figures 8.3a and 8.3b we see the comparison between the two schemes.

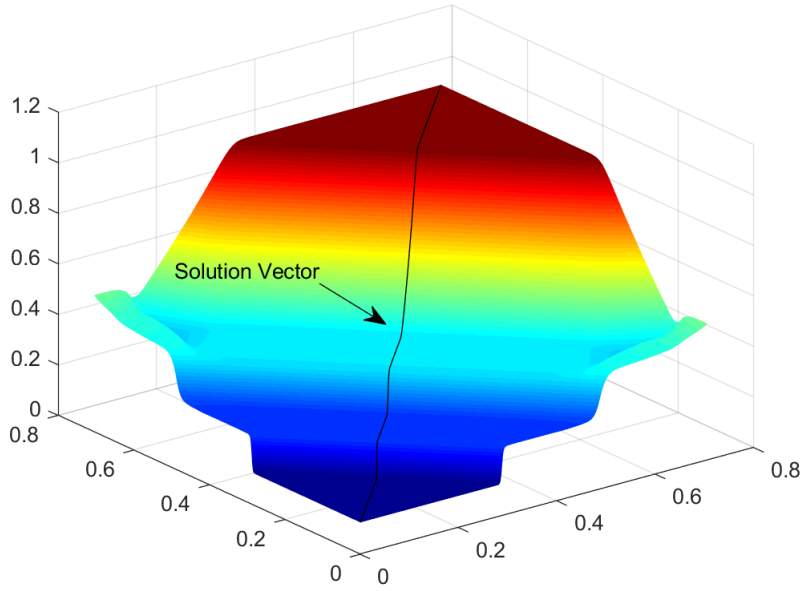

FIGURE 8.2: Density 2D plot at $T = 0.168$ and the solution vector we keep in order to compare with the 1D case.

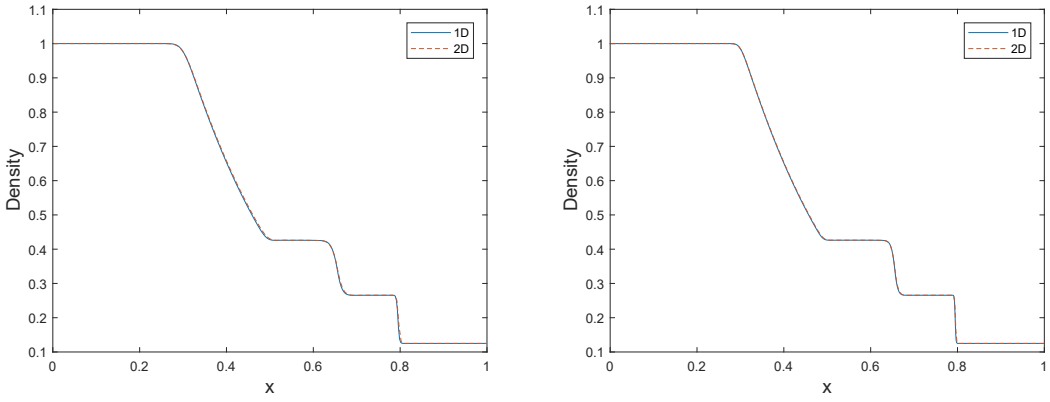

(a) 1D(400pts.) vs 2D(200 pts.).

(b) 1D(800pts.) vs 2D(400 pts.).

FIGURE 8.3: Sod shock tube. Comparison between 1D and 2D code with CFL $= 0.7$.

8.2 Riemann Tests

These tests are adopted from [72]. These tests are not low mach and the purpose of these runs is to check the ability of the proposed scheme to capture shocks like an explicit scheme. We run four different cases which are composed either of rarefaction waves or shock waves or a mixture of them. Comparing quantitatively our results we observe a great agreement with the results from the literature. In order to initialize the 2D Riemann cases we have to split the domain in equal quarters. With this in mind we write the initial conditions :

$$(\rho, u, v, p) = \begin{cases} (\rho_1, u_1, v_1, p_1), & x > 0.5,\ y > 0.5 \\ (\rho_2, u_2, v_2, p_2), & x < 0.5,\ y > 0.5 \\ (\rho_3, u_3, v_3, p_3), & x < 0.5,\ y < 0.5 \\ (\rho_4, u_4, v_4, p_4), & x > 0.5,\ y < 0.5 \end{cases} \tag{8.4}$$

8.2.1 Four Forward Rarefaction Waves

First we run a test with four forward rarefaction waves. We use $N = 200$ with an acoustic CFL number equal to 0.5. We observe the same ripples as the literature at the final time $T = 0.2$ (Figures 8.4b and 8.5b. Using the aforementioned notation, the initial conditions are:

$$\begin{pmatrix} \rho \\ u \\ v \\ p \end{pmatrix}_2 = \begin{pmatrix} 0.5197 \\ -0.7259 \\ 0 \\ 0.4 \end{pmatrix}, \qquad \begin{pmatrix} \rho \\ u \\ v \\ p \end{pmatrix}_1 = \begin{pmatrix} 1 \\ 0 \\ 0 \\ 1 \end{pmatrix},$$

$$\begin{pmatrix} \rho \\ u \\ v \\ p \end{pmatrix}_3 = \begin{pmatrix} 0.1072 \\ -0.7259 \\ -1.4045 \\ 0.0439 \end{pmatrix}, \qquad \begin{pmatrix} \rho \\ u \\ v \\ p \end{pmatrix}_4 = \begin{pmatrix} 0.2579 \\ 0 \\ -1.4045 \\ 0.15 \end{pmatrix}.$$

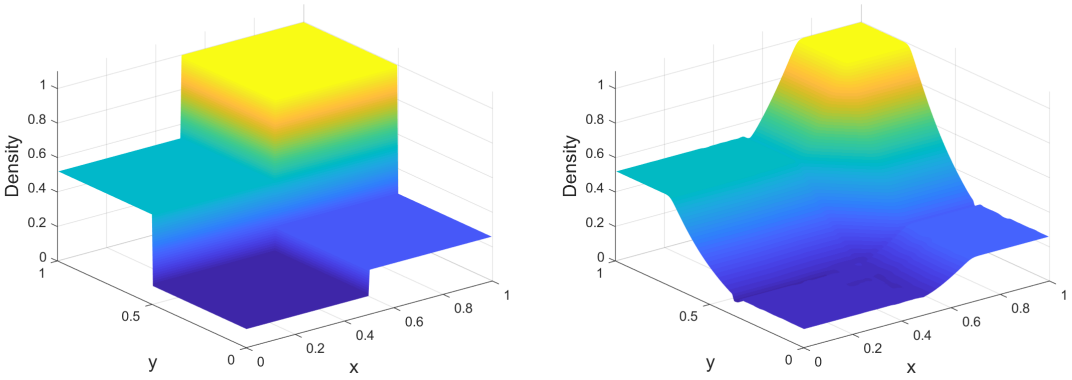

(a) Initial conditions. (b) Solution at final time $T = 0.2$.

FIGURE 8.4: Density surfs for the four rarefaction waves test case computed with $N = 200$ and CFL $= 0.5$.

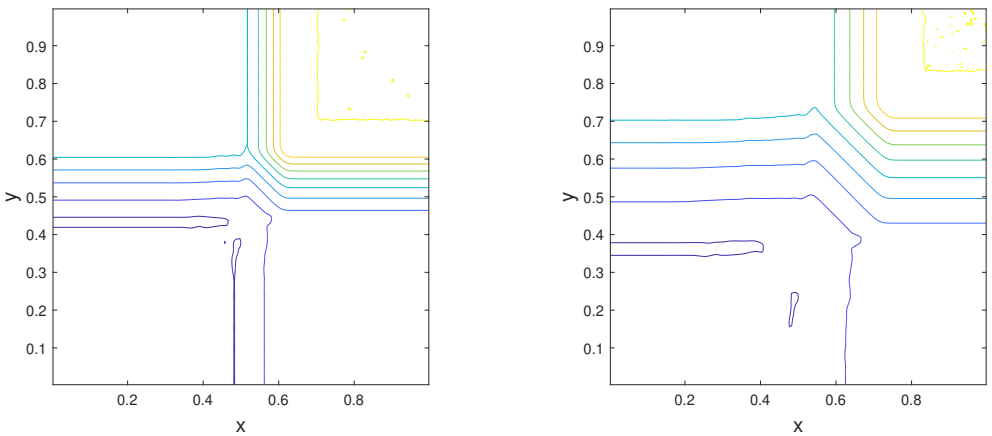

(a) Solution at the time $T = 0.1$. (b) Solution at final time $T = 0.2$.

FIGURE 8.5: Density contour plots for the four rarefaction waves test case computed with $N = 200$ and CFL $= 0.5$.

8.2.2 Two Forward and Two Backward Rarefaction Waves

Now we run a similar test case with the only difference that the two rarefaction waves are moving forward. Again we use $N = 200$ with an acoustic CFL number equal to 0.5. The initial conditions are:

$$\begin{pmatrix} \rho \\ u \\ v \\ p \end{pmatrix}_2 = \begin{pmatrix} 0.5197 \\ -0.7259 \\ 0 \\ 0.4 \end{pmatrix}, \qquad \begin{pmatrix} \rho \\ u \\ v \\ p \end{pmatrix}_1 = \begin{pmatrix} 1 \\ 0 \\ 0 \\ 1 \end{pmatrix},$$

$$\begin{pmatrix} \rho \\ u \\ v \\ p \end{pmatrix}_3 = \begin{pmatrix} 1 \\ -0.7259 \\ -0.7259 \\ 1 \end{pmatrix}, \qquad \begin{pmatrix} \rho \\ u \\ v \\ p \end{pmatrix}_4 = \begin{pmatrix} 0.5197 \\ 0 \\ -0.7259 \\ 0.4 \end{pmatrix}.$$

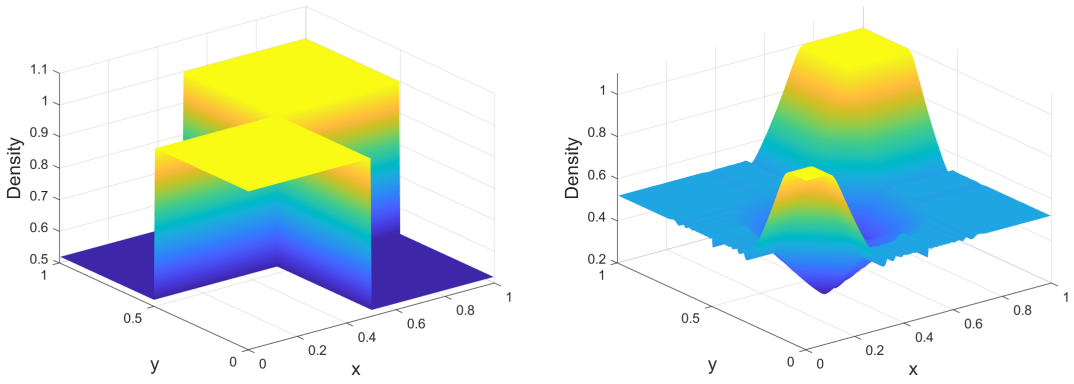

(a) Initial conditions.

(b) Solution at final time $T = 0.2$.

FIGURE 8.6: Density surfs for the two forward and two backward rarefaction waves test case computed with $N = 200$ and CFL $= 0.5$.

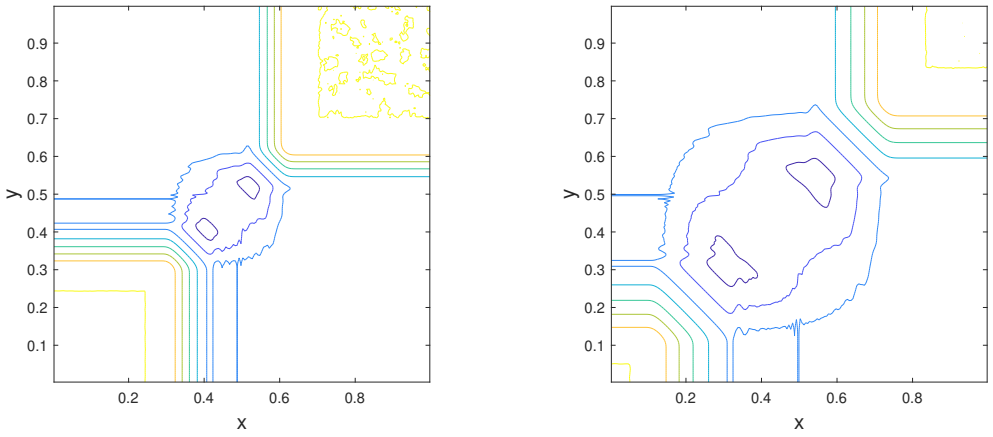

(a) Solution at the time $T = 0.1$.

(b) Solution at final time $T = 0.2$.

FIGURE 8.7: Density contour plots for the two forward and two backward rarefaction waves test case computed with $N = 200$ and CFL $= 0.5$.

8.2.3 Four Backward Shock Waves

Afterwards, we run a test case which is combined of four shock waves. We use the same points and CFL number with the difference that the final time for this test is $T = 0.3$. Again, we observe a good quantitative agreement with the results from the literature.

$$\begin{pmatrix} \rho \\ u \\ v \\ p \end{pmatrix}_2 = \begin{pmatrix} 0.5323 \\ 1.206 \\ 0 \\ 0.3 \end{pmatrix}, \qquad \begin{pmatrix} \rho \\ u \\ v \\ p \end{pmatrix}_1 = \begin{pmatrix} 1.5 \\ 0 \\ 0 \\ 1.5 \end{pmatrix},$$

$$\begin{pmatrix} \rho \\ u \\ v \\ p \end{pmatrix}_3 = \begin{pmatrix} 0.138 \\ 1.206 \\ 1.206 \\ 0.029 \end{pmatrix}, \qquad \begin{pmatrix} \rho \\ u \\ v \\ p \end{pmatrix}_4 = \begin{pmatrix} 0.5323 \\ 0 \\ 1.206 \\ 0.3 \end{pmatrix}.$$

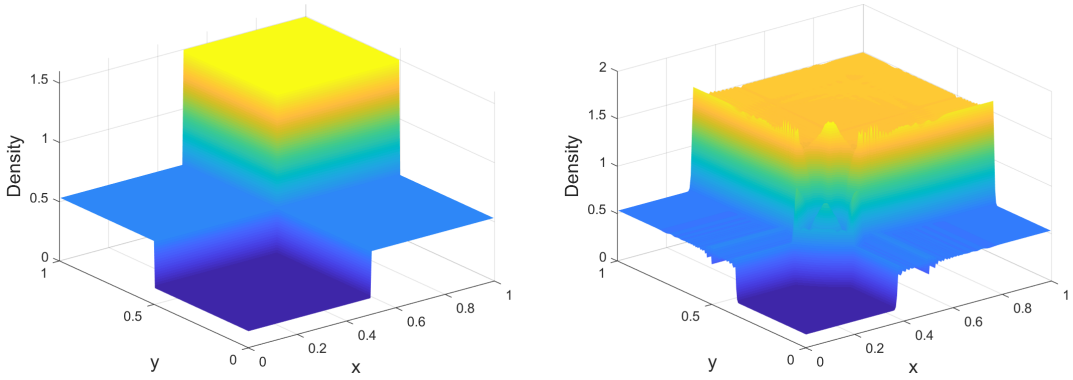

(a) Initial conditions.

(b) Solution at final time $T = 0.3$.

FIGURE 8.8: Density surfs for the four backward shock waves test case computed with $N = 200$ and CFL $= 0.5$.

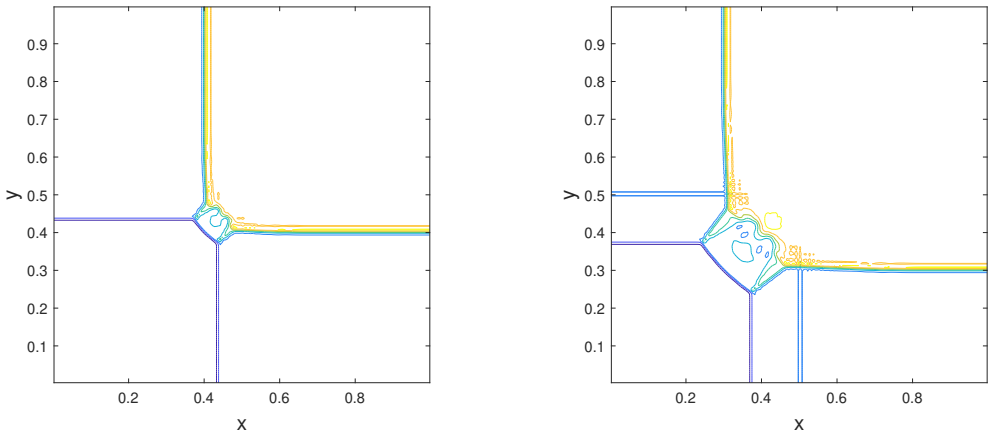

(a) Solution at the time $T = 0.15$.

(b) Solution at final time $T = 0.3$.

FIGURE 8.9: Density contour plots for the four backward shock waves test case computed with $N = 200$ and CFL $= 0.5$.

8.2.4 Two Forward and Two Backward Shock Waves

Now we run the last test of this Riemann test cases series. This test is consisted of two forward shock waves and two backward. The parameters still the same, i.e. $N = 200$ and the CFL number is regulated to 0.5 while the final time now is $T = 0.25$. We observe great agreement with the literature for all the Riemann test cases. The initial conditions for this case are:

$$\begin{pmatrix}\rho\\u\\v\\p\end{pmatrix}_2 = \begin{pmatrix}0.5065\\0.8939\\0\\0.35\end{pmatrix}, \qquad \begin{pmatrix}\rho\\u\\v\\p\end{pmatrix}_1 = \begin{pmatrix}1.1\\0\\0\\1.1\end{pmatrix},$$

$$\begin{pmatrix}\rho\\u\\v\\p\end{pmatrix}_3 = \begin{pmatrix}1.1\\0.8939\\0.8939\\1.1\end{pmatrix}, \qquad \begin{pmatrix}\rho\\u\\v\\p\end{pmatrix}_4 = \begin{pmatrix}0.5065\\0\\0.8939\\0.35\end{pmatrix}.$$

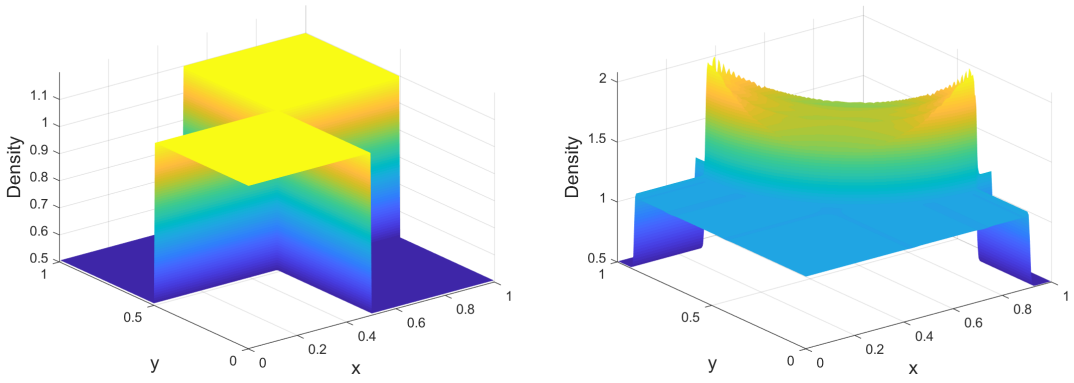

(a) Initial conditions.

(b) Solution at final time $T = 0.2$.

FIGURE 8.10: Density surfs for the two forward and two backward shock waves test case computed with $N = 200$ and CFL $= 0.5$.

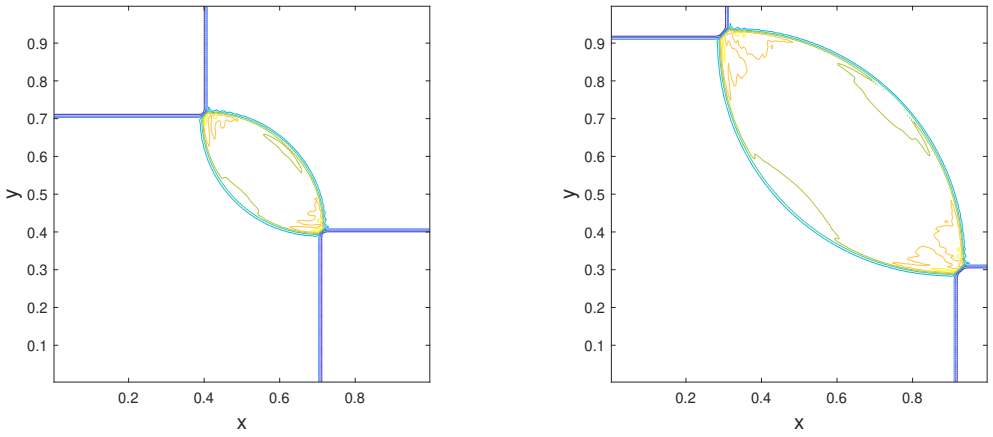

(a) Solution at the time $T = 0.1$.

(b) Solution at final time $T = 0.2$.

FIGURE 8.11: Density contour plots for the two forward and two backward shock waves test case computed with $N = 200$ and CFL $= 0.5$.

8.3 Gresho Vortex

In this test we apply our scheme to the Gresho vortex problem. This is done in order to check the capability of the semi-implicit scheme to deal with very low Mach number problems with very little numerical diffusion. The Gresho vortex is a stationary solution of the Euler equations. We run the test with different values of Mach number $M = 0.1, 0.01, 0.001$ in order to compare the results of the numerical scheme with the initial conditions. To perform this test we assume a square domain $\Omega = [-0.5, 0.5] \times [-0.5, 0.5]$ and we center the vortex to $(x, y) = (0, 0)$. The initial conditions of the problem in polar coordinates are given by:

$$\big(u_\phi(r), p(r)\big) = \begin{cases} \big(5r,\, p_0 + \frac{25}{2}r^2\big)\,, & 0 \le r < 0.2, \\ \big(2 - 5r,\, p_0 + \frac{25}{2}r^2 + 4(1 - 5r - \ln(0.2) + \ln(r))\big)\,, & 0.2 \le r < 0.4, \\ \big(0,\, p_0 - 2 + 4\ln(2)\big)\,, & 0.4 \le r. \end{cases}$$

where $p_0 = \rho/\gamma M^2$ and the density is constant $\rho = 1$ in the whole domain. We introduce a modified CFL number called $\mathrm{CFL}_{\mathrm{IM}}$ and we calculate the timestep as follows:

$$\Delta t = \mathrm{CFL}_{\mathrm{IM}} \frac{\Delta x}{\max |u| + \max |v|}. \tag{8.5}$$

The $\mathrm{CFL}_{\mathrm{IM}}$ number used for this test is 0.15 which corresponds to $\mathrm{CFL} = 170$ for $M = 0.001$. In Figures 8.12 and 8.13 we plot the pressure profiles at the center of the domain in both directions. We observe that the scheme preserves the stationary solution for a wide range of Mach numbers.

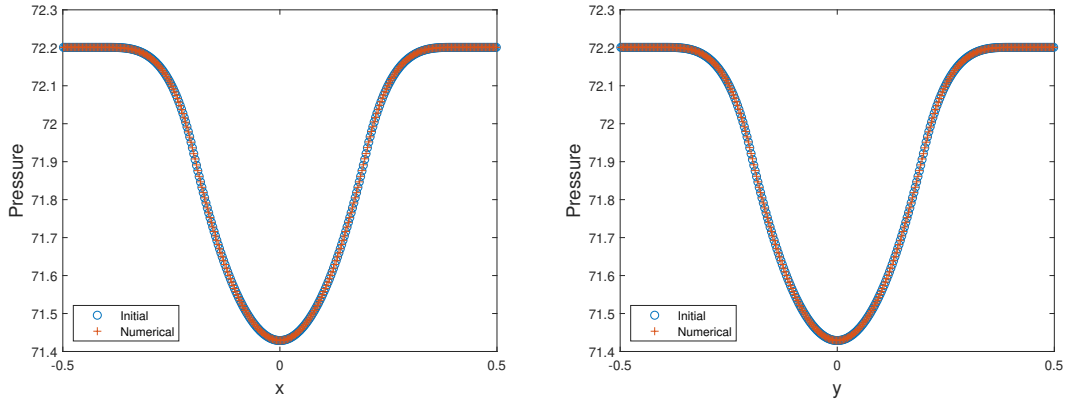

(a) x-direction. (b) y-direction.

FIGURE 8.12: Pressure Profiles, $M = 0.1$ at $T = 0.4\pi$ (320pts).

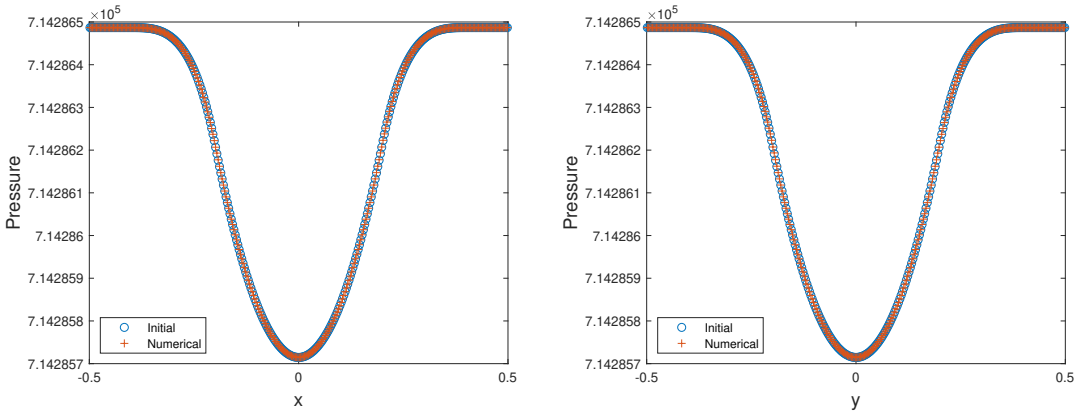

(a) x-direction. (b) y-direction.

FIGURE 8.13: Pressure Profiles, $M = 0.001$ at $T = 0.4\pi$ (320pts).

We perform a convergence test by computing the so-called EOC (experimental order of convergence). In order to compute the EOC we use as reference

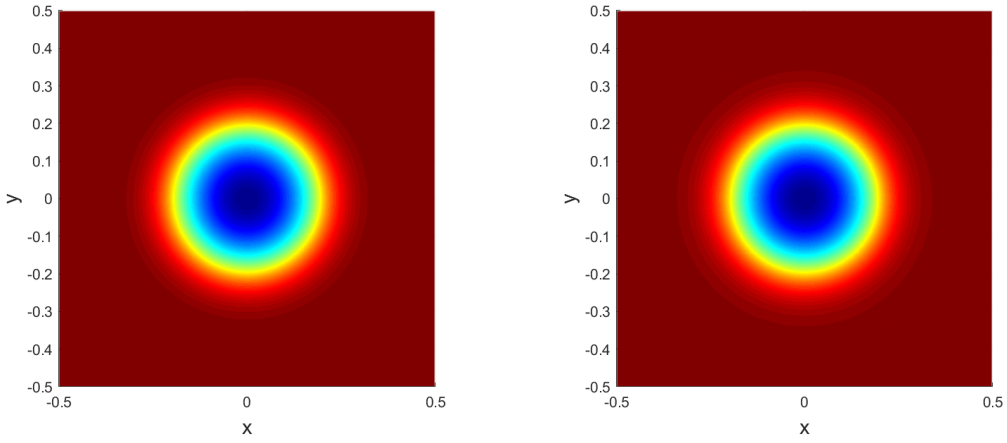

(a) Initial Conditions. (b) Final $T = 0.4\pi$.

FIGURE 8.14: Pseudocontour plot of pressure, $M = 0.1$ at $T = 0.4\pi$ (320pts).

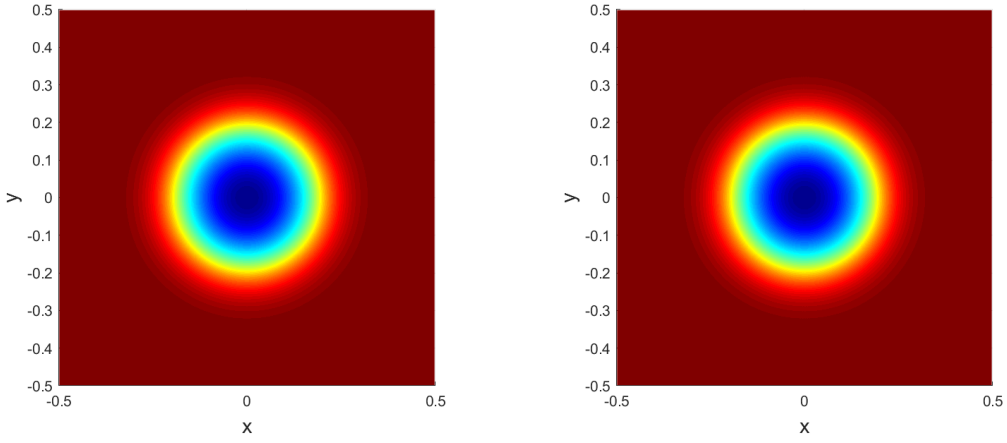

(a) Initial Conditions. (b) Final $T = 0.4\pi$.

FIGURE 8.15: Pseudocontour plot of pressure, $M = 0.001$ at $T = 0.4\pi$ (320pts).

solution the initial conditions of the problem. Thus we calculate the error by using the following formula:

$$e_N = \frac{||U_N - U_I||_{L^1}}{||U_I||_{L^1}}, \tag{8.6}$$

where U_N is the numerical solution calculated on a grid with $N \times N$ points and U_I is the initial condition of the problem taken as a reference solution. Then the EOC is calculated:

$$EOC := \log_2 \left(\frac{e_N}{e_{2N}} \right) \tag{8.7}$$

Pressure errors and the corresponding EOC for the Gresho vortex test are presented in table 8.1. We observe that for moderate to very low Mach number the convergence rate is close to second order, which is the formal order of the scheme. On the other hand, for intermediate values of the Mach number an order reduction is observed. The phenomenon of order reduction is typical of IMEX schemes applied to stiff problems, and has been analyzed in the context of hyperbolic systems with relaxation in several papers [17, 15]. In Figure 8.16 we plot the evolution of the kinetic energy $E_{Kin}(t)$, normalized with respect to the initial value $E_{Kin}(0)$, for two different meshes 40×40 (dotted line) and 80×80 (cross line) with $CFL_{IM} = 0.25$. For each mesh we use all the values of $M = 10^{-1}, 10^{-2}, 10^{-3}$ and we observe that the lines are indistinguishable. Finally, in Figure 8.17 we plot the percentage loss of the total kinetic energy at the final time. Here we use different CFL_{IM} numbers and we observe that the energy loss percent remains almost constant for each mesh regardless of the M and the CFL_{IM} number that we choose.

N	M=0.1 ($T = 0.4\pi$)		M=0.01 ($T = 0.4\pi$)		M=0.001 ($T = 0.4\pi$)	
	L^1 error	L^1 order	L^1 error	L^1 order	L^1 error	L^1 order
40	1.95e-04	-	3.38e-06	-	1.35e-07	-
80	5.50e-05	1.8277	3.80e-07	3.1549	3.72e-09	5.1851
160	1.77e-05	1.6380	1.21e-07	1.6455	1.03e-09	1.8525
320	4.24e-06	2.0586	7.97e-08	0.6079	2.75e-10	1.9018

TABLE 8.1: Convergence table for the Gresho vortex.

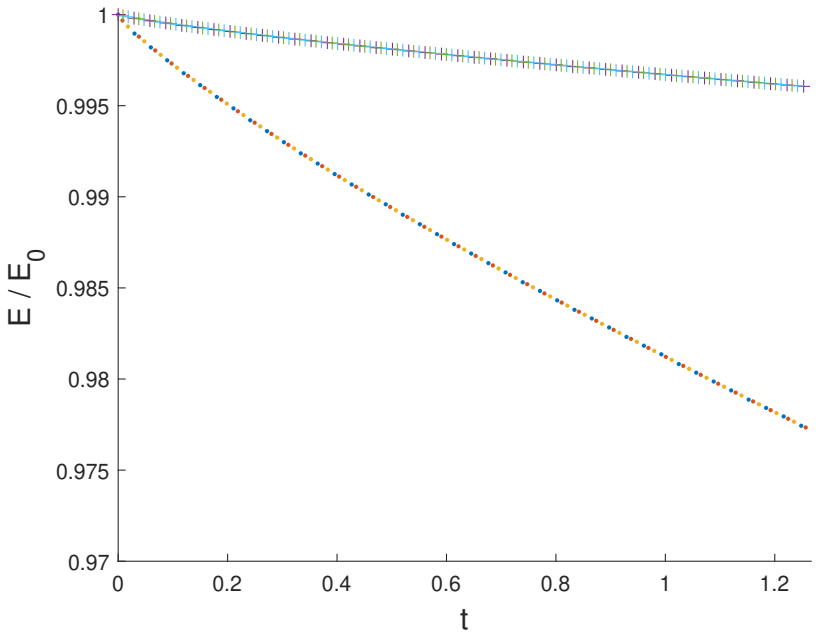

FIGURE 8.16: Evolution of the total Kinetic energy normalized with respect to the initial Kinetic energy. The dotted line is for the 40×40 grid and the cross line is for the 80×80 grid. We use $M = 10^{-1}, 10^{-2}, 10^{-3}$ for both meshes.

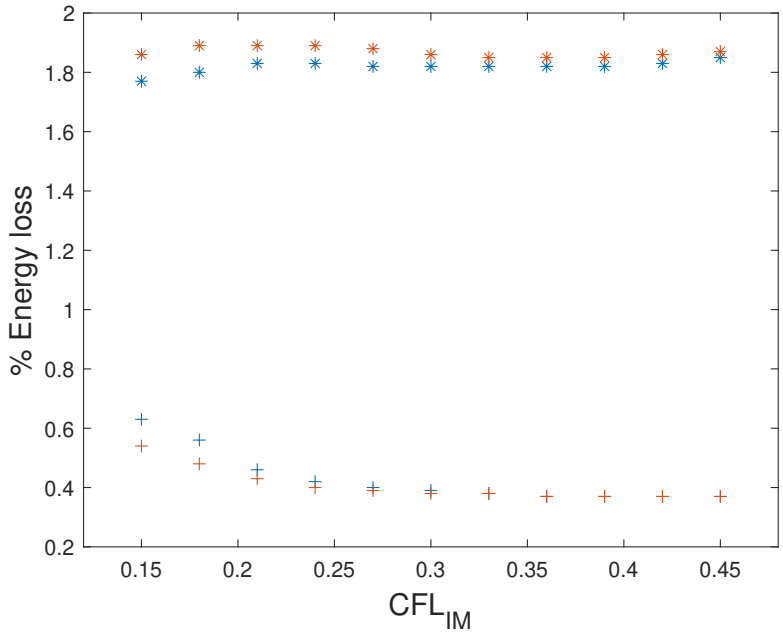

FIGURE 8.17: Percentage loss of the total Kinetic energy at the final time $T = 0.4\pi$ for $CFL_{IM} = 0.15 \ldots 0.45$ numbers. The star points are for the 40×40 grid and the cross points are for the 80×80 grid. We use $M = 10^{-1}$ (blue points) and $M = 10^{-3}$ (red points) for both meshes.

8.4 Double Vortex Sheet

Here we compare the result of the scheme to an accurate solution of incompressible Euler equations. This test was used before in some recent publications [18, 19, 5]. We use the same Low Mach number scaling for the equations as [18] and we introduce a parameter ϵ which is a global Mach number. System (6.1) becomes:

$$\begin{cases} \dfrac{\partial \rho}{\partial t} + \nabla \cdot \mathbf{m} = 0, \\ \dfrac{\partial \mathbf{m}}{\partial t} + \nabla \cdot \left(\dfrac{\mathbf{m} \otimes \mathbf{m}}{\rho} \right) + \dfrac{1}{\epsilon^2} \nabla p = 0, \\ \dfrac{\partial E}{\partial t} + \nabla \cdot (h\mathbf{m}) = 0, \end{cases} \tag{8.8}$$

where the enthalpy stands for:

$$h = \frac{(E+p)}{\rho} \tag{8.9}$$

and the equation of state (6.2) becomes:

$$p = (\gamma - 1)\left(E - \frac{\epsilon^2}{2}\rho(u^2 + v^2)\right). \tag{8.10}$$

The accurate reference solution is obtained by a Fourier-spectral method applied to incompressible Euler equations in the vorticity-stream function formulation. For more details we refer the reader to Appendix A.

The vorticity:

$$\omega = \frac{\partial v}{\partial x} - \frac{\partial u}{\partial y}, \tag{8.11}$$

is initialized as follows:

$$\omega(x,y,0) = \begin{cases} \delta\cos x - \dfrac{1}{\sigma}\operatorname{sech}^2((y-\pi/2)/\sigma)), & y \le \pi, \\ \delta\cos x - \dfrac{1}{\sigma}\operatorname{sech}^2((3\pi/2-y)/\sigma)), & y > \pi, \end{cases}$$

where $\delta = 0.05$ and $\sigma = \pi/15$.

The density and the pressure for this test are set equal to 1 on the whole domain and we assume periodic boundary conditions. The final time is $T = 6$, the $\mathrm{CFL}_{\mathrm{IM}}$ number is 0.35, corresponding to CFL $= 8.5$ ($\epsilon = 0.1$), and as reference solution (Figure 8.18f) we consider a very accurate solution obtained by Fourier spectral discretization in space and a fourth order Runge-Kutta method in time.

By comparing the reference solution with the solution obtained with the 2D scheme for the compressible Euler equations with exactly the same initial conditions as the incompressible case (Figure 8.18e), we observe that for small values of ϵ there is a qualitative agreement.

In Figure 8.19 we show the behavior of the L^1 norm as the difference between the velocities of the numerical solution of the compressible Euler equations and a reference solution of the incompressible Euler equations obtained by the aforementioned spectral method in a very fine grid. For this test we use $\sigma = \pi/10$ and the final time is $T = 1$.

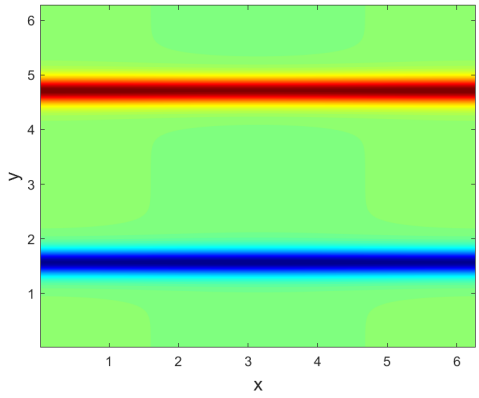

(a) Initial Conditions $T = 0$.

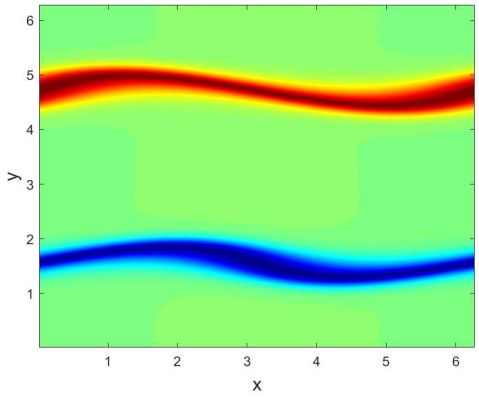

(b) Numerical solution at $T = 3$.

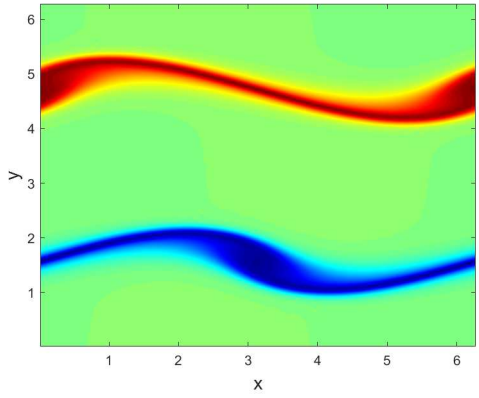

(c) Numerical solution at $T = 4$.

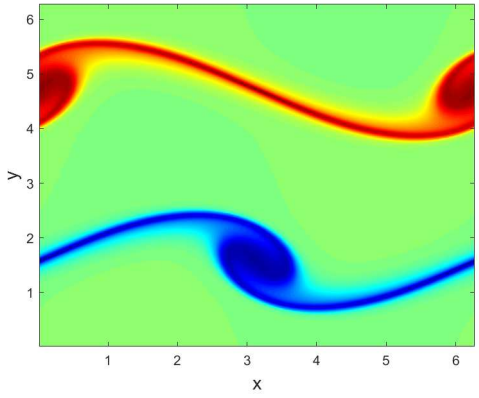

(d) Numerical solution at $T = 5$.

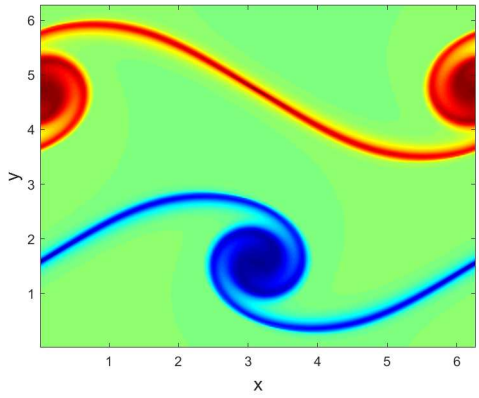

(e) Numerical solution at $T = 6$.

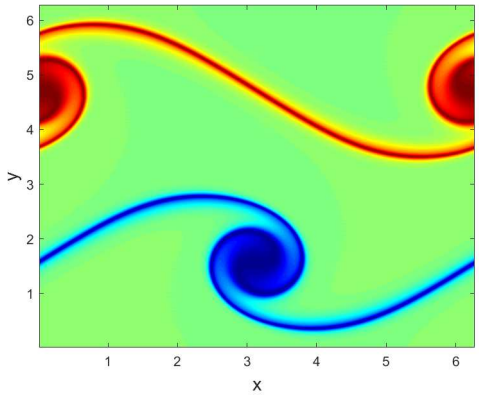

(f) Reference Solution.

FIGURE 8.18: Pseudo contour plot of Evolution of the Vortex Dipole with $\epsilon = 0.0001$ obtained on a 256×256 grid and comparison at the final time with the reference solution

The discrepancy between the two solutions is due to two causes: first, we are solving two different equations, compressible and incompressible Euler, so there is a difference between the two solutions, that we shall call modeling error which vanishes as the Mach number approaches zero. A second source of error is due to the finite size of the grid in space and time. We call this discretization error. For a coarse grid and relatively small Mach number, the discretization error is dominant, is almost independent of the Mach number, and decreases as the grid is refined, showing a second order accuracy in space and time. For fine enough meshes, the error saturates to an approximately constant value, which does no longer depend on the grid, but only on the Mach number, the modeling error.

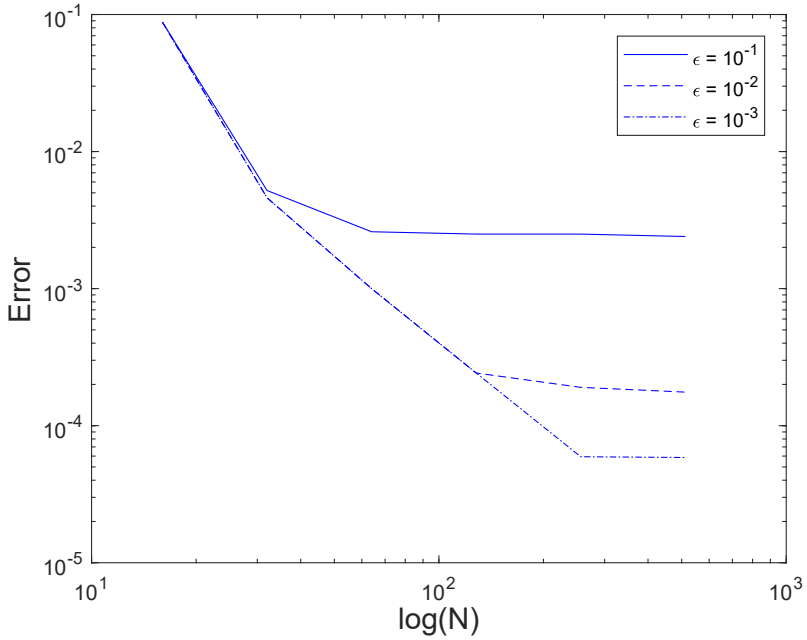

FIGURE 8.19: L^1 norm of the difference between the solution obtained by the 2D compressible Euler equations scheme and a reference solution of the incompressible Euler equations obtained by Fourier-spectral method and fourth order Runge-Kutta, as a function of the number of grid points per direction, for various Mach numbers.

Chapter 9

Conclusions for Euler Equations

We propose a novel all Mach number scheme for gas dynamics. The general idea is that explicit differential operators in space relative to convective or material speeds are discretized upwind. The linear implicit operators, pertaining to acoustic waves, are discretized by central differences. We have compared the results of such schemes on a series of one-dimensional test problems including classical shock tube tests in one and two dimensions. Also we have considered low-mach number acoustic wave propagation tests, Riemann tests, Gresho vortex and shear flow in the incompressible limit. We found that there is no scheme that outperforms the others over the whole Mach number range. In contrast, there exist implicit schemes that are robust enough to work in all regimes. Furthermore, for low-mach number flows, implicit schemes are far more accurate and efficient compared to explicit ones for given precision.

Chapter 10

Shallow Water Equations

At the second part of this thesis we are dealing with the shallow water equations and by extension with the Exner model. Our motivation occurs from the multiscale nature of the Exner model. In some cases when one is interested for the evolution of the sediment and being indifferent for the fully resolved water waves, by using the our scheme is able to use larger timesteps overpassing the classical CFL restriction. This has multiple advantages, starting from the efficiency of the scheme where the computational time is dramatically reduced. Moreover, numerical diffusion occurs when one uses explicit schemes and in the case of Exner model this affects the solution of the sediment. Here we manage to reduce the numerical diffusion on the solution by making less computations compared to an explicit scheme for a given runtime. In this Chapter we describe the derivation of the shallow water equations. In order to do this we must first derive the Navier-Stokes equations from the conservation laws. Then under certain assumptions and by following a procedure we derive the shallow water equations (for more details see [109]).

10.1 Conservation of Mass

By following the same procedure done in Section 2.1 we have:

$$\frac{\partial \rho}{\partial t} + \nabla \cdot (\mathbf{m}) = 0, \tag{10.1}$$

where $\mathbf{m} = \rho \mathbf{u}$ stands for the momentum.

10.2 Conservation of Linear Momentum

Let us now consider the linear momentum balance over a control volume W in the integral form:

$$\frac{\partial}{\partial t}\int_W \rho \mathbf{u} dV = -\int_{\partial W} (\rho \mathbf{u})\mathbf{u}\cdot\mathbf{n} dA + \int_W \rho \mathbf{b} dV + \int_{\partial W} \mathbf{T}\mathbf{n} dA \tag{10.2}$$

where $\mathbf{b}$ is the body force density per unit mass acting on the fluid, $\mathbf{T}$ is the Cauchy stress tensor and $\mathbf{n}$ the normal outward vector defined at each point of ∂W.

Using Gauss theorem we rewrite the Equation 10.2 in the following form:

$$\frac{\partial}{\partial t}\int_W \rho \mathbf{u} dV + \int_W \nabla\cdot(\rho\mathbf{u}\otimes\mathbf{u}) dV - \int_W \rho\mathbf{b} dV - \int_W \nabla\cdot\mathbf{T} dV = 0. \tag{10.3}$$

Under the assumption that the subregion W is fixed and does not change with time, Equation 10.3 becomes:

$$\int_W \left(\frac{\partial}{\partial t}(\rho\mathbf{u}) + \nabla\cdot(\rho\mathbf{u}\otimes\mathbf{u}) - \rho\mathbf{b} - \nabla\cdot\mathbf{T}\right) dV = 0. \tag{10.4}$$

Because the control volume W was arbitrary the integral vanishes and we obtain:

$$\frac{\partial}{\partial t}(\rho\mathbf{u}) + \nabla\cdot(\rho\mathbf{u}\otimes\mathbf{u}) - \rho\mathbf{b} - \nabla\cdot\mathbf{T} = 0. \tag{10.5}$$

In order to derive Navier-Stokes equations we assume that the density of fluid does not depends on pressure. Moreover the salinity of the fluid and the temperature are constant throughout the whole domain. Under these assumption we obtain that the fluid is incompressible and thus:

$$\begin{cases} \nabla\cdot\mathbf{u} = 0 \\ \dfrac{\partial}{\partial t}\rho\mathbf{u} + \nabla\cdot(\rho\mathbf{u}\otimes\mathbf{u}) = \rho\mathbf{b} + \nabla\cdot\mathbf{T} \end{cases} \tag{10.6}$$

Assuming that the fluid is Newtonian and that the body forces are essentially the gravity the System (10.6) becomes:

$$\begin{cases} \nabla \cdot \mathbf{u} = 0 \\ \dfrac{\partial}{\partial t}\rho\mathbf{u} + \nabla \cdot (\rho\mathbf{u} \otimes \mathbf{u} + pI) = \rho g\mathbf{k} \end{cases} \tag{10.7}$$

Let us write now the System (10.7) in a simplified form where the equation of the mass conservation becomes:

$$\frac{\partial}{\partial x}u + \frac{\partial}{\partial y}v + \frac{\partial}{\partial z}w = 0, \tag{10.8}$$

and the conservation of momentum:

$$\frac{\partial}{\partial t}(\rho u) + \frac{\partial}{\partial x}(\rho u^2) + \frac{\partial}{\partial y}(\rho uv) + \frac{\partial}{\partial z}(\rho uw) = -\frac{\partial p}{\partial x} \tag{10.9a}$$

$$\frac{\partial}{\partial t}(\rho v) + \frac{\partial}{\partial x}(\rho uv) + \frac{\partial}{\partial y}(\rho v^2) + \frac{\partial}{\partial z}(\rho vw) = -\frac{\partial p}{\partial y} \tag{10.9b}$$

$$\frac{\partial}{\partial t}(\rho w) + \frac{\partial}{\partial x}(\rho uw) + \frac{\partial}{\partial y}(\rho vw) + \frac{\partial}{\partial z}(\rho w^2) = -\frac{\partial p}{\partial z} - g \tag{10.9c}$$

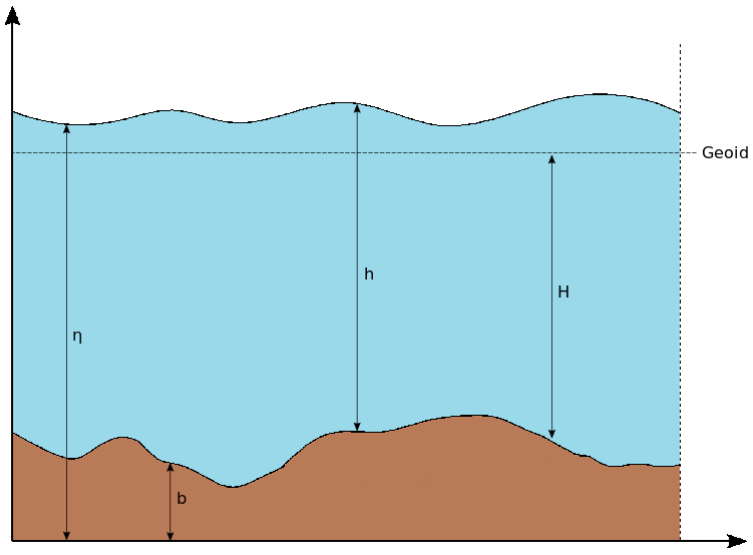

FIGURE 10.1: Water column

Due to the main condition for shallow-water model is that the horizontal length-scale far exceed the vertical length-scale, many terms in Eq. (3) can be neglected in such it reduces to the simple hydrostatic balance:

Now we assume that the horizontal wavelength-scale far exceed the vertical length-scale and the Equation (10.9c) becomes:

$$\frac{\partial}{\partial t}(\rho w) = -\frac{\partial p}{\partial z} - \rho g \tag{10.10}$$

Then we neglect vertical accelerations (i.e. is like a boundary layer method) and the Equation (10.10) reduces to the simple hydrostatic balance:

$$-\frac{\partial p}{\partial z} - \rho g = 0 \Leftrightarrow \frac{\partial p}{\partial z} = -\rho g. \tag{10.11}$$

Integrating the Equation (10.11) on gets:

$$p = \rho g(h - H - z) + p_0. \tag{10.12}$$

The vertical pressure gradients are almost hydrostatic ans the horizontal gradients are computed as:

$$\frac{\partial p}{\partial x} = -\rho g \frac{\partial}{\partial x}(h - H) \tag{10.13a}$$

$$\frac{\partial p}{\partial y} = -\rho g \frac{\partial}{\partial y}(h - H). \tag{10.13b}$$

Substituting the pressure terms in System (10.9) by using the Equations (10.13) we obtain:

$$\frac{\partial}{\partial t}(u) + \frac{\partial}{\partial x}(u^2) + \frac{\partial}{\partial y}(uv) + \frac{\partial}{\partial z}(uw) = -g\frac{\partial}{\partial x}(h - H) \tag{10.14a}$$

$$\frac{\partial}{\partial t}(v) + \frac{\partial}{\partial x}(uv) + \frac{\partial}{\partial y}(v^2) + \frac{\partial}{\partial z}(vw) = -g\frac{\partial}{\partial y}(h - H). \tag{10.14b}$$

Now under the main assumption of the SWE, that horizontal scales are much larger than vertical scales, we integrate the Equation (10.8) and we obtain:

$$\frac{\partial}{\partial t}h + \frac{\partial}{\partial x}(hu) + \frac{\partial}{\partial y}(hv) = 0. \tag{10.15}$$

Finally we can write the shallow water equations in two dimensions:

$$\begin{cases} \frac{\partial h}{\partial t} + \frac{\partial}{\partial x}(hu) + \frac{\partial}{\partial y}(hv) = 0, \\ \frac{\partial}{\partial t}(hu) + \frac{\partial}{\partial x}(hu^2 + \frac{1}{2}gh^2) + \frac{\partial}{\partial y}(huv) = -gh\frac{\partial b}{\partial x}, \\ \frac{\partial}{\partial t}(hv) + \frac{\partial}{\partial x}(huv) + \frac{\partial}{\partial y}(hv^2 + \frac{1}{2}gh^2) = -gh\frac{\partial b}{\partial y}. \end{cases} \tag{10.16}$$

In order to derive the one dimensional model, we set the derivatives with respect to y equal to zero and the velocity $v = 0$. Thus we obtain:

$$\begin{cases} \frac{\partial h}{\partial t} + \frac{\partial}{\partial x}(hu) = 0, \\ \frac{\partial}{\partial t}(hu) + \frac{\partial}{\partial x}(hu^2 + \frac{1}{2}gh^2) = -gh\frac{\partial b}{\partial x}. \end{cases} \tag{10.17}$$

10.3 Exner Model 1D

Let us now introduce the Exner model [44]. In order to describe the evolution of the sediment in a channel we use the shallow water equations but we add an extra equation for the sediment transport. This equation is the so-called Exner equation which stands for:

$$(z_b)_t + (q_b)_x = 0, \tag{10.18}$$

where z_b is the height of the sediment layer and q_b is the solid transport discharge parameter which for now is computed using the Grass model:

$$q_b = \xi A_g u \|u\|^{m-1} \tag{10.19}$$

where $1 \leq m \leq 4, 0 < A_g < 1$ and $\xi = 1/(1-\rho_0)$ where ρ_0 is the porosity of the sediment layer.

This equation gives an extra term at the shallow water equations which is nothing more than an extra bedload term. Adding this term we can rewrite the System (10.16) in the following form:

$$\begin{cases} \dfrac{\partial h}{\partial t} + \dfrac{\partial}{\partial x}(hu) = 0, \\ \dfrac{\partial}{\partial t}(hu) + \dfrac{\partial}{\partial x}(hu^2 + \dfrac{1}{2}gh^2) = -gh\dfrac{\partial b}{\partial x}, \\ \dfrac{\partial}{\partial t}(z_b) + \dfrac{\partial}{\partial x}(q_b) = 0. \end{cases} \tag{10.20}$$

10.4 Hyperbolicity for Exner Model 1D

Let us now proceed to the following analysis which was initially proposed in [92] and [95]. Additional articles which they deal with the hyperbolicity of the Exner mode are [33] and [36] We write the PDE System (11.10), by assuming for the sake of simplicity that the bottom topography is flat ($b_x = 0$), in the following non conservative form:

$$W_t + A(W)W_x = 0, \tag{10.21}$$

where:

$$W = \begin{pmatrix} h \\ q \\ z_b \end{pmatrix}, \qquad A(W) = \begin{pmatrix} 0 & 1 & 0 \\ gh - u^2 & 2u & gh \\ \alpha & \beta & 0 \end{pmatrix}$$

where $\alpha = \frac{\partial q_b}{\partial h}$ and $\beta = \frac{\partial q_b}{\partial q}$.

The system (11.10) is strictly hyperbolic if and only if, the characteristic polynomial:

$$p_\lambda(\lambda) = -\lambda\left((u-\lambda)^2 - gh\right) + gh(\beta\lambda + \alpha)$$

has three distinct roots such as $\lambda_1 < \lambda_2 < \lambda_3$.

The motivation for the derivation of the semi-implicit scheme was the nature of the system. Such eigenvalues represent the wavespeeds of the system. This multiscale nature of the equations inspired us to propose a semi-implicit scheme for the Exner model. By assuming that the interaction between the water and the sediment is weak, we are looking for the eigenvalue whose value is closer to zero. The wavespeed of the sediment is much smaller compared with the wavespeed of the water, therefore we assume that the corresponding eigenvalue for the sediment transport is the intermediate root λ_2 which is closer to zero. This analysis is essential in order

to minimize the numerical diffusion effect and optimize our scheme. Classical approaches for the numerical viscosity terms lead to a very diffusive solution for the sediment.

10.5 Exner Model 2D

Let us now describe he Exner model in two dimensions. The philosophy is the same as one dimension with the difference that extra terms occur in two dimensions. First we introduce the Exner equation for the sediment evolution:

$$(z_b)_t + (q_{b,x})_x + \left(q_{b,y}\right)_y = 0, \tag{10.22}$$

where z_b is the height of the sediment layer and qb_x, qb_y are the solid transport discharge parameters which are computed using the Grass model:

$$q_{b,x} = \xi A_g u \left(u^2 + v^2\right)^{\frac{m-1}{2}}, \tag{10.23a}$$

$$q_{b,y} = \xi A_g v \left(u^2 + v^2\right)^{\frac{m-1}{2}}. \tag{10.23b}$$

where $1 \leq m \leq 4, 0 < A_g < 1$ and $\xi = 1/\left(1 - \rho_0\right)$ where ρ_0 is the porosity of the sediment layer.

Recalling the shallow water equations in two dimensions, one write the Exner model:

$$\begin{cases} \dfrac{\partial h}{\partial t} + \dfrac{\partial}{\partial x}(hu) + \dfrac{\partial}{\partial y}(hv) = 0, \\ \dfrac{\partial}{\partial t}(hu) + \dfrac{\partial}{\partial x}(hu^2 + \dfrac{1}{2}gh^2) + \dfrac{\partial}{\partial y}(huv) = -gh\dfrac{\partial b}{\partial x}, \\ \dfrac{\partial}{\partial t}(hv) + \dfrac{\partial}{\partial x}(huv) + \dfrac{\partial}{\partial y}(hv^2 + \dfrac{1}{2}gh^2) = -gh\dfrac{\partial b}{\partial y}, \\ \dfrac{\partial h}{\partial t}\left(z_b\right) + \dfrac{\partial}{\partial x}\left(q_{b,x}\right) + \dfrac{\partial}{\partial y}\left(q_{b,y}\right) = 0. \end{cases} \tag{10.24}$$

10.6 Hyperbolicity for Exner Model 2D

Let us now do the same analysis as 1D for the eigenvalues of the system. The scope of this analysis is to identify the eigenvalues that are connected with the sediment evolution, because such values are very useful at the derivation of he semi-implicit scheme.

By assuming that the bottom topography is flat, the system (13.1) can be written in the following form:

$$W_t + A_1(W)W_x + A_2(W)W_y = 0,$$

where

$$W = \begin{pmatrix} h \\ \mathsf{m} \\ \mathsf{n} \\ z_b \end{pmatrix}, \qquad A_1(W) = \begin{pmatrix} 0 & 1 & 0 & 0 \\ gh - u^2 & 2u & 0 & gh \\ -uv & v & u & 0 \\ \alpha & \beta_1 & \beta_2 & 0 \end{pmatrix},$$

$$A_2(W) = \begin{pmatrix} 0 & 0 & 1 & 0 \\ -uv & v & u & 0 \\ gh - v^2 & 0 & 2v & gh \\ \gamma & \delta_1 & \delta_2 & 0 \end{pmatrix}.$$

Moreover $\alpha = \frac{\partial q_{b,x}}{\partial h}$, $\beta_1 = \frac{\partial q_{b,x}}{\partial \mathsf{m}}$ and $\beta_2 = \frac{\partial q_{b,x}}{\partial \mathsf{n}}$. Respectively, $\gamma = \frac{\partial q_{b,y}}{\partial h}$, $\delta_1 = \frac{\partial q_{b,y}}{\partial \mathsf{m}}$ and $\delta_2 = \frac{\partial q_{b,y}}{\partial \mathsf{n}}$.

Given an unitary vector $\mathbf{n} = (n_1, n_2)$ we define:

$$A(\mathbf{n}) = A_1 n_1 + A_2 n_2 \tag{10.25}$$

The system (13.1) is hyperbolic if for all unit vector $\mathbf{n}$, the matrix $A(\mathbf{n})$ has real eigenvalues and a complete set of eigenvectors [37].

In the case where $\mathbf{n} = (1, 0)$ the characteristic polynomial is defined:

$$p_\lambda(\lambda, \mathbf{n}) = -\lambda\left((u-\lambda)^2 - gh\right) + gh(\beta_1\lambda + \alpha + \beta_2 v)$$

while for $\mathbf{n} = (0, 1)$ one writes:

$$p_\mu(\mu, \mathbf{n}) = -\mu\left((v-\mu)^2 - gh\right) + gh(\delta_2\mu + \alpha + \delta_1 u)$$

The eigenvalues λ_2 and μ_2 are directly connected with the evolution of the sediment. These eigenvalues, later at the derivation of the semi-implicit scheme, are going to be used as viscosity parameters for the LLF fluxes.

Chapter 11

Semi-implicit Scheme for 1D Exner Model

In this chapter we present the semi-implicit scheme for the one dimensional shallow water equations. First we want to present a new technique which we are using. Keeping in mind the approximations described in in Chapter 3, we want to introduce a new reconstruction for the computation of the finite volume derivative that we use for the sediment evolution.

11.1 CWENO Reconstruction

Let us now describe the procedure of the CWENO reconstruction [80, 82, 81]. Our goal is to reconstruct the cell averages. First we introduce the meaning of the optimal polynomial on a cell j where:

$$P_j(x) = P_{OPT,j}(x), \tag{11.1}$$

where $P_{OPT,j}(x)$ is the parabola that interpolates the cell averages $\overline{u}^n_{j-1}, \overline{u}^n_j, \overline{u}^n_{j+1}$ in the cell $I_j := \left[x_{j-1/2}, x_{j+1/2}\right]$ where $x_j = jh$.

The polynomial is computed as follows:

$$P_{\mathrm{OPT},j}(x) = u^n_j + u'_j\left(x - x_j\right) + \frac{1}{2}u''_j\left(x - x_j\right)^2, \tag{11.2}$$

where:

$$
\begin{aligned}
u_j^n &= \overline{u}_j^n - \frac{1}{24}\left(\overline{u}_{j+1}^n - 2\overline{u}_j^n + \overline{u}_{j-1}^n\right), \\
u_j' &= \frac{\overline{u}_{j+1}^n - \overline{u}_{j-1}^n}{2\Delta x}, \\
u_j'' &= \frac{\overline{u}_{j-1}^n - 2\overline{u}_j^n + \overline{u}_{j+1}^n}{\Delta x^2}.
\end{aligned}
\tag{11.3}
$$

Moreover smoothness indicators are introduced in order to capture discontinuities. For this reason the methodology constructs an ENO interpolant as a convex combination of polynomials which are based on different stencils. For this reason, in the cell j one writes:

$$
P_j(x) = \sum_i w_i^j P_i^j(x), \quad \sum_i w_i^j = 1, \quad w_i \geq 0, \quad i \in \{\mathrm{L}, \mathrm{C}, \mathrm{R}\}
\tag{11.4}
$$

where P_R and P_L are linear functions made from the interpolation on the right and the left stencil respectively and P_C is a quadratic polynomial.

The polynomials P_R and P_L are defined as:

$$
\begin{aligned}
P_{\mathrm{R}}(x) &= \overline{u}_j^n + \frac{\overline{u}_{j+1}^n - \overline{u}_j^n}{\Delta x}\left(x - x_j\right), \\
P_{\mathrm{L}}(x) &= \overline{u}_j^n + \frac{\overline{u}_j^n - \overline{u}_{j-1}^n}{\Delta x}\left(x - x_j\right).
\end{aligned}
\tag{11.5}
$$

Finally the centered polynomial P_C is defined as:

$$
P_{\mathrm{OPT}}(x) = C_{\mathrm{L}} P_{\mathrm{L}}(x) + C_{\mathrm{R}} P_{\mathrm{R}}(x) + C_{\mathrm{C}} P_{\mathrm{C}}(x), \quad \sum_i C_i = 1, \quad i \in \{\mathrm{L}, \mathrm{C}, \mathrm{R}\}.
\tag{11.6}
$$

The choice of the coefficients C_i must be symmetric in order to provide the desired accuracy, i.e. in [80] the authors suggest that $C_L = C_R = 1/4$. Using these coefficients the centered polynomial is computed:

$$
P_{\mathrm{C}}(x) = 2P_{\mathrm{OPT}}(x) - \frac{1}{2}\left(P_{\mathrm{R}}(x) + P_{\mathrm{L}}(x)\right)
\tag{11.7}
$$

Now we have to define the weights, where:

$$w_i = \frac{\alpha_i}{\sum_k \alpha_k}, \quad \alpha_i = \frac{C_i}{(\varepsilon + IS_i)^p}, \quad i,k \in \{\mathrm{L},\mathrm{C},\mathrm{R}\}. \tag{11.8}$$

Finally smoothness indicators IS_i are introduced which are responsible for detecting discontinuities and are defined as:

$$\begin{aligned} IS_{\mathrm{L}} &= \left(\overline{u}_j^n - \overline{u}_{j-1}^n\right)^2, \\ IS_{\mathrm{R}} &= \left(\overline{u}_{j+1}^n - \overline{u}_j^n\right)^2, \\ IS_{\mathrm{C}} &= \frac{13}{3}\left(\overline{u}_{j+1}^n - 2\overline{u}_j^n + \overline{u}_{j-1}^n\right)^2 + \frac{1}{4}\left(\overline{u}_{j+1}^n - \overline{u}_{j-1}^n\right)^2. \end{aligned} \tag{11.9}$$

Using the aforementioned techniques we recall the Exner model in one dimension where:

$$\begin{cases} \dfrac{\partial h}{\partial t} + \dfrac{\partial}{\partial x}(hu) = 0, \\ \dfrac{\partial}{\partial t}(hu) + \dfrac{\partial}{\partial x}(hu^2 + \dfrac{1}{2}gh^2) = -gh\dfrac{\partial b}{\partial x}, \\ \dfrac{\partial}{\partial t}\left(z_b\right) + \dfrac{\partial}{\partial x}\left(q_b\right) = 0. \end{cases} \tag{11.10}$$

For the computation of the solid transport discharge term q_b we use the Grass model where:

$$q_b = \xi A_g u \|u\|^{m-1} \tag{11.11}$$

.

11.2 1st Order Discretization in Time

Let us discretize now the governing equations in time. We use backward differences over a time step Δt, thus the first-order accurate temporal discretization is given by:

$$\frac{U^{n+1} - U^n}{\Delta t} = \mathcal{H}\left(U^n, U^{n+1}\right), \tag{11.12}$$

where $n+1$ denotes the value at the next time step $t + \Delta t$. Now we have to describe the spatial discretization of the term $\mathcal{H}\left(U^n, U^{n+1}\right)$.

11.3 1st Order Discretization in Space

Now we introduce a scheme derived from an implicit treatment of the surface water waves, while the slow wave corresponding to sediment evolution is treated explicitly.

We introduce a new variable (see Figure 11.1).

$$\eta = h + b + z_b, \tag{11.13}$$

and combining (11.10) and (11.13) we obtain a new system:

$$\begin{cases} \dfrac{\partial \eta}{\partial t} + \dfrac{\partial}{\partial x}(q + q_b) = 0 \\ \dfrac{\partial q}{\partial t} + \dfrac{\partial}{\partial x}(qu) + gh\left(\dfrac{\partial \eta}{\partial x}\right) = 0 \\ \dfrac{\partial}{\partial t}(z_b) + \dfrac{\partial}{\partial x}(q_b) = 0. \end{cases} \tag{11.14}$$

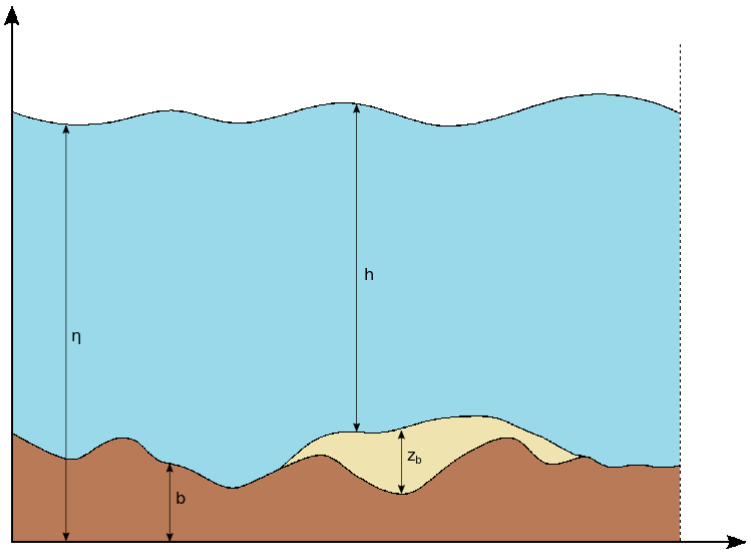

FIGURE 11.1: Water column with sediment layer

We denote by $\hat{D}_x$ the derivative that is treated explicitly using finite volume approximation and D_x the centred derivative. Then we discretize the system

(11.14) at a time interval $[t_n, t_{n+1}]$:

$$\begin{cases} \eta^{n+1} = \eta^n - \Delta t D_x(q_b^n) - \Delta t D_x(q^{n+1}) & \text{(11.15a)} \\ q^{n+1} = q^n - \Delta t \hat{D}_x(q^n u^n) - \Delta t (g h^n) D_x(\eta^{n+1}) & \text{(11.15b)} \\ z_b^{n+1} = z_b^n - \Delta t \hat{D}_x(q_b^n). & \text{(11.15c)} \end{cases}$$

Writing the Equation (11.15b) in the following form:

$$q^{n+1} = \underbrace{q^n - \Delta t \hat{D}_x(q^n u^n)}_{q^*} - \Delta t (g h^n) D_x(\eta^{n+1}). \tag{11.16}$$

Plugging (11.16) to (11.15a) we derive:

$$\eta^{n+1} = \underbrace{\eta^n - \Delta t D_x(q_b^n) - \Delta t D_x(q^*)}_{\eta^*} + g \Delta t^2 D_x(h^n D_x(\eta^{n+1})). \tag{11.17}$$

Posing for the sake of simplicity $k = g\left(\frac{\Delta t}{\Delta x}\right)^2$ we obtain from (11.17):

$$\eta_j^{n+1}\left(1 + k(h_{j+1/2} + h_{j-1/2})\right) - \eta_{j-1}^{n+1}\left(k h_{j-1/2}\right) - \eta_{j+1}^{n+1}\left(k h_{j+1/2}\right) = \eta_j^*. \tag{11.18}$$

This in an invertible linear system which can be solved to find η^{n+1}. Afterwards, q^{n+1} can be computed from (11.15b). The quantity z_b^{n+1} is computed explicitly from (11.15c) by using LLF scheme.

Here the key element is to find the appropriate value of numerical viscosity in the LLF flux. We are seeking for a value such as the numerical diffusion to be the least possible and the stability of the scheme is not affected. Using the analysis from 10.4 we are seeking for the intermediate eigenvalue λ_2, which is closer to zero, in order to be used as the numerical viscosity in the LLF flux. This root can be found easily by a root finding algorithm (Newton's method etc.) and used as the numerical viscosity parameter for the corresponding equation i.e. the sediment transport. Finally, h^{n+1} can be computed from (11.13).

11.4 Second order

In order to obtain a second order scheme in space we use a second order piecewise conservative linear reconstruction for the finite volume approximated derivative in the momentum equation, a third order CWENO reconstruction [**levy_puppo_russo_1999**] for the transport discharge term and classical three point central scheme for the rest. Second order in time is achieved through an implicit-explicit Runge-Kutta scheme initially proposed in [11]. Higher order extension can be done by using higher order reconstruction and higher order Runge-Kutta methods. On the other hand the nature of the semi-implicit scheme, where some derivatives are computed using centred approximations, may lead to some problems. An extension of the grid might bee needed for such cases. Fore the moment we limit ourselves to second order accuracy while we are using a CWENO3 reconstruction for the sediment in order to reduce the diffusion on this term. This third order reconstruction does not affect the efficiency and the speed of the computations because the gain that we achieve from the bigger timesteps is much bigger than this reconstruction step.

Chapter 12

Numerical Tests for 1D Exner Model

In these tests we check the ability of the scheme to compute the solution efficiently and fast. Our goal is to use a CFL number greater than one in order to reduce the computation time. To achieve the maximum CFL number, we have to avoid some small disturbances at the beginning of the test which can restrict us to smaller CFL numbers. To achieve that we do the following procedure. We assume that the sediment layer is fixed bathymetry and then we solve an explicit scheme with a very small CFL number until the system reaches a stationary solution. Finally, we use this solution as initial conditions for the semi implicit scheme.

In Figure 12.1a we have an original dummy set of initial conditions. By treating the sediment as bottom topography we initialize an explicit scheme. Once the explicit scheme reaches a stationary state we use this solution as initial condition for the semi implicit scheme 12.1b. We observe the difference at the water surface that makes the set of initial conditions appropriate in order to use higher CFL numbers while we avoid the small disturbances.

12.1 Transport of parabolic sediment layer

The domain here is $[0, 1000]$ and is discretized with 200 points. We initialize the test setting $\eta = 10$, $q = 10$, $b = 0$ and

$$z_b = \begin{cases} 0.1 + sin^2\left(\frac{\pi(x-300)}{200}\right), & 300 \leq x \leq 500 \\ 0.1, & \text{otherwise.} \end{cases}$$

The Grass model parameters are set to $A_g = 0.001$, $m_g = 3$ and $\rho_0 = 0.4$. CFL number is regulated to 7.5 corresponding to a material CFL of 0.77. The results shown at Figure 12.2 are obtained at the final time.

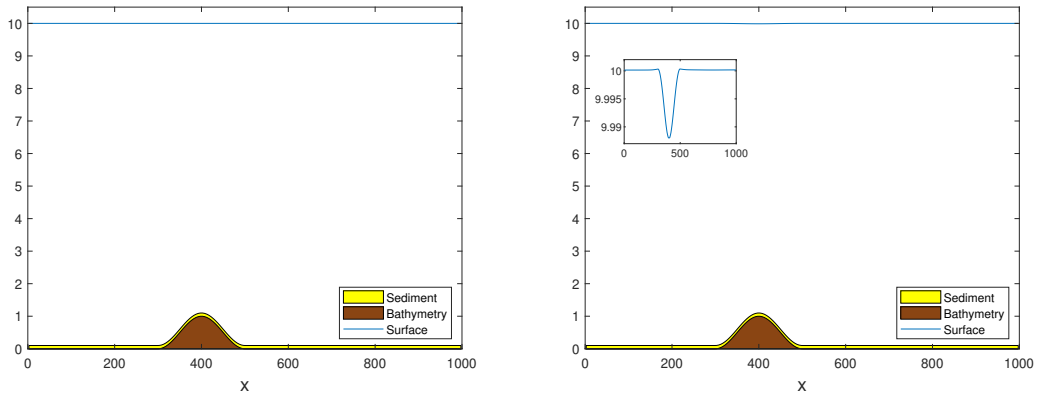

(a) Original initial conditions (b) Modified initial conditions

FIGURE 12.1: Initialization procedure for the semi implicit scheme in order to use higher CFL numbers.

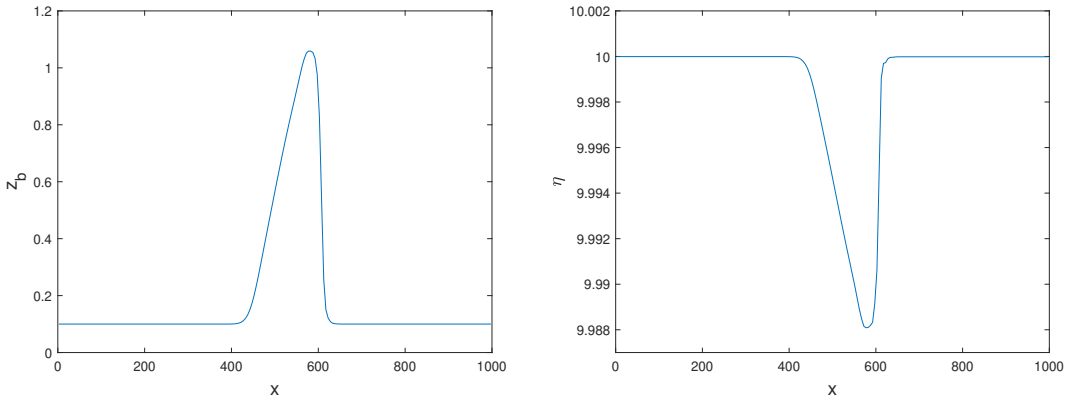

(a) Sediment (b) Surface

FIGURE 12.2: Parabolic sediment layer test results at the final time $t = 238000$.

We observe at the Figures 12.3 and 12.4 that the solution of the proposed semi implicit scheme introduces less dissipation compared with the explicit scheme. Moreover, the computational time is incomparable i.e. the semi implicit scheme computes the solution 22 time faster than the explicit scheme.

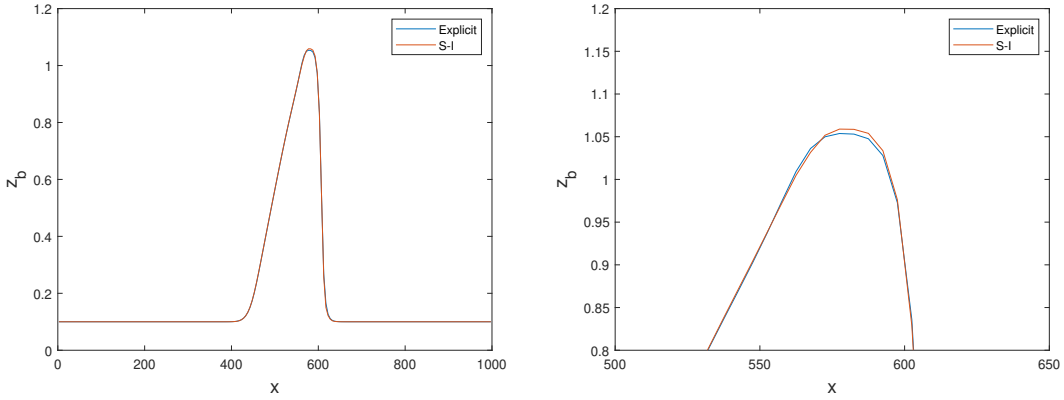

(a) Sediment (b) Zoomed sediment

FIGURE 12.3: Explicit scheme with CFL= 0.3 vs the Semi implicit scheme with CFL= 7.5. at the final time evaluated with 200 points.

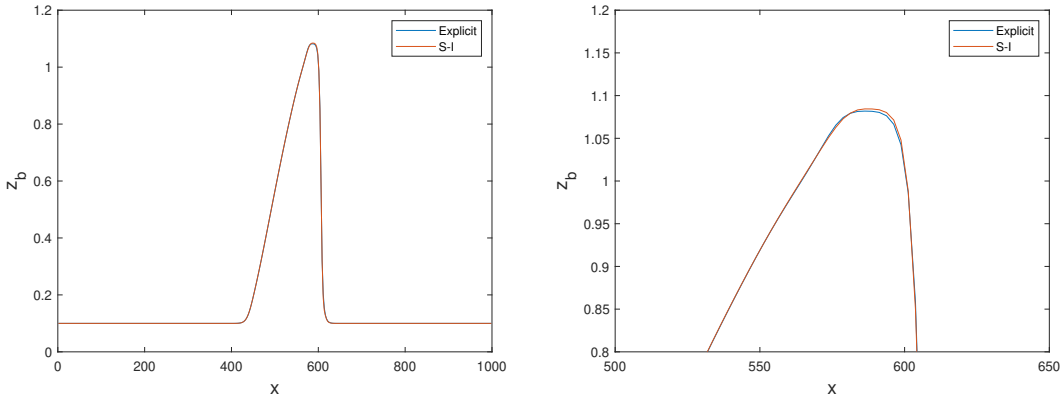

(a) Sediment (b) Zoomed sediment

FIGURE 12.4: Explicit scheme with CFL= 0.3 vs the Semi implicit scheme with CFL= 7.5. at the final time evaluated with 400 points.

Chapter 13

Semi-implicit Scheme for 2D Exner Model

We recall the Exner model in 2D, where:

$$\begin{cases} \dfrac{\partial h}{\partial t} + \dfrac{\partial \mathsf{m}}{\partial x} + \dfrac{\partial \mathsf{n}}{\partial y} = 0, & \text{(13.1a)} \\ \dfrac{\partial \mathsf{m}}{\partial t} + \dfrac{\partial}{\partial x}(\mathsf{m}u + \dfrac{1}{2}gh^2) + \dfrac{\partial}{\partial y}(\mathsf{m}v) = -gh\dfrac{\partial b}{\partial x}, & \text{(13.1b)} \\ \dfrac{\partial \mathsf{n}}{\partial t} + \dfrac{\partial}{\partial x}(\mathsf{n}u) + \dfrac{\partial}{\partial y}(\mathsf{n}v + \dfrac{1}{2}gh^2) = -gh\dfrac{\partial b}{\partial y}, & \text{(13.1c)} \\ \dfrac{\partial h}{\partial t}(z_b) + \dfrac{\partial}{\partial x}(q_{b,x}) + \dfrac{\partial}{\partial y}(q_{b,y}) = 0. & \text{(13.1d)} \end{cases}$$

where h is the water height, m and n are the water discharges in the x and y direction respectively. Moreover, $u = \frac{\mathsf{m}}{h}$ and $v = \frac{\mathsf{n}}{h}$ are the velocities, b is the bottom topography ($b_t = 0$).

Finally, z_b is the height of the sediment layer and $q_{b,x}$,$q_{b,y}$ are the solid transport discharge parameters which are computed using the Grass model:

$$q_{b,x} = \xi A_g u \left(u^2 + v^2\right)^{\frac{m-1}{2}} \tag{13.2}$$

$$q_{b,y} = \xi A_g v \left(u^2 + v^2\right)^{\frac{m-1}{2}} \tag{13.3}$$

where $1 \leq m \leq 4$, $0 < A_g < 1$ and $\xi = 1/(1-\rho_0)$ where ρ_0 is the porosity of the sediment layer.

13.1 CWENO Reconstruction

Now we want to describe a well known reconstruction technique, which was first introduced in **[levy_puppo_russo_1999]**, in order to derive the semi-implicit scheme for the Exner model. We use the same procedures described in Chapter 6 for the water column height and the momentum terms, while for the sediment evolution equation we introduce a new reconstruction procedure in two dimensions. Using the same notation as Section 11.1 we can write the reconstruction on a cell i, j as:

$$P_{i,j}(x,y) = \sum_k w_k^{i,j} P_k^{i,j}(x,y), \quad k \in \{\mathrm{NE}, \mathrm{NW}, \mathrm{SE}, \mathrm{SW}, \mathrm{C}\}, \tag{13.4}$$

where $\sum_k w_k^{i,j} = 1$.

We denote with $P_{\mathrm{NE}}, P_{\mathrm{NW}}, P_{\mathrm{SE}}$, and P_{SW} the one sided linear reconstructions while with P_{C} the centered quadratic reconstruction.

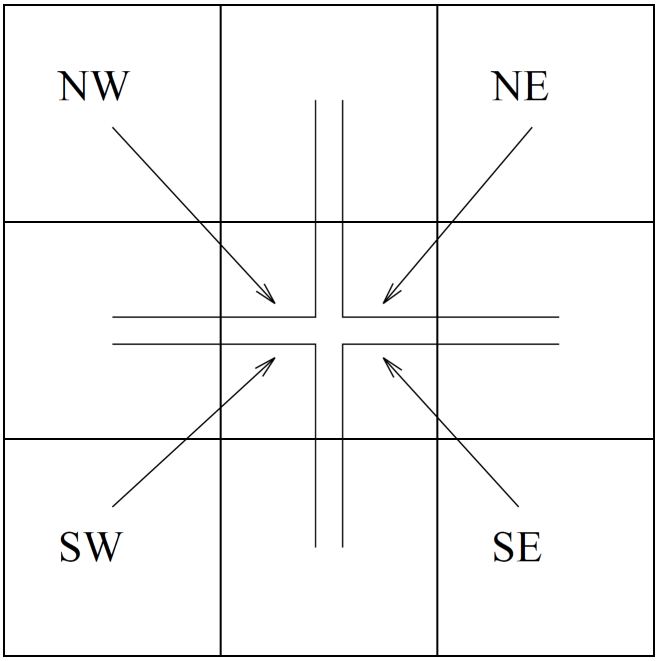

FIGURE 13.1: CWENO reconstruction 2D stencil.

The four linear one-sided reconstructions are given by:

$$
\begin{aligned}
P_{\mathrm{NE}}(x,y) &= \overline{u}^n_{i,j} + \frac{\overline{u}^n_{i+1,j} - \overline{u}^n_{i,j}}{\Delta x}(x - x_i) + \frac{\overline{u}^n_{i,j+1} - \overline{u}^n_{i,j}}{\Delta y}(y - y_j) \\
P_{\mathrm{NW}}(x,y) &= \overline{u}^n_{i,j} + \frac{\overline{u}^n_{i,j} - \overline{u}^n_{i-1,j}}{\Delta x}(x - x_i) + \frac{\overline{u}^n_{i,j+1} - \overline{u}^n_{i,j}}{\Delta y}(y - y_j) \\
P_{\mathrm{SW}}(x,y) &= \overline{u}^n_{i,j} + \frac{\overline{u}^n_{i,j} - \overline{u}^n_{i-1,j}}{\Delta x}(x - x_i) + \frac{\overline{u}^n_{i,j} - \overline{u}^n_{i,j-1}}{\Delta y}(y - y_j) \\
P_{\mathrm{SE}}(x,y) &= \overline{u}^n_{i,j} + \frac{\overline{u}^n_{i+1,j} - \overline{u}^n_{i,j}}{\Delta x}(x - x_i) + \frac{\overline{u}^n_{i,j} - \overline{u}^n_{i,j-1}}{\Delta y}(y - y_j).
\end{aligned}
\tag{13.5}
$$

Then the centred polynomial is defined such as:

$$
P_{\mathrm{OPT}}(x,y) = \sum_k C_k P_k(x,y), \quad k \in \{\mathrm{NE}, \mathrm{NW}, \mathrm{SE}, \mathrm{SW}, \mathrm{C}\}, \tag{13.6}
$$

where $\sum_k C_k = 1$.

Now we define the optimal polynomial which is computed as follows:

$$
\begin{aligned}
P_{\mathrm{OPT}}(x,y) = u^n_{i,j} + u'_{i,j}(x - x_i) + u^{\backprime}_{i,j}(y - y_j) + u^{\wedge}_{i,j}(x - x_i)(y - y_j) \\
+ \frac{1}{2}u''_{i,j}(x - x_i)^2 + \frac{1}{2}u^{\backprime\backprime}_{i,j}(y - y_j)^2
\end{aligned}
\tag{13.7}
$$

where:

$$
\begin{aligned}
u^n_{i,j} &= \overline{u}_{i,j} - \frac{1}{24}\left((\Delta x)^2 u''_{i,j} + (\Delta y)^2 u^{\backprime\backprime}_{i,j}\right) \\
u'_{i,j} &= \frac{\overline{u}^n_{i+1,j} - \overline{u}^n_{i-1,j}}{2\Delta x}, \quad u^{\backprime}_{i,j} = \frac{\overline{u}^n_{i,j+1} - \overline{u}^n_{i,j-1}}{2\Delta y} \\
u''_{i,j} &= \frac{\overline{u}^n_{i+1,j} - 2\overline{u}^n_{i,j} + \overline{u}^n_{i-1,j}}{\Delta x^2}, \quad u^{\backprime\backprime}_{i,j} = \frac{\overline{u}^n_{i,j+1} - 2\overline{u}^n_{i,j} + \overline{u}^n_{i,j-1}}{\Delta y^2} \\
u^{\wedge}_{i,j} &= \frac{\overline{u}^n_{i+1,j+1} + \overline{u}^n_{i-1,j-1} - \overline{u}^n_{i+1,j-1} - \overline{u}^n_{i-1,j+1}}{4\Delta x \Delta y}.
\end{aligned}
\tag{13.8}
$$

A possible choice of the parameters C_K in order to achieve a third-order reconstruction for the quarter cell-averages is $C_{\mathrm{NE}} = C_{\mathrm{NW}} = C_{\mathrm{SW}} = C_{\mathrm{SE}} =$

1/8 and finally $C_C = 1/2$. Using these constants and the Equation 13.6 one writes the central polynomial as follows:

$$P_C(x,y) = 2P_{OPT}(x,y) - \frac{1}{4}\left[P_{NE}(x,y) + P_{NW}(x,y) + P_{SW}(x,y) + P_{SE}(x,y)\right] \tag{13.9}$$

Now we define the weight where:

$$w_k^{i,j} = \frac{\alpha_k^{i,j}}{\sum_l \alpha_l^{i,j}}, \quad \alpha_k^{i,j} = \frac{C_k^{i,j}}{\left(\varepsilon + IS_k^{i,j}\right)^p}, \quad k,l \in \{\mathrm{NE},\mathrm{NW},\mathrm{SE},\mathrm{SW},\mathrm{C}\}. \tag{13.10}$$

At the end we have to compute the smoothness indicators which are responsible for the manipulation of the discontinuities. Assuming that $\Delta x = \Delta y = h$ one writes for the four one-sided linear reconstructions:

$$IS_k = h^2\left[\left(\hat{u}'\right)^2 + \left(\hat{u}'\right)^2\right], \tag{13.11}$$

while for the centered polynomial:

$$IS_C = h^2\left[\left(u'\right)^2 + \left(u`\right)^2\right] + \frac{h^4}{3}\left[13\left(u''\right)^2 + 14\left(u'`\right)^2 + 13\left(u``\right)^2\right]. \tag{13.12}$$

Now in the same philosophy as before, we introduce a new variable, namely:

$$\eta = h + b + z_b, \tag{13.13}$$

and combining (13.1) and (13.13) we obtain a new system:

$$\begin{cases} \dfrac{\partial \eta}{\partial t} + \dfrac{\partial}{\partial x}(\mathsf{m} + q_{b,x}) + \dfrac{\partial}{\partial y}(\mathsf{n} + q_{b,y}) = 0, \\ \dfrac{\partial \mathsf{m}}{\partial t} + \dfrac{\partial}{\partial x}(\mathsf{m}u) + \dfrac{\partial}{\partial y}(\mathsf{m}v) + gh\left(\dfrac{\partial \eta}{\partial x}\right) = 0, \\ \dfrac{\partial \mathsf{n}}{\partial t} + \dfrac{\partial}{\partial y}(\mathsf{n}v) + \dfrac{\partial}{\partial x}(\mathsf{n}u) + gh\left(\dfrac{\partial \eta}{\partial y}\right) = 0, \\ \dfrac{\partial h}{\partial t}(z_b) + \dfrac{\partial}{\partial x}(q_{b,x}) + \dfrac{\partial}{\partial y}(q_{b,y}) = 0. \end{cases} \tag{13.14}$$

13.2 1st Order Discretization in Time

Recalling the first order discretization in time from Section 3.5 we write the System (13.14)

$$\frac{U^{n+1} - U^n}{\Delta t} = \mathcal{H}\left(U^n, U^{n+1}\right), \tag{13.15}$$

where $n+1$ denotes the value at the next time step $t + \Delta t$. Now we are going to describe the spatial discretization of the term $\mathcal{H}\left(U^n, U^{n+1}\right)$.

13.3 1st Order Discretization in Space

Here we follow the same procedure as Chapter 11 in order to obtain a first order semi implicit scheme. In the same philosophy, we treat implicitly the fast surface water waves while the sediment which has a much smaller wave speed explicitly. By using the same notation where $\hat{D}_x$ is the derivative that is treated explicitly using finite volume approximation and D_x the centred derivative. By discretizing the system (13.14) at a time interval $[t_n, t_{n+1}]$ we obtain:

$$\begin{cases} \eta^{n+1} = \eta^n - \Delta t D_x(q^n_{b,x}) + \Delta t D_y(q^n_{b,y}) \\ \qquad\qquad - \Delta t D_x(\mathsf{m}^{n+1}) - \Delta t D_y(\mathsf{n}^{n+1}) & \text{(13.16a)} \\ \mathsf{m}^{n+1} = \mathsf{m}^n - \Delta t \hat{D}_x(\mathsf{m}^n u^n) - \Delta t \hat{D}_y(\mathsf{m}^n v^n) \\ \qquad\qquad - \Delta t (g h^n) D_x(\eta^{n+1}) & \text{(13.16b)} \\ \mathsf{n}^{n+1} = \mathsf{n}^n - \Delta t \hat{D}_y(\mathsf{n}^n v^n) - \Delta t \hat{D}_x(\mathsf{n}^n u^n) \\ \qquad\qquad - \Delta t (g h^n) D_y(\eta^{n+1}) & \text{(13.16c)} \\ z_b^{n+1} = z_b^n - \Delta t \hat{D}_x(q^n_{b,x}) - \Delta t \hat{D}_y(q^n_{b,y}). & \text{(13.16d)} \end{cases}$$

Plugging (13.16b) and (13.16c) to (13.16a) we derive:

$$\begin{aligned} \eta^{n+1} = \eta^n &- \Delta t D_x(q^n_{b,x}) - \Delta t D_y(q^n_{b,y}) \\ &- \Delta t D_x(\mathsf{m}^*) + g \Delta t^2 D_x(h^n D_x(\eta^{n+1})) \\ &- \Delta t D_y(\mathsf{n}^*) + g \Delta t^2 D_y(h^n D_y(\eta^{n+1})), \end{aligned} \tag{13.17}$$

where

$$\begin{aligned} \mathsf{m}^* &= \mathbf{m}^n - \Delta t \hat{D}_x(\mathsf{m}^n u^n) - \Delta t \hat{D}_y(\mathsf{m}^n v^n), \\ \mathsf{n}^* &= \mathbf{n}^n - \Delta t \hat{D}_y(\mathsf{n}^n v^n) - \Delta t \hat{D}_x(\mathsf{n}^n u^n). \end{aligned} \tag{13.18}$$

By posing

$$\eta^* = \eta^n - \Delta t D_x(q^n_{b,x}) - \Delta t D_y(q^n_{b,y}) - \Delta t D_x(\mathsf{m}^*) - \Delta t D_y(\mathsf{n}^*)$$

and by substituting $k_x = g\left(\frac{\Delta t}{\Delta x}\right)^2$ and $k_y = g\left(\frac{\Delta t}{\Delta y}\right)^2$ we obtain from (13.17):

$$\begin{aligned} &\eta^{n+1}_{i,j}\left(1 + k_x(h_{i,j+1/2} + h_{i,j-1/2}) + k_y(h_{i+1/2,j} + h_{i-1/2,j})\right) \\ &-\eta^{n+1}_{i,j-1}\left(k_x h_{i,j-1/2}\right) - \eta^{n+1}_{i,j+1}\left(k_x h_{i,j+1/2}\right) \\ &-\eta^{n+1}_{i-1,j}\left(k_y h_{i-1/2,j}\right) - \eta^{n+1}_{i+1,j}\left(k_y h_{i+1/2,j}\right) = \eta^*_j. \end{aligned} \tag{13.19}$$

This is a system of linear equations that can be solved in order to find η^{n+1}. Then, m^{n+1} and n^{n+1} are computed from (13.16b) and (13.16c) respectively. Moreover, the sediment evolution is computed explicitly from (13.16d).

Again, we are seeking for the appropriate viscosity parameters in the LLF fluxes that we use for the sediment evolution. The purpose of this scheme is to capture accurately the evolution of the sediment when the interaction is small. For this reason we assume that he corresponding numerical viscosity terms for the LLF fluxes in the x and y dimension are the eigenvalues closer to zero, i.e. λ_2 and μ_2 (see Section 10.6), due to the fact that the wave speed of the sediment is very small.

In order to compute these eigenvalues, we use an iterative root finding algorithm (for example Newton method). When we obtain the requested numerical viscosity terms, we compute the evolution of the sediment from (13.16d). Finally, h^{n+1} can be computed from (13.13).

13.4 Second order

Here, in order to achieve second order in space we use the same procedure. For the FV numerical approximation we use a piece-wise conservative linear reconstruction with minmod flux limiter. Moreover, because the scheme is mainly focused on the sediment evolution, we use a third order CWENO reconstruction just for the derivatives in (13.16d). Second order in time is achieved by using the same implicit-explicit Runge-Kutta scheme from [11].

Chapter 14

Numerical Tests for 2D Exner Model

In these tests we are checking our scheme in 2D. Again, in order to achieve the maximum CFL number that can be used for each test, we choose to initialize the tests by assuming that the sediment is not moving. We set the bottom topography as the sum of the sediment layer and the real bathymetry and we initialize the explicit solver. Once the explicit scheme reaches a stationary state we use this solution as initial conditions for the semi implicit scheme.

14.1 2D transport of parabolic sediment layer

This test is adopted from [37]. We use this test in order to compare the results obtain in the 1D case with 2D. We initialize this test by extending the parabolic shape of the sediment layer shown previously on Chapter 12.1 across the y axis. The same procedure can be done also in x axis, but for sake of simplicity we just present this case. The domain here is the square $[0, 1000] \times [0, 1000]$ and it's discretized with 10,000 finite volumes while the final time is $T = 238000$. We set the total water column height $\eta = 10$ and the bottom topography equal to zero. We initialize the flow by setting $\mathsf{m} = 10$ and $\mathsf{n} = 0$. Finally we set:

$$z_b = \begin{cases} 0.1 + sin^2\left(\frac{\pi(x-300)}{200}\right), & 200 \leq x \leq 300 \\ 0.1, & \text{otherwise.} \end{cases}$$

After the initialization with the explicit scheme we obtain the initial conditions for the semi implicit scheme depicted in Figure 14.1. The Grass parameters that we used for this test are $A_g = 0.001$, $m_g = 3$ and $\rho_0 = 0.4$. CFL

number is regulated to 10 corresponding to a material CFL of 0.55. The results at the final time $T = 238000$. By comparing the 1D with the 2D scheme, we observe at Figure 14.3 that evolution of the sediment and the water column height are almost indistinguishable.

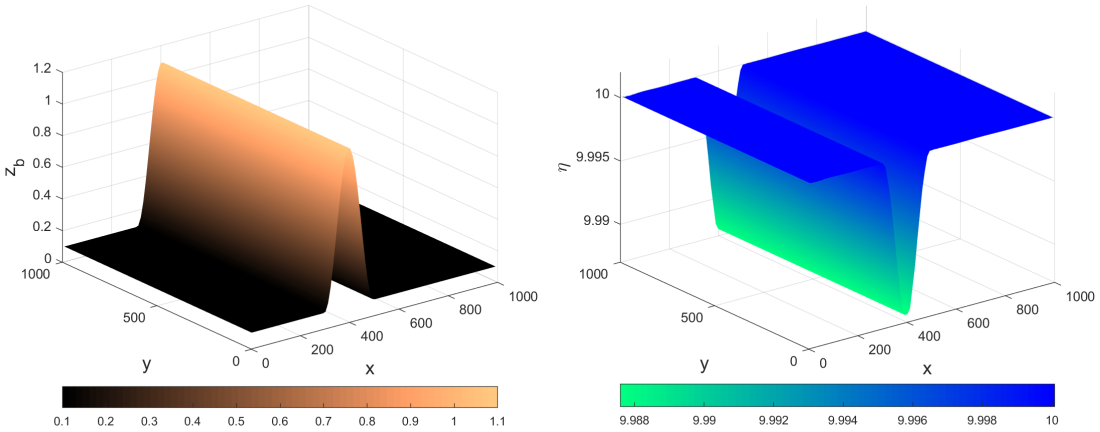

(a) Sediment (b) Surface

FIGURE 14.1: 2D parabolic sediment layer initial conditions.

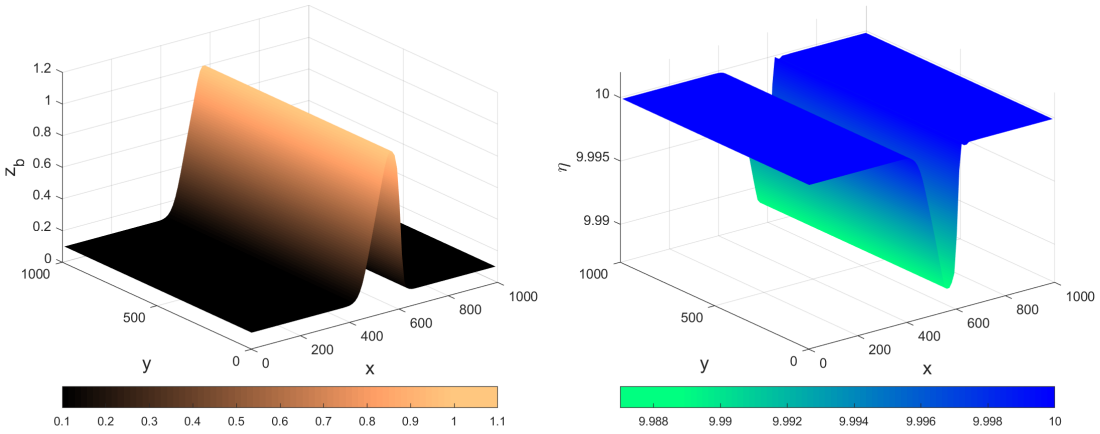

(a) Sediment (b) Surface

FIGURE 14.2: 2D parabolic sediment layer test results at the final time $t = 238000$.

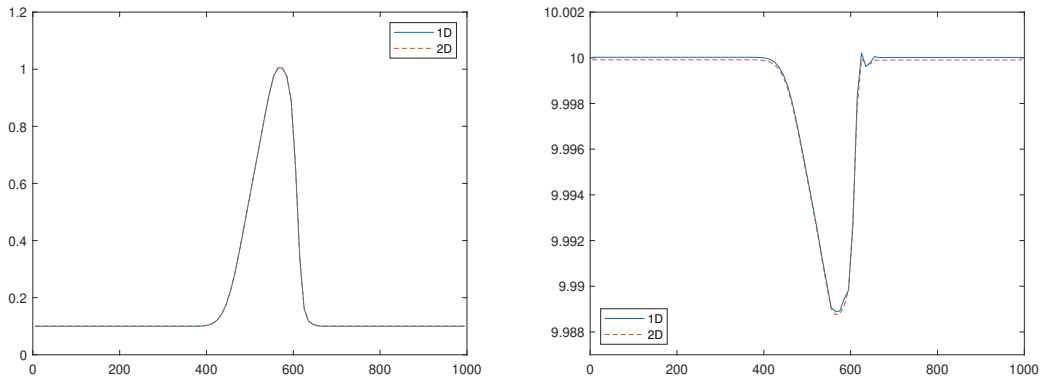

(a) Sediment (b) Surface

FIGURE 14.3: 1D vs. 2D parabolic sediment layer test results at the final time $t = 238000$.

14.2 Conical dune

This test was initially proposed in [60]. It's purely 2D test which can be initialized with various values of A_g in order the check the ability of the proposed scheme on capturing the sediment evolution accurately even if the water and the sediment interact fast. For this reason we run the test with two different values of A_g. The test is initialized by setting $\eta = 10$, $\mathsf{m} = 10$ and $\mathsf{n} = 0$. The sediment layer is initialized as follows:

$$z_b = \begin{cases} 0.1 + sin^2\left(\frac{\pi(x-300)}{200}\right) sin^2\left(\frac{\pi(y-400)}{200}\right), & 200 \leq x \leq 300, \\ & 400 \leq y \leq 600, \\ 0.1, & \text{otherwise.} \end{cases}$$

Again, we use an explicit scheme to initialize properly the test in order to avoid small disturbances at the water surface. After a stationary state is reached we have the well prepared initial conditions for the semi implicit scheme Figure 14.4.

First we initialize the test on a 100×100 numerical grid and we set the Grass model parameters $A_g = 0.001$, $m_g = 3$ and the porosity $\rho_0 = 0.4$. The final time for this test is $T = 360000$ and the results are shown in Figure 14.5.

Finally we use exactly the same initial conditions, but here we set $A_g = 1$ which represents a strong interaction between the sediment and the water. For this reason the final time here is $T = 500$. The results are shown on Figure 14.6

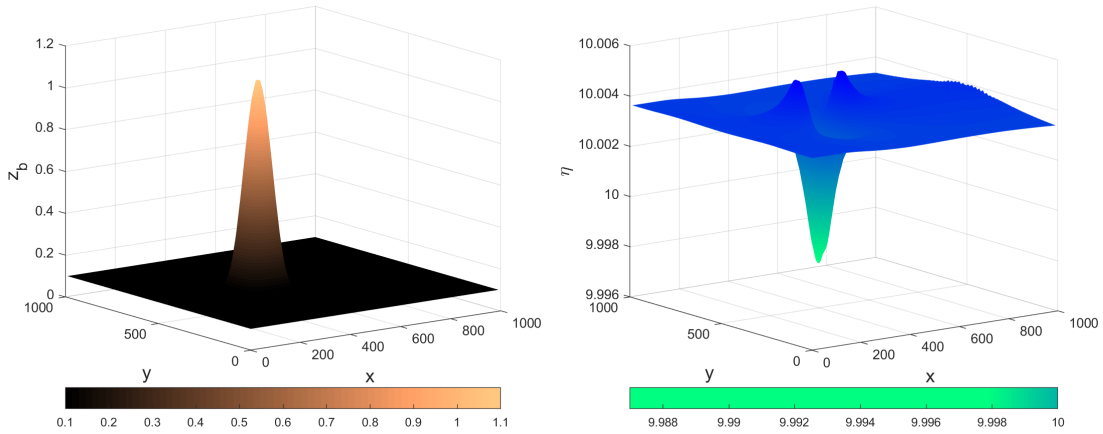

(a) Sediment (b) Surface

FIGURE 14.4: Initial conditions of conical dune test case

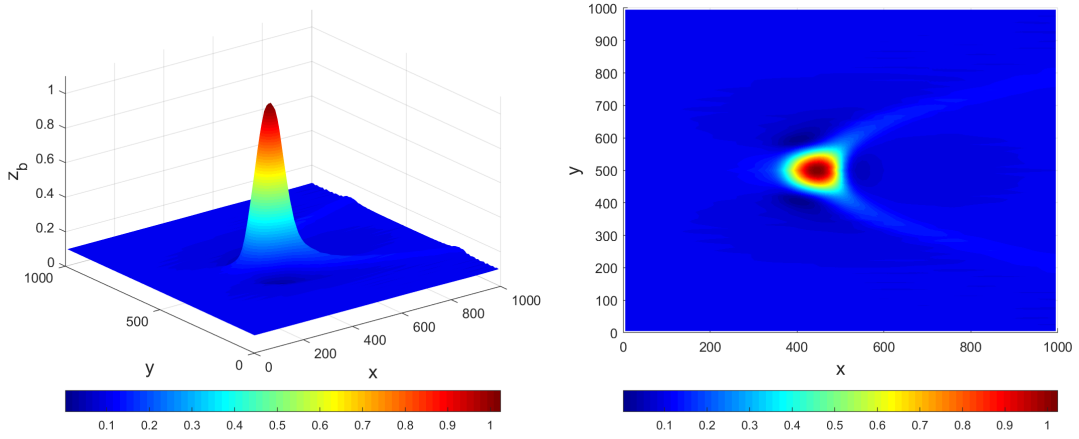

(a) Sediment (b) Sediment top view

FIGURE 14.5: Conical dune test case at the final time $T = 360000$ with small interaction $A_g = 0.001$.

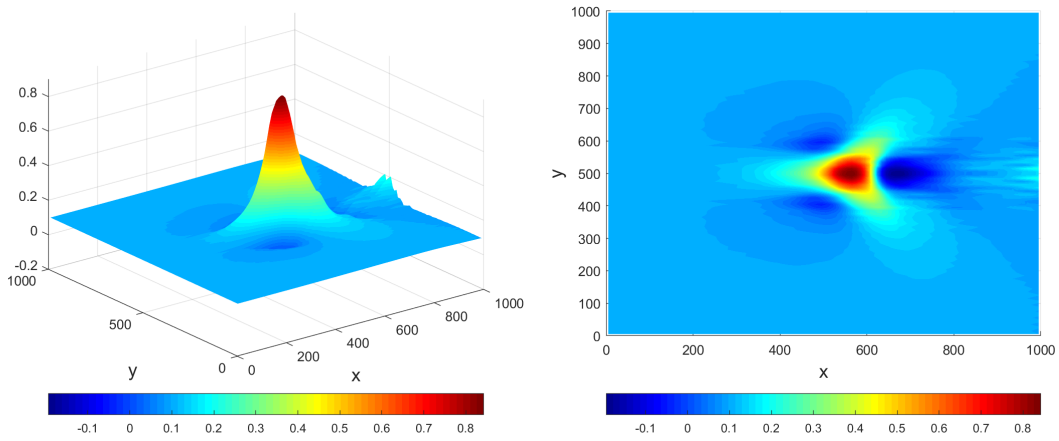

(a) Sediment (b) Sediment top view

FIGURE 14.6: Conical dune test case at the final time $T = 500$ with strong interaction $A_g = 1$.

Chapter 15

Conclusions for Exner Model

We propose an efficient fast and very robust scheme. Motivated from the multiscale nature of the Exner model we built a scheme that is focused on the sediment evolution. Moreover the scheme can be used (with the classical CFL condition) for the evolution of the fast water waves if one is interested for the surface waves. Bigger CFL numbers can be used when one is interested for the sediment layer evolution and this leads to less diffusive results while explicit schemes, which obey the classical CFL condition, suffer from numerical dissipation. We managed to achieve a remarkable decrease at the computation time while we observe less dissipation in the solution.

Appendix A

Fourier-Spectral Method

Here we briefly describe the Fourier-spectral method that we used in Section 8.4. We assume the problem is in a domain $[0, 2\pi]^2$, with periodic boundary conditions.

The vorticity satisfies the equation

$$\frac{\partial \omega}{\partial t} + \mathbf{u} \cdot \nabla \omega = 0. \tag{A.1}$$

Because $\nabla \cdot \mathbf{u} = 0$ there exists a stream function ψ such that:

$$\mathbf{u} = \left(-\frac{\partial \psi}{\partial y}, \frac{\partial \psi}{\partial x} \right).$$

Plugging this expression into Eq.(8.11) we obtain the Poisson equation for ψ:

$$-\Delta \psi = \omega. \tag{A.2}$$

The Fourier-spectral method works as follows: let Ω be a discretisation of ω on a $M \times M$ grid. Then Ω satisfies the system of ODE's:

$$\frac{d\Omega}{dt} = F(\Omega). \tag{A.3}$$

The right hand side is computed as follows: First compute the Fast Fourier Transform of Ω as

$$\hat{\Omega}(k_x, k_y) = \mathcal{F}(\Omega, k_x, k_y).$$

Then compute the Fourier transform $\hat{\psi}$ of ψ from the Poisson equation (A.2):

$$\hat{\psi} = \hat{\Omega} / (k_x^2 + k_y^2).$$

where we note that $\hat{\Omega}(0,0) = 0$ because Ω has zero mean. The two components of the velocity, U, V, are given by:

$$U = \mathcal{F}^{-1}(-ik_y\hat{\psi}), \quad V = \mathcal{F}^{-1}(ik_x\hat{\psi}).$$

The space derivatives of Ω are given by:

$$\Omega_x = \mathcal{F}^{-1}(ik_x\hat{\Omega}), \quad \Omega_y = \mathcal{F}^{-1}(ik_y\hat{\Omega})$$

Finally, the right hand side of Eq.(A.3) is given by

$$F = -(U\Omega_x + V\Omega_y). \tag{A.4}$$

System (A.3) can then be solved by an accurate ODE solver.

Bibliography

[1] Emanuela Abbate, Angelo Iollo, and Gabriella Puppo. "An all-speed relaxation scheme for gases and compressible materials". In: *Journal of Computational Physics* 351 (2017), pp. 1 –24. ISSN: 0021-9991. DOI: https://doi.org/10.1016/j.jcp.2017.08.052. URL: http://www.sciencedirect.com/science/article/pii/S0021999117306332.

[2] Rémi Abgrall. "How to Prevent Pressure Oscillations in Multicomponent Flow Calculations: A Quasi Conservative Approach". In: *Journal of Computational Physics - J COMPUT PHYS* 125 (Apr. 1996), pp. 150–160. DOI: 10.1006/jcph.1996.0085.

[3] Ann S Almgren et al. "Low Mach number modeling of type Ia supernovae. I. Hydrodynamics". In: *The Astrophysical Journal* 637.2 (2006), p. 922.

[4] Uri M Ascher, Steven J Ruuth, and Raymond J Spiteri. "Implicit-explicit Runge-Kutta methods for time-dependent partial differential equations". In: *Applied Numerical Mathematics* 25.2 (1997), pp. 151–167.

[5] Stavros Avgerinos et al. "Linearly implicit all Mach number shock capturing schemes for the Euler equations". In: *Journal of Computational Physics* 393 (2019), pp. 278 –312. ISSN: 0021-9991. URL: http://www.sciencedirect.com/science/article/pii/S0021999119302530.

[6] Silvia Bertoluzza et al. *Numerical Solutions of Partial Differential Equations*. Jan. 2009. ISBN: 978-3-7643-8939-0. DOI: 10.1007/978-3-7643-8940-6.

[7] G. Bispen. "IMEX finite volume methods for the shallow water equations". In: *Ph.D. thesis, Johannes Gutenberg-Universität* (2015).

[8] S. Boscarino, G. Russo, and L. Scandurra. "All Mach Number Second Order Semi-Implicit Scheme for the Euler Equations of Gasdynamics". In: (2017).

[9] Sebastiano Boscarino. "On an accurate third order implicit-explicit Runge–Kutta method for stiff problems". In: *Applied Numerical Mathematics* 59.7 (2009), pp. 1515–1528.

[10] Sebastiano Boscarino, Francis Filbet, and Giovanni Russo. "High order semi-implicit schemes for time dependent partial differential equations". In: *Journal of Scientific Computing* (2016), pp. 1–27.

[11] Sebastiano Boscarino, Francis Filbet, and Giovanni Russo. "High Order Semi-implicit Schemes for Time Dependent Partial Differential Equations". In: *Journal of Scientific Computing* 68.3 (2016), pp. 975–1001. ISSN: 1573-7691. DOI: 10.1007/s10915-016-0168-y.

[12] Sebastiano Boscarino, Philippe G LeFloch, and Giovanni Russo. "High-order asymptotic-preserving methods for fully nonlinear relaxation problems". In: *SIAM Journal on Scientific Computing* 36.2 (2014), A377–A395.

[13] Sebastiano Boscarino, Lorenzo Pareschi, and Giovanni Russo. "Implicit-explicit Runge–Kutta schemes for hyperbolic systems and kinetic equations in the diffusion limit". In: *SIAM Journal on Scientific Computing* 35.1 (2013), A22–A51.

[14] Sebastiano Boscarino and Giovanni Russo. "Flux-explicit IMEX Runge–Kutta schemes for hyperbolic to parabolic relaxation problems". In: *SIAM Journal on Numerical Analysis* 51.1 (2013), pp. 163–190.

[15] Sebastiano Boscarino and Giovanni Russo. "Implicit-Explicit Runge-Kutta schemes for hyperbolic systems with stiff relaxation and applications". In: (June 2013).

[16] Sebastiano Boscarino and Giovanni Russo. "On a class of uniformly accurate IMEX Runge-Kutta schemes and applications to hyperbolic systems with relaxation". In: *SIAM Journal on Scientific Computing* 31.3 (2009), pp. 1926–1945.

[17] Sebastiano Boscarino and Giovanni Russo. "On a Class of Uniformly Accurate IMEX Runge–Kutta Schemes and Applications to Hyperbolic Systems with Relaxation". In: *SIAM J. Scientific Computing* 31 (Jan. 2009), pp. 1926–1945. DOI: 10.1137/080713562.

[18] Sebastiano Boscarino, Giovanni Russo, and Leonardo Scandurra. "All Mach Number Second Order Semi-implicit Scheme for the Euler Equations of Gas Dynamics". In: *Journal of Scientific Computing* 77.2 (Nov. 2018), pp. 850–884. DOI: 10.1007/s10915-018-0731-9.

[19] Sebastiano Boscarino et al. "A high order semi-implicit IMEX WENO scheme for the all-Mach isentropic Euler system". In: *Journal of Computational Physics* 392 (May 2019). DOI: 10.1016/j.jcp.2019.04.057.

[20] Sebastiano Boscarino et al. "On linearly implicit IMEX Runge-Kutta methods for degenerate convection-diffusion problems modeling polydisperse sedimentation". In: *Bulletin of the Brazilian Mathematical Society, New Series* 47.1 (2016), pp. 171–185.

[21] Christopher A. Kennedy Carpenter and Mark H. "Additive Runge-Kutta Schemes for Convection-Diffusion-Reaction Equations". In: *Applied Numerical Mathematics* 44 (2003), pp. 139–181.

[22] V. Casulli and D. Greenspan. "Pressure method for the numerical solution of transient, compressible fluid flows". In: *International Journal for Numerical Methods in Fluids* 4.11 (1984), pp. 1001–1012. DOI: 10.1002/fld.1650041102.

[23] Gui Qiang Chen, C David Levermore, and Tai-Ping Liu. "Hyperbolic conservation laws with stiff relaxation terms and entropy". In: *Communications on Pure and Applied Mathematics* 47.6 (1994), pp. 787–830.

[24] Alexandre J. Chorin. "Numerical solution of the Navier-Stokes equations". In: *Mathematics of Computation* 22 (1968), pp. 745–762.

[25] Alexandre J. Chorin and Jerrold E. Marsden. *A Mathematical Introduction to Fluid Mechanics*. Texts in Applied Mathematics. Springer New York, 2013. ISBN: 9781461208839. URL: https://books.google.gr/books?id=HBXSBwAAQBAJ.

[26] F Coquel et al. "Lagrange-projection scheme for two-phase flows 1. Applications to realistic test cases". In: *PAMM* 7.1 (2007), pp. 2020021–2020022.

[27] Frédéric Coquel et al. "Entropy-satisfying relaxation method with large time-steps for Euler IBVPs". In: *Mathematics of Computation* 79.271 (2010), pp. 1493–1533.

[28] Frédéric Coquel et al. "Large time step positivity-preserving method for multiphase flows". In: *Hyperbolic Problems: Theory, Numerics, Applications*. Springer Berlin Heidelberg, 2008, pp. 849–856.

[29] Frédéric Coquel et al. "Local time stepping applied to implicit-explicit methods for hyperbolic systems". In: *Multiscale Modeling & Simulation* 8.2 (2010), pp. 540–570.

[30] Frédéric Coquel et al. "Local time stepping with adaptive time step control for a two-phase fluid system". In: *ESAIM: Proceedings*. Vol. 29. EDP Sciences. 2009, pp. 73–88.

[31] Frédéric Coquel et al. "Multiresolution technique and explicit–implicit scheme for multicomponent flows". In: *Journal of Numerical Mathematics jnma* 14.3 (2006), pp. 187–216.

[32] Floraine Cordier, Pierre Degond, and Anela Kumbaro. "An Asymptotic-Preserving all-speed scheme for the Euler and Navier–Stokes equations". In: *Journal of Computational Physics* 231.17 (2012), pp. 5685 – 5704. ISSN: 0021-9991. DOI: 10.1016/j.jcp.2012.04.025.

[33] S. Cordier, M.H. Le, and T. Morales de Luna. "Bedload transport in shallow water models: Why splitting (may) fail, how hyperbolicity (can) help". In: *Advances in Water Resources* 34.8 (2011), pp. 980 –989. ISSN: 0309-1708. DOI: https://doi.org/10.1016/j.advwatres.2011.05.002. URL: http://www.sciencedirect.com/science/article/pii/S0309170811000935.

[34] G. Costigan and P.B. Whalley. "Measurements of the speed of sound in air-water flows". In: *Chemical Engineering Journal* 66.2 (1997), pp. 131 –135. ISSN: 1385-8947. DOI: http://dx.doi.org/10.1016/S1385-8947(96)03169-5. URL: http://www.sciencedirect.com/science/article/pii/S1385894796031695.

[35] R. Courant and K. O. Friedrichs. *Supersonic flow and shock waves*. 1948.

[36] M.J. Castro Díaz, E.D. Fernández-Nieto, and A.M. Ferreiro. "Sediment transport models in Shallow Water equations and numerical approach by high order finite volume methods". In: *Computers & Fluids* 37.3 (2008), pp. 299 –316. ISSN: 0045-7930. DOI: https://doi.org/10.1016/j.compfluid.2007.07.017. URL: http://www.sciencedirect.com/science/article/pii/S0045793007001454.

[37] M.J. Castro Dıáz et al. "Two-dimensional sediment transport models in shallow water equations. A second order finite volume approach on unstructured meshes". In: *Computer Methods in Applied Mechanics and Engineering* 198.33 (2009), pp. 2520 –2538. ISSN: 0045-7825. DOI: https://doi.org/10.1016/j.cma.2009.03.001. URL: http://www.sciencedirect.com/science/article/pii/S0045782509001169.

[38] P. Degond, S. Jin, and J.-G. Liu. "Mach-number uniform asymptotic-preserving gauge schemes for compressible flows". In: *Bull. Inst. Math., Acad. Sin.* Vol. 2.No. 4 (2007), pp. 851–892.

[39] P. Degond and M. Tang. "All speed scheme for the low mach number limit of the Isentropic Euler equations". In: *Commun. Comput. Phys.* Vol. 10.No. 1 (2011), pp. 1–31.

[40] Pierre Degond and Min Tang. "All speed scheme for the low mach number limit of the Isentropic Euler equation". In: *arXiv preprint arXiv:0908.1929* (2009).

[41] Stéphane Dellacherie. "Analysis of Godunov type schemes applied to the compressible Euler system at low Mach number". In: *Journal of Computational Physics* 229.4 (2010), pp. 978–1016.

[42] M. Dumbser et al. "A divergence-free semi-implicit finite volume scheme for ideal, viscous, and resistive magnetohydrodynamics". In: *International Journal for Numerical Methods in Fluids* 89.1-2 (2019). cited By 0, pp. 16–42. DOI: 10.1002/fld.4681. URL: https://www.scopus.com/inward/record.uri?eid=2-s2.0-85058455601&doi=10.1002%2ffld.4681&partnerID=40&md5=2eb3729740d153a856fcc34106375aa1.

[43] Michael Dumbser and Casulli Vincenzo. "A conservative, weakly nonlinear semi-implicit finite volume scheme for the compressible Navier-Stokes equations with general equation of state". In: *Applied Mathematics and Computation* 272 (Jan. 2016), pp. 479–497. DOI: 10.1016/j.amc.2015.08.042.

[44] Fernández-Nieto, Enrique D. et al. "Formal deduction of the Saint-Venant-Exner model including arbitrarily sloping sediment beds and associated energy". In: *ESAIM: M2AN* 51.1 (2017), pp. 115–145. DOI: 10.1051/m2an/2016018. URL: https://doi.org/10.1051/m2an/2016018.

[45] Heinrich Freistühler and Gerald Warnecke. *Hyperbolic Problems: Theory, Numerics, Applications: Eighth International Conference in Magdeburg, February/March 2000 Volume 1*. Jan. 2001. ISBN: 978-3-0348-9537-8. DOI: 10.1007/978-3-0348-8370-2.

[46] Daniel Fuster and Stephane Popinet. "An all-Mach method for the simulation of bubble dynamics problems in the presence of surface tension". In: *Journal of Computational Physics* 374 (2018), pp. 752 –768.

[47] Thierry Gallouet et al. "Convergence of the MAC scheme for the compressible stationary Navier-Stokes equations". In: *arXiv preprint arXiv:1607.01968* (2016).

[48] Edwige Godlewski and Pierre-Arnaud Raviart. *Numerical Approximation of Hyperbolic Systems of Conservation Laws*. Springer, 2014.

[49] Sigal Gottlieb and Chi-Wang Shu. "Total Variation Diminishing Runge-Kutta Schemes." In: *Mathematics of Computation* 67 (Aug. 1996). DOI: 10.1090/S0025-5718-98-00913-2.

[50] Sigal Gottlieb, Chi-Wang Shu, and Eitan Tadmor. "Strong Stability-Preserving High-Order Time Discretization Methods". In: *SIAM Review* 43 (May 2001). DOI: 10.1137/S003614450036757X.

[51] Jeffrey Haack, Shi Jin, and Jian-Guo Liu. "An all-speed asymptotic-preserving method for the isentropic Euler and Navier-Stokes equations". In: *Communications in Computational Physics* 12.04 (2012), pp. 955–980.

[52] E. Hairer, S. P. Nørsett, and G. Wanner. *Solving Ordinary Differential Equations I (2Nd Revised. Ed.): Nonstiff Problems*. New York, NY, USA: Springer-Verlag New York, Inc., 1993. ISBN: 0-387-56670-8.

[53] E. Hairer and G. Wanner. *Solving Ordinary Differential Equations II. Stiff and Differential-Algebraic Problems. (2Nd Revised. Ed.)* Vol. 14. Springer Series in Comput. Mathematics. New York, NY, USA: Springer-Verlag New York, Inc., 1996.

[54] Natalie Happenhofer et al. "A low Mach number solver: Enhancing applicability". In: *Journal of Computational Physics* 236 (2013), pp. 96 –118. ISSN: 0021-9991. DOI: https://doi.org/10.1016/j.jcp.2012.11.002. URL: http://www.sciencedirect.com/science/article/pii/S0021999112006572.

[55] Douglas S. Harned and W. Kerner. "Semi-Implicit Method for Three-Dimensional Resistive Magnetohydrodynamic Simulation of Fusion Plasmas". In: *Nuclear Science and Engineering* 92.1 (1986), pp. 119–125.

[56] Ami Harten and Stanley Osher. "Uniformly high-order accurate nonoscillatory schemes. I". In: *SIAM Journal on Numerical Analysis* 24.2 (1987), pp. 279–309.

[57] Amiram. Harten, Peter D. Lax, and Bram van. Leer. "On Upstream Differencing and Godunov-Type Schemes for Hyperbolic Conservation Laws". In: *SIAM Review* 25.1 (1983), pp. 35–61. DOI: 10.1137/1025002. eprint: https://doi.org/10.1137/1025002. URL: https://doi.org/10.1137/1025002.

[58] Raphaèle Herbin, Walid Kheriji, and Jean-Claude Latche. "Staggered schemes for all speed flows". In: *ESAIM: Proceedings*. Vol. 35. EDP Sciences. 2012, pp. 122–150.

[59] D.R. van der Heul, C. Vuik, and P. Wesseling. "A conservative pressure-correction method for flow at all speeds". In: *Computers & Fluids* 32.8 (2003), pp. 1113 –1132. ISSN: 0045-7930. DOI: http://dx.doi.org/10.1016/S0045-7930(02)00086-5. URL: http://www.sciencedirect.com/science/article/pii/S0045793002000865.

[60] Justin Hudson. "Numerical Techniques for Morphodynamic Modelling". PhD thesis. University of Whiteknights, 2001.

[61] Antony Jameson. "Numerical Solution of the Euler Equations by Finite Volume methods Using Runge-Kutta Time-Stepping Schemes". In: (Jan. 1981).

[62] Matthew Jemison, Mark Sussman, and Marco Arienti. "Compressible, multiphase semi-implicit method with moment of fluid interface representation". In: *Journal of Computational Physics* 279 (2014), pp. 182 –217.

[63] Guang-Shan Jiang and Eitan Tadmor. "Nonoscillatory central schemes for multidimensional hyperbolic conservation laws". In: *SIAM Journal on Scientific Computing* 19.6 (1998), pp. 1892–1917.

[64] Shi Jin. "Efficient asymptotic-preserving (AP) schemes for some multiscale kinetic equations". In: *SIAM Journal on Scientific Computing* 21.2 (1999), pp. 441–454.

[65] Samet Y Kadioglu and Dana A Knoll. "A fully second order implicit/explicit time integration technique for hydrodynamics plus nonlinear heat conduction problems". In: *Journal of Computational Physics* 229.9 (2010), pp. 3237–3249.

[66] Samet Y Kadioglu et al. "A second order primitive preconditioner for solving all speed multi-phase flows". In: *Journal of computational physics* 209.2 (2005), pp. 477–503.

[67] Samet Y Kadioglu et al. "A second order self-consistent IMEX method for radiation hydrodynamics". In: *Journal of Computational Physics* 229.22 (2010), pp. 8313–8332.

[68] Kentaro Kan and Takao Yoshinaga. "Instability of a planar liquid sheet with surrounding fluids between two parallel walls". In: *Fluid Dynamics Research* 39.5 (2007), pp. 389–412. DOI: 10.1016/j.fluiddyn.2006.08.001. URL: https://doi.org/10.1016%2Fj.fluiddyn.2006.08.001.

[69] Sergiu Klainerman and Andrew Majda. "Compressible and incompressible fluids". In: *Communications on Pure and Applied Mathematics* 35.5 (1982), pp. 629–651. ISSN: 1097-0312. DOI: 10.1002/cpa.3160350503. URL: http://dx.doi.org/10.1002/cpa.3160350503.

[70] Sergiu Klainerman and Andrew Majda. "Singular limits of quasilinear hyperbolic systems with large parameters and the incompressible limit of compressible fluids". In: *Communications on Pure and Applied Mathematics* 34.4 (1981), pp. 481–524. ISSN: 1097-0312. DOI: 10.1002/cpa.3160340405. URL: http://dx.doi.org/10.1002/cpa.3160340405.

[71] R. Klein. "Semi-implicit extension of a Godunov-type scheme based on low Mach number asymptotics. I: One-dimensional flow". In: *J. Comput. Phys.* Vol. 121.No. 2 (1995), pp. 213–237.

[72] Alexander Kurganov and Eitan Tadmor. "Solution of Two-Dimensional Riemann Problems for Gas Dynamics Without Riemann Problem Solvers". In: *Numerical Methods for Partial Differential Equations* 18 (Sept. 2002). DOI: 10.1002/num.10025.

[73] Nipun Kwatra et al. "A method for avoiding the acoustic time step restriction in compressible flow". In: *Journal of Computational Physics* 228.11 (2009), pp. 4146–4161.

[74] Nipun Kwatra et al. "A method for avoiding the acoustic time step restriction in compressible flow". In: *Journal of Computational Physics* 228.11 (2009), pp. 4146 –4161.

[75] L Landau and E Lifshitz. *Fluid Mechanics: Landau and Lifshitz: Course of Theoretical Physics*. Sept. 2013. ISBN: 9781483161044.

[76] Olivier Le Métayer and Richard Saurel. "The Noble-Abel Stiffened-Gas equation of state". In: *Physics of Fluids* 28.4 (2016), p. 046102. DOI: 10.1063/1.4945981. eprint: https://doi.org/10.1063/1.4945981. URL: https://doi.org/10.1063/1.4945981.

[77] Bram van Leer. "Towards the ultimate conservative difference scheme. V. A second-order sequel to Godunov's method". In: *Journal of Computational Physics* 32.1 (1979), pp. 101 –136. ISSN: 0021-9991. DOI: https://doi.org/10.1016/0021-9991(79)90145-1. URL: http://www.sciencedirect.com/science/article/pii/0021999179901451.

[78] Randall J. LeVeque. *Finite Volume Methods for Hyperbolic Problems*. Cambridge Texts in Applied Mathematics. Cambridge University Press, 2002. DOI: 10.1017/CBO9780511791253.

[79] Randall J. LeVeque. *Numerical Methods for Conservation Laws*. Lectures in Mathematics ETH Zürich, Department of Mathematics Research Institute of Mathematics. Springer, 1992. ISBN: 9783764327231. URL: https://books.google.gr/books?id=3WhqLPcMdPsC.

[80] D. Levy, G. Puppo, and G. Russo. "Compact Central WENO Schemes for Multidimensional Conservation Laws". In: *SIAM Journal on Scientific Computing* 22.2 (2000), pp. 656–672. DOI: 10.1137/S1064827599359461.

[81] Doron Levy, Gabriella Puppo, and Giovanni Russo. "A Fourth-Order Central WENO Scheme for Multidimensional Hyperbolic Systems of Conservation Laws". In: *Siam Journal on Scientific Computing* 24 (Oct. 2002). DOI: 10.1137/S1064827501385852.

[82] Doron Levy, Gabriella Puppo, and Giovanni Russo. "Central WENO schemes for hyperbolic systems of conservation laws". In: *ESAIM: M2AN* 33.3 (1999), pp. 547–571. DOI: 10.1051/m2an:1999152. URL: https://doi.org/10.1051/m2an:1999152.

[83] Tai Ping Liu. "Quasilinear hyperbolic systems". In: *Comm. Math. Phys.* 68.2 (1979), pp. 141–172. URL: https://projecteuclid.org:443/euclid.cmp/1103905309.

[84] C. Madroñal and Manuel Castro. "On the well-balanced property of Roe's method for nonconservative hyperbolic systems. Applications to shallow-water systems". In: *ECCOMAS 2004 - European Congress on Computational Methods in Applied Sciences and Engineering* 38 (Jan. 2004).

[85] F. Miczek, F.K. Röpke, and P.V.F. Edelmann. "A new numerical solver for flows at various Mach numbers". In: *Astronomy & Astrophysics* Vol. 576 (2015), A50.

[86] Miczek, F., Röpke, F. K., and Edelmann, P. V. F. "New numerical solver for flows at various Mach numbers". In: *A&A* 576 (2015), A50. DOI: 10.1051/0004-6361/201425059. URL: https://doi.org/10.1051/0004-6361/201425059.

[87] C-D Munz et al. "The extension of incompressible flow solvers to the weakly compressible regime". In: *Computers & Fluids* 32.2 (2003), pp. 173–196.

[88] Haim Nessyahu and Eitan Tadmor. "Non-oscillatory central differencing for hyperbolic conservation laws". In: *Journal of computational physics* 87.2 (1990), pp. 408–463.

[89] S. Noelle et al. "An asymptotic preserving all Mach number scheme for the Euler equations of gas dynamics". In: *Technical Report 348, IGPM , RWTH-Aachen, Germany* (2012).

[90] Andrew Nonaka et al. "MAESTRO: An adaptive low Mach number hydrodynamics algorithm for stellar flows". In: *The Astrophysical Journal Supplement Series* 188.2 (2010), p. 358.

[91] S Osher and F Solomon. "Upwind difference schemes for hyperbolic systems of conservation laws". In: *Mathematics of Computation* (1982).

[92] Carlos Parés and Manuel Castro. "On the well-balance property of Roe's method for nonconservative hyperbolic systems. Applications to shallow-water systems". en. In: *ESAIM: Mathematical Modelling and Numerical Analysis - Modélisation Mathématique et Analyse Numérique* 38.5 (2004), pp. 821–852. DOI: 10.1051/m2an:2004041. URL: http://www.numdam.org/item/M2AN_2004__38_5_821_0.

[93] Lorenzo Pareschi and Giovanni Russo. "Implicit-explicit Runge-Kutta schemes and applications to hyperbolic systems with relaxation". In: *Journal of Scientific computing* 25.1-2 (2005), pp. 129–155.

[94] JH Park and C-D Munz. "Multiple pressure variables methods for fluid flow at all Mach numbers". In: *International journal for numerical methods in fluids* 49.8 (2005), pp. 905–931.

[95] Carlos Parés. "Numerical methods for nonconservative hyperbolic systems: a theoretical framework." In: *SIAM Journal on Numerical Analysis* 44.1 (2006), pp. 300–321. DOI: 10.1137/050628052.

[96] J.-M. Qiu and C.-W. Shu. "Conservative high order semi-Lagrangian finite difference WENO methods for advection in incompressible flow". In: *J. Comput. Phys.* Vol. 230.No. 4 (2011), pp. 863–889.

[97] Jianxian Qiu and Chi-Wang Shu. "Finite Difference WENO Schemes with Lax–Wendroff-Type Time Discretizations". In: *Siam Journal on Scientific Computing* 24 (May 2003). DOI: 10.1137/S1064827502412504.

[98] P L Roe. "Characteristic-Based Schemes for the Euler Equations". In: *Annual Review of Fluid Mechanics* 18.1 (1986), pp. 337–365. DOI: 10.1146/annurev.fl.18.010186.002005.

[99] P.L Roe. "Approximate Riemann solvers, parameter vectors, and difference schemes". In: *Journal of Computational Physics* 43.2 (1981), pp. 357–372. ISSN: 0021-9991. DOI: https://doi.org/10.1016/0021-9991(81)90128-5. URL: http://www.sciencedirect.com/science/article/pii/0021999181901285.

[100] Sabine Roller and Claus-Dieter Munz. "A low Mach number scheme based on multi-scale asymptotics". In: *Computing and Visualization in Science* 3.1 (2000), pp. 85–91. ISSN: 1433-0369. DOI: 10.1007/s007910050055. URL: http://dx.doi.org/10.1007/s007910050055.

[101] Giovanni Russo. *High order shock capturing schemes for balance laws*. Dipartimento di Matematica e Informatica - Universit'a di Catania, 2008.

[102] Giovanni Russo and Alexander Khe. "High order well-balanced schemes based on numerical reconstruction of the equilibrium variables". In: *Waves and Stability in Continuous Media*. Vol. 1. 2010, pp. 230–241.

[103] Giovanni Russo and Alexander Khe. "High order well balanced schemes for systems of balance laws". In: *Hyperbolic problems: theory, numerics and applications*. Vol. 67. Proc. Sympos. Appl. Math. Amer. Math. Soc., Providence, RI, 2009, pp. 919–928. DOI: 10.1090/psapm/067.2/2605287. URL: http://dx.doi.org/10.1090/psapm/067.2/2605287.

[104] Steven Ruuth, Raymond Spiteri, and J. Ruuth. "A New Class of Optimal High-Order Strong-Stability-Preserving Time Discretization Methods". In: *SIAM J. Numer. Anal.* 40 (Feb. 2002). DOI: 10.1137/S0036142901389025.

[105] A H Shapiro. *The Dynamics and Thermodynamics of Compressible Fluid Flow*. May 1953.

[106] Chi-Wang Shu. "Essentially non-oscillatory and weighted essentially non-oscillatory schemes for hyperbolic conservation laws". In: *Advanced numerical approximation of nonlinear hyperbolic equations*. Springer Berlin Heidelberg, 1998, pp. 325–432.

[107] Chi-Wang Shu. "Total-Variation-Diminishing Time Discretizations". In: *Siam Journal on Scientific and Statistical Computing* 9 (Nov. 1988). DOI: 10.1137/0909073.

[108] Chi-Wang Shu and Stanley Osher. "Efficient implementation of essentially non-oscillatory shock-capturing schemes". In: *Journal of Computational Physics* 77.2 (1988), pp. 439 –471. ISSN: 0021-9991. DOI: https://doi.org/10.1016/0021-9991(88)90177-5. URL: http://www.sciencedirect.com/science/article/pii/0021999188901775.

[109] James J. Stoker. *Water Waves: The Mathematical Theory with Applications*. Interscience Publishers Inc., New York, 1957. ISBN: 9780471570349.

[110] Gallouet Thierry, Jean-Marc Hérard, and Nicolas Seguin. "Some recent Finite Volume schemes to compute Euler equations using real gas EOS". In: *International Journal for Numerical Methods in Fluids* 39 (Aug. 2002), pp. 1073–1138. DOI: 10.1002/fld.346.

[111] Eleuterio Toro. "Riemann Solvers and Numerical Methods for Fluid Dynamics: A Practical Introduction". In: Jan. 2009. DOI: 10.1007/b79761.

[112] Eleuterio Toro. "Shock-Capturing Methods for Free-Surface Shallow Flows / E.F. Toro." In: (Jan. 2001).

[113] Eleuterio Toro and Elena Vázquez-Cendón. "Flux splitting schemes for the Euler equations". In: *Computers & Fluids* 70 (Nov. 2012). DOI: 10.1016/j.compfluid.2012.08.023.

[114] Eleuterio F Toro. *Riemann solvers and numerical methods for fluid dynamics: a practical introduction. Third edition*. 2009.

[115] Eli Turkel. "Preconditioned methods for solving the incompressible and low speed compressible equations". In: *Journal of computational physics* 72.2 (1987), pp. 277–298.

[116] Deepak Varma R S and Praveen Chandrashekar. "A second-order well-balanced finite volume scheme for Euler equations with gravity". In: *Computers & Fluids* 181 (Mar. 2018). DOI: 10.1016/j.compfluid.2019.02.003.

[117] Cécile Viozat. *Implicit Upwind Schemes for Low Mach Number Compressible Flows*. Tech. rep. RR-3084. INRIA, Jan. 1997. URL: https://hal.inria.fr/inria-00073607.

[118] Feng Xiao. "Unified formulation for compressible and incompressible flows by using multi-integrated moments I: one-dimensional inviscid compressible flow". In: *Journal of Computational Physics* 195.2 (2004), pp. 629 –654.